bioRxiv preprint doi: https://doi.org/10.1101/2021.01.29.428913; this version posted April 2, 2021. The copyright holder for this preprint (which was not certified by peer review) is the author/funder, who has granted bioRxiv a license to display the preprint in perpetuity. It is made available under aCC-BY 4.0 International license.

Atg8 licenses adipokine nuclear exit

Michelle E. Poling[1, #], Camille E. Sullivan[1, #], Ava E. Brent[1#], Terry L. Hafer[1, 2] and Akhila Rajan[1, 2, *].

[1] Basic Sciences Division, Fred Hutch, Seattle, WA 98109, USA.

[2] Graduate Program in Molecular and Cellular Biology, University of Washington, Seattle, USA.

[#]equal contribution. * corresponding author: akhila@fredhutch.org

Abstract

Adipokines released from adipocytes function as a systemic 'adipometer' and signal satiety[1, 2]. For organisms to accurately sense surplus and scarcity, adipocytes must switch adeptly between adipokine release and retention[3]. Despite the central requirement for adipocytes to retain adipokines to enable organismal adaptation to nutrient deprivation[1], how fasting induces adipokine retention remains to be fully characterized. Here we investigated how Unpaired2 (Upd2), a fruit fly ortholog of the human adipokine Leptin[4], is retained during fasting. Unexpectedly, we observe that on fasting Upd2 accumulates in the nucleus and discover that fasting-induced Upd2 nuclear accumulation is regulated by Atg8. Atg8 is a ubiquitin like protein which conjugates to a lipid moiety[5]. We find that, Atg8 based on its own lipidation status promotes adipokine nuclear exit in fed cells and adipokine retention in starved cells- we term this 'adipokine licensing'. Then, we show that Atg8 lipidation is the rate-limiting step in adipokine licensing. We then illustrate how organisms use adipokine licensing to survive nutrient deprivation. Additionally, we show that adipokine nuclear retention, controlled by Atg8, stimulates post-fasting hunger; thus, Atg8-mediated nuclear retention sensitizes adipokine signaling after fasting. Hence, our findings point to a new mechanism to tackle adipokine resistance[6, 7], an underlying cause of common obesity. Collectively, we have identified a novel cell-intrinsic mechanism that orchestrates systemic response to energy flux and uncovered an unexpected role for Atg8 in context-dependent protein localization.

Introduction

Organisms constantly evaluate their basal nutritional reserves to decide on whether to allocate resources to expensive functions that enhance fitness or to conserve energy. Adipokines, secreted by fat cells provide an accurate assessment of nutrient-reserve information. Leptin in mammals [1] and its functional ortholog in fruit-flies, Unpaired2 (Upd2) [4], are primary adipokines that are released in proportion to fat stores [8-10]. They impinge on brain circuits that control energy expenditure, appetite and overall metabolism [4, 11, 12]. In surplus nutrient states, adipokines convey a permissive signal, indicating that energy resources can be devoted

bioRxiv preprint doi: https://doi.org/10.1101/2021.01.29.428913; this version posted April 2, 2021. The copyright holder for this preprint (which was not certified by peer review) is the author/funder, who has granted bioRxiv a license to display the preprint in perpetuity. It is made available under aCC-BY 4.0 International license.

to costly activities like immunity and reproduction. During periods of scarcity, their circulation is reduced, signaling an energy deficit, and enabling organisms to conserve energy.

Starvation-induced reduction in Leptin/Upd2 levels is crucial for an organism's neuroendocrine response to reduced energy reserves; this has been well-documented in humans [8, 9], mice [1, 6] and flies [3, 4]. Specifically, Leptin injections, during fasting, dysregulates neuroendocrine physiology, and decreases survival capacity in mice [1]. Based on this study [1], Flier and colleagues have proposed that "*the primary physiologic role of Leptin is to provide a signal of energy deficit to the CNS*" [6, 13]. Similarly, flies with reduced levels of Upd2 display increased starvation survival [4], suggesting that reduced Upd2 levels enable flies to develop resilience to starvation.

Despite the central requirement for adipocytes to retain adipokines during starvation in order to allow organismal adaptation to nutrient deprivation, how fasting induces adipokine retention remains to be fully characterized. Importantly, hyperleptinemia, i.e., high levels of circulating leptin, has been identified as a primary cause of 'leptin resistance'- a state wherein Leptin is unable to effectively signal satiety state to the brain [14], resulting in dysfunctional feeding behavior and decreased energy expenditure. Hence, understanding how adipokine retention is regulated in fat cells will provide mechanistic insights that can be applied to intervene in hyperleptinemia-induced adipokine signaling resistance.

We previously showed that in *Drosophila* cells, both Upd2 and human Leptin adopt a unconventional secretion route for release into circulation [3]. We also showed that during nutrient deprivation, increased circulating levels of the starvation hormone Glucagon impinges on fat cells to inhibit adipokine release via this route, ultimately enabling fat cells to retain adipokines [3]. This mechanistic insight is consistent with the idea of using glucagon like peptides (GLPs) to treat obesity and sensitize Leptin signaling [15]. While our work [3] provided clues on how systemic signals, including glucagon, impinge on fat cells to regulate adipokine retention, what cell intrinsic mechanisms mediate fasting induced adipokine retention remained an open question, and a central focus of our investigations.

A primary mechanism by which organisms adapt to metabolic stress is the nutrient scavenging pathway called autophagy [16, 17]. In adipocytes, autophagy controls lipid metabolism by a process known as lipophagy [18, 19]. A central player in the autophagy pathway is a ubiquitin-like protein family member [20] called LC3/GABARAP in mammals, and Atg8 in flies and yeast [21].

bioRxiv preprint doi: https://doi.org/10.1101/2021.01.29.428913; this version posted April 2, 2021. The copyright holder for this preprint (which was not certified by peer review) is the author/funder, who has granted bioRxiv a license to display the preprint in perpetuity. It is made available under aCC-BY 4.0 International license.

Atg8 is widely distributed in the nucleus [22] and during starvation, it translocates to the cytoplasm [23] where its gets conjugated to the lipid moiety phosphatidylethanolamine (PE) [5]. Lipidated Atg8 regulates fusion of autophagosomes to lysosomes, resulting in cargo degradation [24]. It is now widely recognized that many core autophagy proteins, including Atg8, play central roles in non-degradative cellular activities [25]. These include, but are not limited to: LC3-associated phagocytosis (LAP) [26], viral replication [27], extracellular vesicle secretion (LDELS) [28], and LC3 associated endocytosis (LANDO) [29]. These non-degradative roles for Atg8 have been documented in the cytosol. But what remains unclear is whether Atg8/LC3 proteins localized to the nucleus [22] play a specific role other than to provide a pool of Atg8 available for lipidation [23], and to help cells cope with oncogenic stress by degrading the nuclear lamina [30].

While investigating cell intrinsic mechanisms which regulate acute adipokine retention, we unexpectedly found a direct, non-degradative role for Atg8 in licensing adipokine nuclear exit in fed cells and promoting adipokine retention during fasting. Furthermore, we found that this mechanism is central to systemic energy balance as it provides a resilience mechanism for flies during fasting and sensitizes adipokine signaling post-fasting. Given, the deep conservation of autophagy machinery between flies and mammals [31, 32], and also the processes governing energy homeostasis, particularly lipid biology, between flies and mammals [33-38], we believe that our findings in the *Drosophila* model, regarding Atg8's role in licensing adipokine release, will be of relevance more broadly.

Results

Fasting induces Upd2 nuclear accumulation:

To explore whether cells have intrinsic mechanisms to retain adipokines during fasting, we probed whether cells retain Upd2/Leptin on amino-acid (AA) deprivation. Note, we chose the AA-starvation regime, because it provided the most consistent results, as opposed to serum starvation or culturing cells in buffers including PBS and EBSS. Upd2, a JAK/STAT pathway agonist, is secreted into media of cultured *Drosophila* S2R+ cells [39]. In previous work, a quantitative assay (ELISA) for Upd2 release was established in the *Drosophila* S2R+ cell culture system [3]. For these experiments a C-terminal GFP-tagged version of Upd2 (*Upd2::GFP*) is transiently transfected into S2R+ cells [3]. *Upd2::GFP* can rescue *upd2Δ* mutants [4], strongly suggesting that GFP tagged version of Upd2 likely recapitulates the function of untagged wild-type (WT) Upd2. Using this previously established quantitative secretion assay (see methods)

bioRxiv preprint doi: https://doi.org/10.1101/2021.01.29.428913; this version posted April 2, 2021. The copyright holder for this preprint (which was not certified by peer review) is the author/funder, who has granted bioRxiv a license to display the preprint in perpetuity. It is made available under aCC-BY 4.0 International license.

we asked whether culturing S2R+ cells in amino acid (AA)-free media affected Upd2::GFP release (hereafter referred to as Upd2-WT). We observed a -76% reduction ($p<0.001$) in Upd2 secretion within 6 hours of AA-starvation. Furthermore, 20 hours post-starvation, Upd2 secretion decreased by -96% ($p=0.0004$) (Fig.1A). These results suggest that *Drosophila* S2R+ cells sense a fasted state and acutely retain a significant portion of the adipokine Upd2 (~76%) within a brief period of AA deprivation (6 hours).

Fasting induced transcriptional [40] and translational [41] controls, are likely to work in concordance with acute mechanisms to retain already transcribed and translated adipokines. Acute adipokine retention mechanisms possibly include a “brake” on the trafficking machinery involved in Upd2 release, and/or degradation of adipokine primed for release. To begin to explore these acute mechanisms, we documented Upd2’s cellular localization during a fasting time-course (imaging fixed cells - every 2-4 hours on AA-fasting). When cells are cultured in complete medium (‘Fed’ state), Upd2 exhibits a punctate cytoplasmic localization, with diffuse and faint nuclear localization (Fig.1Ba). Within 4-8 hours of AA fasting, increased Upd2 nuclear accumulation is observable (Fig.1Bb- Starved (Stv), 8hr). Upd2 nuclear accumulation is detected even at 16 hours of AA-starvation (Fig.1Bc- Stv, 16hr). We also noted that Upd2, at time points assayed (4-24hr), exhibits a punctate cytoplasmic localization (Fig.1Bb, Bc). While it is possible that this cytoplasmic pool of Upd2 is retained or degraded, we did not further define or characterize the fasting-induced acute adipokine retention mechanisms in the cytoplasm (See Discussion).

Instead, intrigued by fasting-induced Upd2 nuclear accumulation, we sought to define and characterize it. To this end, we performed independent fasting-time series experiments with 50-100 cells per time-point (these were blinded experiments-see methods) and quantified the ratio of Upd2 nuclear intensity versus the whole cell at each time point (Fig.1B’). Across such independent experiments, we observed a similar dynamic in Upd2 nuclear accumulation. No significant increase in Upd2 nuclear accumulation was observable at 2 hours of AA-fasting. However, within 4 hours we observed, on average, a +25% increase ($p=9.9E-7$) in Upd2 nuclear accumulation. This upward trend in Upd2 nuclear accumulation peaks at 8-12 hours post-AA starvation with a 30-50% increase in Upd2 nuclear accumulation ($p= 1.2E-8$). At 16 hours, Upd2 nuclear accumulation while higher than fed state (+17%; $p=5.1E-3$), was lower than the peak at 8-12 hours (Fig.1B’).

bioRxiv preprint doi: https://doi.org/10.1101/2021.01.29.428913; this version posted April 2, 2021. The copyright holder for this preprint (which was not certified by peer review) is the author/funder, who has granted bioRxiv a license to display the preprint in perpetuity. It is made available under aCC-BY 4.0 International license.

Next, we asked whether refeeding restores Upd2 release. On performing a quantitative ELISA for Upd2-WT in cells from three different nutrient states--fed, starved, and re-fed--we observed that by 5 hours after refeeding (Fig.1C), the amount of Upd2-WT released into the media was 104% higher than the starved state (p=1.2E-6). This indicates that cells can toggle between retention and release within a 5-hour period; strikingly, this mirrors the temporal dynamics of adipokine retention (Fig.1A). Next, we examined the correlation between refeeding and Upd2 nuclear accumulation. As observed previously (Fig.1B, B'), within 8 hours of starvation, significantly higher Upd2 nuclear accumulation can be seen (+43%; p=6.8E-14; Fig.1Db, D'). Within 4 hours of refeeding, Upd2 nuclear accumulation is about +14% higher (p=0.0001) than fed cells (Fig.1Dc, D'). By 6 hours after refeeding, Upd2 nuclear accumulation is reduced and closer to the 'original' fed levels (+6%; p=0.07/ns; see Fig.1Dd, D'); this correlates with Upd2 release within 5-hours on refeeding. Taken together these observations indicate that fasting-induced nuclear accumulation is an acute adipokine retention mechanism, and that refeeding reverses Upd2 nuclear accumulation within a similar timeframe (4-6 hours). For the rest of this study, we focused on understanding the mechanisms that regulate the early phase (4-8 hours) of acute adipokine Upd2 nuclear accumulation.

Atg8 regulates nucleocytoplasmic localization of Upd2:

We then sought to identify mechanisms that link nutrient state to adipokine nuclear retention. AA-starvation triggers autophagy, a nutrient scavenging pathway [42], of which Atg8/LC3, a ubiquitin-like protein, is a primary component [21]. In fasted cells, Atg8 undergoes a ubiquitin-like conjugation to a lipid moiety phosphatidylethanolamine (PE) [5]. Subsequent to its lipidation Atg8 regulates fusion of autophagosomes to lysosomes, resulting in cargo degradation [24]. It is now widely recognized that many core autophagy proteins, including Atg8, play central roles in non-degradative cellular activities [25]. For instance, Atg8 is well-documented for its involvement in the unconventional secretion of a wide variety of cargoes including, but not limited to, yeast Acb1, mammalian interleukins and RNA binding proteins [43-47].

In a previous study, our lab demonstrated that the adipokine Upd2 and its human ortholog Leptin (hLeptin), adopts an unconventional secretory route [3]. Given Atg8's role in AA-deprivation triggered nutrient-scavenging [21], and its documented role in unconventional secretion [43-45, 47], we specifically examined the effect of removing Atg8 on Upd2 release. In fed *Drosophila* S2R+ cells, dsRNA mediated knockdown of Atg8 (Atg8-KD) results in an -85% reduction (p=0.048) in Upd2 secretion (Fig.2A), phenocopying the effect of fasting on Upd2 release. Moreover, this

bioRxiv preprint doi: https://doi.org/10.1101/2021.01.29.428913; this version posted April 2, 2021. The copyright holder for this preprint (which was not certified by peer review) is the author/funder, who has granted bioRxiv a license to display the preprint in perpetuity. It is made available under aCC-BY 4.0 International license.

observation, that Atg8 is required for Upd2 release, is consistent with both Atg8's role in unconventional secretion [28, 48] and our prior report that Upd2 is a cargo of the unconventional secretion pathway [3].

To better understand this reduced secretion phenotype, we examined cellular localization of Upd2 following *Atg8-KD* (Fig.2Bb) compared to a control dsRNA (*LacZ-KD*) (Fig.2Ba). While punctate cytoplasmic Upd2 is still present, nuclear Upd2 accumulation is clear in *Atg8-KD* cells by confocal microscopy. On quantifying, *Atg8-KD* resulted in a +34% (p=0.0035) to +60% (p=3.9E-5) increase in Upd2 nuclear accumulation (Fig.2B'). Collectively, these observations are consistent with Atg8 reduction, even in fed cells, correlating with increased Upd2 nuclear accumulation.

As Atg8 itself is degraded by autophagy [49], we considered that in *Atg8-KD*, reduced Atg8 levels perhaps signify a nutrient scavenging state; hence an increase in Upd2 nuclear accumulation could be a 'passive' outcome. An alternate, but not mutually exclusive, hypothesis is that Atg8 plays an 'active'/ direct role that ultimately results in fasting-induced adipokine localization. This latter hypothesis is consistent with the idea that Upd2 might interact in a complex with Atg8, directly or via adapter molecules. To test this, we co-transfected Myc::Atg8-WT and Upd2-WT::GFP and performed GFP and Myc pull downs, we found that Upd2-WT co-immunoprecipitates (Co-IPs) with Atg8-WT (Fig.2C, lane 1).

Next, we wanted to test whether Upd2's interaction with Atg8 is reliant on a short linear protein domain known as the AIM (Atg8-interacting motif), which contains the consensus sequence W/F/Y-X-X-L/I/V, and is present in *bona fide* Atg8 interaction proteins [50]. On analyzing protein sequences, we found that Upd2 has AIM-like sequences (Figure. 2D). Mutating Upd2's AIM (using an established approach of mutating W and L to A [51];here after referred to as Upd2-AIM$^-$) impaired the interaction between Upd2 and Atg8, as assayed by a co-immunoprecipitation experiment (Fig.2C, lane 2). Upd2 is usually found at very low levels in the lysate of S2R+ cells because of its constitutively secreted (see GFP-IP lane 1 in Fig.2C). We noted that Upd2-AIM$^-$ levels appeared higher than Upd2-WT in lysate (GFP-IP lane 2 in Fig.2C). Despite being present at a higher level it does not effectively complex with Atg8 (RFP-IP lane 2 in Fig.2C). Furthermore, the higher levels of Upd2-AIM$^-$ in the lysate is suggestive of a defect in release of Upd2-AIM$^-$.

To test whether Upd2-AIM$^-$ impairs Upd2 release, we performed a quantitative ELISA and found that single amino acid point mutations of the AIM motif of Upd2 (W and L to A) reduced

bioRxiv preprint doi: https://doi.org/10.1101/2021.01.29.428913; this version posted April 2, 2021. The copyright holder for this preprint (which was not certified by peer review) is the author/funder, who has granted bioRxiv a license to display the preprint in perpetuity. It is made available under aCC-BY 4.0 International license.

secretion by -96% (p=4.29E-05) (Fig.2D). This reduction in Upd2-AIM- release phenocopies *Atg8-KD* (Fig.2A) and fasting-induced states (Fig.1A). Hence, we examined whether Upd2-AIM$^-$ exhibits increased nuclear accumulation as occurs in an *Atg8-KD* (Fig.2Eb). We observed a significant increase in Upd2 nuclear localization (Fig.1E). Specifically, Upd2-AIM- (Fig.1Eb, b') exhibited a diffuse but highly enriched Upd2 nuclear localization (+72%; p=1.7E-11 compared to control Fig.1E'). Furthermore, as evidenced by both confocal (Fig.1Eb) and super-resolution images (Fig.1Eb'), Upd2-AIM- is contained within the nuclear lamina, and distinct cytosolic puncta are not readily detectable. The absence of punctate cytosolic localization of Upd2-AIM- contrasts with Upd2 localization following both *Atg8-KD* (Fig.2Bb) and fasting-induced Upd2 nuclear accumulation (Fig.1Bb, 1Db), and represents a stronger retention (-96% reduction in secretion and an increased nuclear accumulation +72%). Given that AIM- significantly impairs Upd2's association with Atg8, we reasoned that Upd2-AIM$^-$ represents an "Atg8-null" state for Upd2, while dsRNA knockdown of *Atg8*, reflects a hypomorphic state (see Discussion).

Altogether, these datasets suggest that when Atg8 levels are reduced (*Atg8-KD*) or when Upd2's interaction with Atg8 is significantly impaired (Upd2-AIM-), Upd2 is retained in the nucleus and is not readily available for secretion. Hence, our results are suggestive of Atg8 playing a central role in Upd2's nucleocytoplasmic localization.

Nucleocytoplasmic shuttling of Upd2 is required for its subsequent release:

Upd2 is a 47 kDa protein. Given the structural restraint of nuclear pore complexes (NPC) to only permit proteins <40kDA to pass through [52], Upd2 is likely to require active nucleocytoplasmic (NC) transport mechanisms that enable transit through the NPC [53]. Hence, we sought to explore whether Upd2's NC localization is regulated by classical NC transport pathways. In such a pathway, cargoes >40kDa (but even some smaller cargoes such as histones) rely on their ability to interact with a set of soluble nuclear transport receptors- 'importins' and 'exportins'- also known as Karyopherins [54, 55].

First, we analyzed Upd2's sequence using a bioinformatic tool- classic NLS (cNLS) mapper- [56-58] to ask whether Upd2 has a predicted NLS. cNLS mapper predicted that Upd2 contains an NLS at residues 141-150 (GRVIKRKHLE) with a score of 10.5. According to cNLS mapper, a GUS-GFP reporter protein fused to an NLS with a score of 8, 9, or 10 is exclusively localized to the nucleus. Next, we asked whether Upd2 is predicted to contain an NES using another tool NetNES [59]. While NetNES predicted an NES like sequence for Upd2 residues 248-

bioRxiv preprint doi: https://doi.org/10.1101/2021.01.29.428913; this version posted April 2, 2021. The copyright holder for this preprint (which was not certified by peer review) is the author/funder, who has granted bioRxiv a license to display the preprint in perpetuity. It is made available under aCC-BY 4.0 International license.

254 (LCEIELTI), residues 251 and 253 do not broach the threshold, thus making it difficult to say if this whole sequence is indeed an NES (see Discussion).

To clarify if Upd2 relies on a classical nuclear export factors, we genetically manipulated nuclear exportin CRM1 [60], also known as Embargoed (Emb) in flies [61]. We asked whether Emb knock-down (*Emb-KD*) affects Upd2 localization in a fed state. We found that transfection of fed S2R+ cells with *Emb dsRNA*, compared to control *LacZ dsRNA* (Fig.3Aa), recapitulated the increase in Upd2 nuclear accumulation (Fig.3Ab) that we had observed in either an AA-starved state (Fig.1Bb, Bc), or following *Atg8-KD* (2Bb). On quantifying (Fig.3A'), we observed that *Emb-KD*, using two independent dsRNAs, resulted in +18% (p=0.0053) and +16% (p=0.024) increase in Upd2 nuclear accumulation (levels akin to 16-hour starvation time point Fig.1B'). We also noted punctate Upd2 localization at the nuclear periphery (blue arrows in Fig.3Ab). We next analyzed the effect of reducing CRM1/Emb on Upd2's release from cells. We observed that, consistent with our previous findings on the inverse correlation between Upd2 nuclear accumulation and its release, that in *Emb-KD* cells, as assayed by ELISA, Upd2 release is reduced by -33 to -49%; p<0.01 (Fig.3B). Altogether, irrespective of whether Upd2 directly interacts with CRM1/Emb or via an adapter due to its "cryptic" NES (See Discussion), these data are indicative of CRM1/Emb export being involved in Upd2 nuclear exit. These observations support the hypothesis that manipulations which impede nuclear export Upd2 nuclear accumulation decreases its subsequent release.

Given the inverse correlation between Upd2's nuclear accumulation and its secretion, we wondered about the opposite condition., i.e., whether manipulations that impede nuclear import increase Upd2 release. In *Drosophila* there are at least four encoded *Importin-α* genes and at least eight *Importin-β* genes [62]. We were concerned that individual knock-down of these 12 genes may not produce a strong effect, should there be redundancy. Our goal was to blunt nuclear import in general and observe its effect on Upd2 release. Therefore, we adopted a pharmacological approach by using a small molecule Importin-β inhibitor, 2,4-diaminoquinazoline, commonly named Importazole [63]. Heald and colleagues have shown that Importazole specifically blocks Importin-β-mediated nuclear import; it does so by impairing Importin-β's interaction with RanGTP, and importantly does not disrupt transportin-mediated nuclear import or CRM1-mediated nuclear export [63]. This drug was established for blocking nuclear import using Xenopus egg extracts and cultured cells [63]. Hence, to block Importin-β based nuclear import, we incubated *Drosophila* S2R+ cells for 6 hours with 40-100μM

bioRxiv preprint doi: https://doi.org/10.1101/2021.01.29.428913; this version posted April 2, 2021. The copyright holder for this preprint (which was not certified by peer review) is the author/funder, who has granted bioRxiv a license to display the preprint in perpetuity. It is made available under aCC-BY 4.0 International license.

Importazole and assayed its effect on Upd2 release using the quantitative sandwich ELISA assay when compared to control treatment (DMSO). Unlike what we predicted, we observed that 40μM Importazole reduced Upd2 secretion by -23% (p=0.15) and that 100μM Importazole reduced Upd2 secretion by -48% (p=0.01) (Fig.3B). We observed the similar reductions in Upd2 release with Importazole treatment, in three independent experiments, with 6 biological replicates per condition per experiment. We were surprised that Importin-β inhibition impaired Upd2 release and wondered whether it affected Upd2 nuclear entry. Therefore, we examined cells treated with Importazole and documented Upd2 NC localization by confocal imaging. As predicted, based on Upd2's NLS sequence, impeding Importin-β-based nuclear transport by treatment with Importazole, reduced Upd2 nuclear localization for both the 40μM Importazole (Fig.3Db) and 100μM Importazole (Fig.3Dc) compared to control DMSO treatment (Fig.3Da). Quantification of reduction in Upd2 nuclear accumulation (Fig.3D') showed a median of -30% reduction (p=0.0032). Significantly, Upd2 does not show an increase in fasting-induced nuclear accumulation (as observed in Fig.1B') when treated with Importazole during a starved state (see Fig.3D': -7% reduction in starved stated compared to fed in Importazole treatment p=0.54). We also noted that compared to control treatment (Fig.3Da), Upd2-WT in Importazole-treated cells (Fig.3Db and 3Dc), was hard to detect in distinct punctate localization. Instead, Upd2-WT in Importazole-treated cells appeared to 'fill' majority of the cytoplasmic compartment (Fig.3Da, 3Dc). Hence, increased Upd2 cytoplasmic accumulation correlates with reduced release. Taken together, these observations suggested to us that Upd2 uses an Importin-β based mechanism for its nuclear import.

It is possible that impairing NC shuttling broadly, including blocking nuclear import by pharmacological means, impacts Upd2 release in an indirect manner. Hence, we sought to precisely manipulate Upd2 so that it remains cytosolic and then assay how such a 'forced' cytosolic localization affects its release. In addition, we also wondered whether forced nuclear export, by appending a strong NES sequence, could 'override' the *Upd2-AIM-* nuclear accumulation phenotype. Studies in *Drosophila* models have shown that appending a particular NES sequence (LDELLELLRL) to the N-terminal of proteins that localize to the nucleus, reliably and actively shuttles those proteins out to the cytosol [64], thus rendering nuclear proteins cytosolic. Hence, we added this strong nuclear export signal (NES^{+}: LDELLELLRL) in the N-terminal (See methods) of Upd2-WT (referred to here-in as *Upd2-NES+*) and Upd2-AIM^{-}(referred to here-in as *Upd2-NES+AIM-*). We then performed confocal imaging of cells

bioRxiv preprint doi: https://doi.org/10.1101/2021.01.29.428913; this version posted April 2, 2021. The copyright holder for this preprint (which was not certified by peer review) is the author/funder, who has granted bioRxiv a license to display the preprint in perpetuity. It is made available under aCC-BY 4.0 International license.

transfected with: *Upd2-WT* (Fig.3Ea, Eb), *Upd2-AIM-* (Fig.3Ec, Ed), *Upd2-NES+* (Fig.3Ee, Ef) and *Upd2-NES+AIM-* (Fig.3Eg, Eh). As previously documented in Fig.1, Upd2-WT in fed cells exhibits a punctate cytosolic localization (Fig.3Ea) and displays significant nuclear accumulation on AA-starvation (Fig.3Eb). Again, as reported in the prior section (Fig.2E), Upd2-AIM$^-$ is nuclear with almost no detectable punctate cytosolic expression in the fed or starved state (Fig.3Ec, Ed). Upd2-NES$^+$ is cytosolic in fed cells (Fig.3Ee) and continues to be cytosolic even in starved cells (Fig.3Ee, see 3E' for quantification). Moreover, like Upd2-WT localization in Importazole treated cells (Fig.3Db, Dc), Upd2-NES+ 'fills' the cytoplasm (Fig.3Ee), instead of exhibiting the punctate localization observed in Upd2-WT fed cells (Fig.3Ea). Like Upd2-NES$^+$, Upd2-NES$^+$AIM$^-$ is cytosolic in fed and starved cells (Fig.3Eg, Eh). Furthermore, the NES$^+$ appended to Upd2-AIM$^-$ overrides the Upd2-AIM$^-$ nuclear accumulation phenotype (Compare Fig.3Ec, Ed to Eg, Eh), indicating that by providing an ectopic active export mechanism, Upd2 can exit the nucleus. But again, just like Upd2-NES+ (Fig.3Ee, Ef), and Importazole treatment Fig.3Db, Dc, the cytosolic Upd2 appears more diffuse in Upd2-NES$^+$AIM$^-$ (Fig.3Ee, Ef). Hence, we asked if engineered nuclear export, which results in Upd2's nuclear export despite being AIM- is sufficient to promote Upd2 release. On performing quantitative ELISA on Upd2-NES$^+$ and Upd2-NES$^+$AIM$^-$, however we observed that both versions exhibit secretion defects (Fig.3F; -64% reduction p=0.0013), suggesting that forced nuclear export of Upd2 while can override the AIM- nuclear retention phenotype, it is unable to direct Upd2's release. This concurs with our observation that interfering with either Upd2's nuclear export (Fig.3B) or its nuclear import (Fig.3C), both affect Upd2 release.

In conclusion, these results suggest that Upd2 needs to be shuttled into the nucleus prior to being secreted. Also, these results are consistent with a model that after translation in the cytoplasm, Upd2 enters the nuclear environment in order to obtain 'licensing' for release.

Upd2 nucleocytoplasmic shuttling licenses its release via Atg8-GRASP pathway:

We surmised that Atg8 could potentially serve as Upd2's 'licensing' factor, by both enabling Upd2 nuclear exit, and then subsequently targeting Upd2 to an appropriate secretion route. To investigate this possibility, we asked whether, in fed cells, the Upd2 cytosolic puncta co-localized or associated with Atg8. First, we performed live imaging of fed cells transfected with Upd2::GFP and mCherry::Atg8 (Fig.4A and Extended Data Fig.1), to gather preliminary information on the dynamics of the Upd2 puncta and Atg8. We observed that Atg8 and Upd2 co-localize in nuclear periphery (Fig.4A, see blue arrows in 0s, 90s and 135s. Similarly, we also observed the two

bioRxiv preprint doi: https://doi.org/10.1101/2021.01.29.428913; this version posted April 2, 2021. The copyright holder for this preprint (which was not certified by peer review) is the author/funder, who has granted bioRxiv a license to display the preprint in perpetuity. It is made available under aCC-BY 4.0 International license.

proteins co-localize in puncta at the cell periphery (Fig.4A, white arrows in 0s-180s). We found that this co-localization was not a stable one, i.e., a complete overlap changed into an association within 45 seconds (see blue arrows in nuclear periphery Fig.4A-135s vs. 180s). Altogether, these imaging datasets indicated that the Upd2 puncta in the cytosol were positive for Atg8, but that the co-localization of Atg8 to Upd2 punctum was dynamic and unstable, and suggesting that in fixed imaging we were likely to observe them overlap partially.

Once we obtained this baseline for dynamics of Atg8 and Upd2 co-localization, we wondered whether colocalization between Upd2 and Atg8 would be different for Upd2-NES+ compared to Upd2-WT. In fed cells co-transfected with Atg8 and either Upd2-WT (Fig.4Ba) or Upd2-NES+(Fig.4Bb), we examined and quantified the co-localization (see Methods) between these two proteins. In >10 cells per condition, we observed that Upd2-WT exhibited partial to complete (yellow arrows in Fig.4Ba) co-localization with Upd2 (quantified in B' : (0-90% co-localization) whereas Upd2-NES+ was almost mutually exclusive to Atg8 (Fig.4Bb, B'; note difference between Upd2-WT and NES+ is significant p=0.006) . This suggested to us that if Upd2 is forcibly shuttled out of the nucleus then, its ability to localize to Atg8 puncta in the cytosol is compromised. Significantly, this observation lends credence to the idea that Upd2 nuclear localization and subsequent exit is key to Upd2's ability to access Atg8 appropriately.

Since Upd2 release is impaired in both Upd2-NES+ (Fig.3F), and Upd2-AIM- (Fig.2A), we reasoned that Upd2's ability to interact with Atg8 is an important step both for its nuclear exit and subsequent secretion. Our lab previously reported that Upd2 uses a GRASP-secretion route [3]. Therefore, we examined the co-localization of GRASP with respect to Upd2-WT and Upd2-AIM-. Imaging fixed cells co-transfected with GRASP and Upd2-WT (Fig.4Ca) versus Upd2-AIM- (Fig.4Cb), showed that GRASP is largely a cytosolic protein and that Upd2-WT puncta co-localize with GRASP, whereas Upd2-AIM- renders Upd2 unable to access the cytosol. Consistent with this, we also observed that while Upd2-WT co-immunoprecipitates with GRASP (Fig.4D; Lane 2), despite being present in much lower amount in the lysate of the cells due to its higher secretion. By contrast, Upd2-AIM-, which is not secreted (Fig.2D), does not co-IP with GRASP (Fig.4D; Lane 2).

Taken together these observations (Fig. 3, 4) are consistent with a model that Upd2's nuclear entry provides Upd2 a 'venue' to have a productive interaction with Atg8 (note Upd2-NES+ co-localization with Atg8 is impaired: Fig.4B, B'). Atg8 then enables Upd2's nuclear exit and provides the context required for Upd2 to be targeted to the GRASP secretory route.

bioRxiv preprint doi: https://doi.org/10.1101/2021.01.29.428913; this version posted April 2, 2021. The copyright holder for this preprint (which was not certified by peer review) is the author/funder, who has granted bioRxiv a license to display the preprint in perpetuity. It is made available under aCC-BY 4.0 International license.

Atg8's lipidation state is the rate-limiting step in Upd2 nuclear exit:

The most well-characterized function of Atg8 is its degradative role in autophagy, where in undergoes a ubiquitin-like conjugation to a lipid moiety phosphatidylethanolamine (PE) [5] and enables the fusion of autophagosomes to lysosomes. Therefore, we asked whether Atg8's lipidation state has an impact on Upd2 nuclear exit.

First, we examined what effect, if any, autophagy induction and its subsequent induction of Atg8 lipidation, has on Upd2 nuclear retention. Torin1, is a highly potent and selective ATP-competitive mTOR inhibitor [65], and is one of the most widely used methods to pharmacologically activate autophagy [66]. Torin1 activated autophagy induces Atg8-lipidation [67]. We treated well-fed *Drosophila* S2R+ cells, cultured in complete media, with Torin1 (50-750nM; see Methods) and assayed its effect on Upd2 nuclear accumulation relative to control (DMSO) treatment (Fig.5A) in 50-150 cells per treatment in independent experiments (Fig.5A'). We observed a dose dependent effect on Upd2 retention (Fig.5Ab-d) in Torin1 treated cells, causing from a +20% (p=1.7E-8) increase with 50nM Torin1 (Fig.5Ab; 5A'), to a +75% (p=1.2E-27) increase with 750nM (Fig.5Ad; 5A'). This striking effect of Torin1 treatment (+75% increase) on Upd2 nuclear retention is consistent with the Upd2 nuclear retention observed during starvation (Fig.1B). Altogether, this suggested to us that induction of autophagy by Torin1 treatment, like AA-withdrawal, induced Upd2 nuclear accumulation.

Atg8-lipidation levels increase during autophagy induction. Atg8 is widely distributed in the nucleus [22]. Whether this nuclear pool of Atg8 has any specific role remains to be fully understood. A study by Liu and colleagues [23], presented compelling evidence that the nuclear pool of Atg8 translocates to the cytosol on starvation, and is the primary source of lipidated Atg8 for autophagosome formation [68]. However, it remains possible that Atg8 has a yet to be uncovered, non-degradative, functions in the nucleus via its actions on AIM/LIR containing proteins such as the adipokine Upd2. Therefore, going a step further, we considered the possibility that AA-starvation induced Atg8-lipidation may result in a depletion of the nuclear pool of Atg8 in *Drosophila* S2R+ cells, a state that would ensure Upd2 remains localized to the nucleus.

To test this directly, we examined the localization of 'normal' wild-type Atg8 (Atg8-WT) versus a lipidation-defective Atg8 [Atg8-PE$^-$; as done in prior studies which defined Atg8 lipidation, [5] we mutated the penultimate glycine, the lipidation acceptor amino acid of Atg8, to an

bioRxiv preprint doi: https://doi.org/10.1101/2021.01.29.428913; this version posted April 2, 2021. The copyright holder for this preprint (which was not certified by peer review) is the author/funder, who has granted bioRxiv a license to display the preprint in perpetuity. It is made available under aCC-BY 4.0 International license.

alanine; see methods]. We transfected N-terminally mCherry tagged- *Atg8-WT* (Fig.5Ba, Bb) or *Atg8-PE-* (Fig.5Bc, Bd) into *Drosophila* S2R+ cells, and examined localization in fed and AA-starved states. We note that these experiments are all performed in WT S2R+ cells that do contain an endogenous Atg8 pool, however our goal was to document the distribution of mCherry-tagged versions of Atg8-WT and Atg8-PE- in the presence of endogenous Atg8. We observed that mCherry::Atg8-WT is distributed diffusely in the nucleus and the cytoplasm (Fig.5Ba) in fed cells, but during a short AA-starvation most of mCherry::Atg8-WT is localized to punctate structures in the cytoplasm (Fig.5Ba). This pattern of Atg8-WT localization in S2R+ cells concurs with what has been shown previously by Baehrecke and colleagues [69], indicating that our Atg8 transgenes and starvation regimes work as would be expected for this cell line (See also Extended Data Fig. 2A, 2B to assess the behavior of *Atg8-WT* and *Atg8-PE-* transgenes in *Drosophila* fat).

Next, we examined the localization of lipidation-defective mcherry::Atg8-PE-. Unlike mCherry::Atg8-WT, which exhibits differential NC localization during starvation (Fig. 5Ba, Bb; 5B'), mCherry::Atg8-PE^{-} exhibited the same diffuse NC distribution in fed (Fig.5Bc) and starved states (Fig.5Bd). Importantly, as quantified in 80-125 cells per genotype per condition (Fig.5B'), lipidation-defective Atg8 showed no reduction in its nuclear localization during starvation (Fig.5B': Atg8 PE^{-} fed vs. starved=+5%; p=0.1). Specifically, Atg8-PE^{-} nuclear pool on starvation increases compared to Atg8-WT (in starved cells Atg8-WT vs. Atg8 PE^{-}= +34%; p=8.5E-10). These results strongly suggest that starvation, because it induces Atg8's lipidation and causes it to re-localize to punctate structures in the cytosol, depletes the Atg8 nuclear pool, while a lipidation-defective Atg8 molecule continues to be present in the nucleus even during starvation, at levels comparable to the fed state. We extended this observation to *Drosophila* adult fat cells (Extended Data Fig.2B), in which we found that on starvation Atg8-WT localizes to punctate cytosolic structures (Extended Data Fig.2Ba; white arrows) and is depleted from the nucleus (Extended Data Fig.2Ba; blue arrows). Lipidation-defective Atg8 (Atg8-PE-), while present in the cytosol, continued to show strong nuclear enrichment, even on starvation (Extended Data Fig.2Bb; blue arrows).

Thus far, our data show that events which induce Atg8-lipidation increase Upd2 nuclear accumulation, including AA-starvation (Fig.1B) and Torin1 treatment (Fig.5A). Hence, we hypothesized that lipidation-induced depletion of Atg8's nuclear pool is a rate-limiting step in Upd2's nuclear exit during starvation. To test this, we co-transfected Upd2-WT, with either

bioRxiv preprint doi: https://doi.org/10.1101/2021.01.29.428913; this version posted April 2, 2021. The copyright holder for this preprint (which was not certified by peer review) is the author/funder, who has granted bioRxiv a license to display the preprint in perpetuity. It is made available under aCC-BY 4.0 International license.

control (empty mCherry vector), mCherry::Atg8-WT (which can undergo lipidation and hence move into the cytosol on starvation; Fig.5Bb), or mCherry::Atg8-PE- (lipidation-defective Atg8 which remains in a nuclear pool even during starvation; Fig.5Bd). See schematic in the top panel of Fig.5C for experimental design. We then quantified (in 65-150 cells per condition) the ability of starvation to induce nuclear accumulation of Upd2, in the presence of these Atg8 transgenes. As documented in the prior section (Fig.1Ba), Upd2 is localized to cytosolic puncta in fed cells. Co-expression of either mCherry empty vector (Fig.5Ca), mCherry::Atg8-WT (Fig.5Cc), or mCherry::Atg8-PE- (Fig.5Ce) in fed cells results in normal Upd2-WT localization (Fig.1Ba). On starving for 8 hours, Upd2-WT exhibits significantly increased nuclear accumulation in mCherry control (Fig.5Cb, 5C', +59%; p=5.1E-6), and in mCherry::Atg8-WT (Fig.5Cd, 5C' , +25%; p=1.5E-7). Strikingly, when co-transfected with mCherry::Atg8-PE-, which continues to remain nuclear in starvation (Fig.5Bd, 5B'), Upd2-WT exhibits no increase in fasting-induced nuclear accumulation (Fig. 5Cf, 5C'; 0.4%, p=0.95). Hence, providing cells a pool of lipidation-defective Atg8, that continues to be nuclear during starvation, interferes with fasting-induced Upd2 nuclear accumulation, and is sufficient to allow Upd2 to exit the nucleus during fasting. Consistent with this, co-IP experiments show that Upd2-WT can complex with Atg8 despite its lipidation-defective state (Extended Data Fig.2C; lane 2). In sum, these observations support a model in which the nuclear pool of Atg8 licenses Upd2's nuclear exit, and during fasting, it is the depletion of the nuclear Atg8 pool due to lipidation that triggers Upd2 nuclear accumulation.

Adipokine nuclear accumulation signals a systemic starvation state:

We next wondered whether our studies of adipokine nuclear accumulation in *Drosophila* S2R+ cells, which are derived from macrophage like cells, are of any relevance to adult fat cells, the source tissue of adipokine signaling. We first examined whether fasting induces adipokine nuclear accumulation like we observed in *Drosophila* S2R+ cells, is visible in fat cells. To do this, we generated endogenous CRISPR engineered tag knock-ins into the Upd2 locus with two different tags (HA and GFP- See Methods) to follow Upd2's endogenous localization. Both these genomic tagged versions of Upd2 were able to rescue the fat storage defects (Extended Data Fig.3 A, B) that have been reported for a upd2-deletion allele (*upd2Δ*) [4]. In addition to the genomic tagged Upd2 alleles, we also used flies that expressed an mCherry-tagged Upd2 cDNA transgene in fly fat (*Lpp-Gal4> UAS-Upd2::mCherry*). We acutely fasted flies with either tissue-specific expression of Upd2-WT::mCherry (Fig. 6Ab, 6A'a) or the endogenously tagged Upd2::HA (Fig.6A'b) and Upd2::GFP(Fig.6A'c) flies. In all these different over-expressed and

bioRxiv preprint doi: https://doi.org/10.1101/2021.01.29.428913; this version posted April 2, 2021. The copyright holder for this preprint (which was not certified by peer review) is the author/funder, who has granted bioRxiv a license to display the preprint in perpetuity. It is made available under aCC-BY 4.0 International license.

endogenously tagged versions of Upd2, we observed that Upd2, which is usually barely detectable in fat cells, and especially their nuclei, exhibited a perceptible increase nuclear localization (Fig.6Ab) of Upd2 levels (Fig.6A'; +41-51% ($p<1.1E-6$)). This increase is comparable to the acute fasting induced Upd2 accumulation in S2R+ cells (Fig.1Bb), providing evidence for conservation of our findings in S2R+ cells.

To ask whether Atg8 controls adipokine accumulation in adult fly fat cells, we first performed fat-tissue specific acute (*Upd2crGFP; ppl-Gal4tubGal80t^{s}*; Fig. 6Ba) and 'mild'-chronic (*Upd2crGFP; Lpp-Gal4*; Fig. 6Bb) and assessed endogenous Upd2 nuclear accumulation. Note for the 'mild-chronic' *Atg8-KD* crosses were maintained at 18c (a temperature at which RNAi based KD is weak in fruit-flies). Then when the F1s were 7 days old, they were shifted to 29c for a 5-7day Atg8 knock down. Tissue-specific knock down of Atg8 using RNAi, using such an acute 5-7 day period, resulted in a moderate (+16%-26%) but statistically significant ($p=0.03$ or $p=0.05$) increase in Upd2 nuclear accumulation. Given we only performed *Atg8-KD* in adult fat for an acute period, these moderate effects are likely due to a weaker Atg8-KD. Nevertheless promisingly, these results (Fig. 6B) of *in vivo* adult fat tissue-specific *Atg8-KD's* effect on Upd2 accumulation are consistent with our findings in *Drosophila* S2R+ cells that *Atg8-KD* increases Upd2 nuclear accumulation.

Then, we reasoned that examination of the *Upd2-AIM-* transgenes was likely to provide the most clarifying result. *Atg8-KD* in fat tissue, even in clones, can have numerous effects that might complicate interpretation. Furthermore, the AIM-mutation represents a "Atg8-null" situation for Upd2, and correlates strongly with *Atg8-KD* phenotype in S2R+ cells. To recap, the Upd2-AIM^{-} mutation does not co-IP with Atg8 (Fig.2C) and displays strong nuclear accumulation (Fig.2Eb, E'). Hence, we examined the effect of the point-mutation to Upd2's AIM, on Upd2's localization in adult fly fat in a *upd2Δ* background (*upd2Δ; Lpp-Gal4> UAS-Upd2-AIM-*). We observed a striking increase in nuclear accumulation of the Upd2-AIM- transgene, even in adult fat cells from well-fed flies (Fig.6Cb), compared to Upd2-WT (Fig.6Ca) which, at the same imaging settings, was barely detectable. In addition, the Upd2-AIM- transgenes displayed similar nuclear accumulation even in a control background (*Lpp-Gal4> UAS-Upd2-AIM-*) where endogenous Upd2 is intact (Extended Data Fig.5Ab). These results suggest that the mechanisms that we uncovered for Atg8's control of Upd2 nuclear exit in *Drosophila* S2R+ cells, are conserved in adult fly fat. Furthermore, they suggest that by examining the effect of Upd2-

bioRxiv preprint doi: https://doi.org/10.1101/2021.01.29.428913; this version posted April 2, 2021. The copyright holder for this preprint (which was not certified by peer review) is the author/funder, who has granted bioRxiv a license to display the preprint in perpetuity. It is made available under aCC-BY 4.0 International license.

AIM- which accumulates in fly fat, we will be able to uncover whether Atg8-mediated regulation of Upd2's nuclear exit, and subsequent release, has an effect on systemic physiology.

In a starved state, insulin (Dilp2, Dilp5) accumulates in the fly insulin producing cells (IPCs) [70]. One of the primary functions of Upd2 in adult fly fat is to remotely signal to the brain to create a permissive environment for insulin release [4, 12]. As expected, based on a prior study [4], compared to background control, *upd2Δ* flies have elevated levels of Dilp2 and Dilp5 fluorescence in the IPCs (Extended Data Fig.4A), and expression of a Upd2-WT transgene (*upd2Δ; Lpp-Gal4>UAS-Upd2-WT*) rescues this defect (Extended Data Fig.4A). Hence, we examined the effect of insulin release when *Upd2-AIM-* was expressed in fly fat (*upd2Δ; Lpp-Gal4> UAS-Upd2-AIM-)* and observed that *Upd2-AIM-* is unable to completely rescue the insulin accumulation phenotype of *upd2Δ* flies (Fig.6D, D', Extended Data Fig. 4B). This suggests that Upd2-AIM- is not able to be released and signal to the IPCs.

Having shown that the Upd2-AIM- variant of Upd2 is localized to the fat cell nucleus (Fig.6Cb), and unable to promote Insulin release when over-expressed in a *upd2Δ* mutant (Fig. 6D, D'), we next wanted to characterize the effect of Upd2-AIM- on gene expression in fat tissue. Upd2 secretion from the fat tissue systemically signals Insulin release from IPCs [4, 12]. Circulating Drosophila Dilps are received by the fat tissue, where they regulate nutrient uptake and utilization, and promote triacylglyerol (TAG) storage of excess nutrients [71, 72]. Additionally, within the fat tissue, stored fats are packaged into lipophorin/lipoprotein particles (LPPs)--complexes of protein and lipid assembled in fat cells—that re-enter circulation to provide essential lipids to tissues [73].

Because the Upd2-Insulin circuit communicates availability of stored energy, we expected that over-expression of Upd2-WT in fat would generate a gene expression profile reflecting TAG storage and active supply of nutrients to other tissues, while over-expression of Upd2-AIM- would not. To test our prediction, we performed qPCR on fat tissue from *upd2Δ* mutants in which either *Upd2-WT* or *Upd2-AIM-* was over-expressed in the fat and examined expression of genes involved in either de-novo lipid synthesis or LPP production (Fig.6E). De-novo lipid synthesis genes included Sterol regulatory element binding protein (SREBP), a master-regulator of lipogenesis that activates transcription of lipogenic genes [74, 75], and Fatty acid synthase 1 (FASN1), required for de novo synthesis of FB-stored TAG [76, 77]. LPP production genes included Apolipophorin (Apolpp) and Microsomal triacylglycerol transfer protein (Mtp), both specifically expressed in fat cells. *Drosophila* Apolpp, a member of the ApoB family, is the main protein

bioRxiv preprint doi: https://doi.org/10.1101/2021.01.29.428913; this version posted April 2, 2021. The copyright holder for this preprint (which was not certified by peer review) is the author/funder, who has granted bioRxiv a license to display the preprint in perpetuity. It is made available under aCC-BY 4.0 International license.

component of LPPs, and provides a scaffold for lipid assembly. Assembly of LPPs requires the activity of Mtp [73].As hypothesized, when compared to either control flies or *upd2Δ* flies expressing Luciferase (Luc) in the FB (*upd2Δ; Lpp-Gal4>UAS-Luc*), the Upd2-WT over-expressing flies (*upd2Δ; Lpp-Gal4>UAS-Upd2-WT*) showed increased expression of SREBP, FASN1, Apolpp, and Mtp (Fig.6E), supporting that Upd2-WT signals availability of excess nutrition for storage as well as Lpp packaging--even in a *upd2Δ* background. By contrast, in the *upd2Δ* flies expressing Upd2-AIM-, expression of SREBP, FASN1, ApoLpp, and Mtp was significantly lower compared to Upd2-WT (Fig.6E). Interestingly, expression of all four genes was reduced, even compared to control (yw) or *upd2Δ* flies (*upd2Δ; Lpp-Gal4>UAS-Luc*), suggesting that Upd2-AIM- may actively repress pathways involved in lipogenesis and Lpp assembly. Fat specific Upd2-AIM- expression resulted in a similar gene expression profile for SREBP, FASN1, ApoLpp, and Mtp even in a WT background (Extended Data Fig.5B). We also noted a slight increase in expression of SREBP, FASN1, Apolpp, and Mtp in the *upd2Δ* flies (*upd2Δ; Lpp-Gal4>UAS-Luc*) compared to yw, signifying that *upd2Δ* flies may compensate for their previously described diminished TAG stores by increasing de novo lipogeneis and Lpp assembly [4].

Since over-expression of Upd2-WT promotes lipogenesis and Lpp assembly, and over-expression of Upd2-AIM- does not, we hypothesized either a cell-autonomous role for Upd2 within the FB, or a systemic role for Upd2 in Insulin release from the IPCs. To examine the latter possibility at the level of FB gene expression, we asked what effect over-expression of either Upd2-WT or Upd2-AIM- has on Insulin signaling within the FB of *upd2Δ* mutants. DILPs activate insulin receptor (InR) signaling by inhibiting the forkhead transcription factor, FOXO. FB expression levels of the FOXO target genes *InR*, *brummer* (*Bmm*), and *4ebp/Thor* can thus provide a readout of Insulin signaling [78]. We found, as expected, that *upd2Δ* mutants (*upd2Δ*; *Lpp-Gal4>UAS-Luc*) showed increased expression of InR, Bmm, and 4ebp compared to yw controls, indicating that systemic Insulin signaling is reduced in the absence of Upd2 (Fig.6F). Moreover, we found that over-expression of Upd2-WT restored expression of all three FOXO targets to control levels, consistent with Upd2-WT's ability to promote Dilp release from *upd2Δ* mutant IPCs [4]. Following Upd2-AIM- over-expression, however, expression levels of InR, Bmm, and 4ebp remained high, underscoring that Upd2-AIM- cannot rescue Dilp release in *upd2Δ* mutants (Fig.6F). Interestingly, we observed that Bmm, which encodes a lipase required for the break-down of stored fats into fatty acids, and 4ebp, which has been shown to function as a

bioRxiv preprint doi: https://doi.org/10.1101/2021.01.29.428913; this version posted April 2, 2021. The copyright holder for this preprint (which was not certified by peer review) is the author/funder, who has granted bioRxiv a license to display the preprint in perpetuity. It is made available under aCC-BY 4.0 International license.

metabolic brake during starvation [79, 80], were expressed at higher levels in the *upd2Δ* flies with over-expressed Upd2-AIM-, compared to the *upd2Δ* flies expressing Luc—suggesting that the presence of Upd2-AIM- may signal a state of chronic starvation to the organism, it also implies that perhaps that the adipokine which is retained in the nucleus has a direct or indirect gene regulatory role (See Discussion).

Atg8-mediated adipokine nuclear accumulation increases resilience to starvation and promotes post-fasting hunger:

We wondered whether Atg8 controlled, fasting-induced adipokine nuclear accumulation (Fig.5C) affords an organism advantages during fasting. Consistent with this idea, we had documented in the prior section that expression of *Upd2-AIM-* signals a chronic starvation state, at least based on its gene expression profile (Fig.6E) and insulin accumulation phenotype (Fig.6C). Given that Upd2-AIM- phenocopies fasting-induced adipokine nuclear accumulation, we used it as a tool to ask what effect constitutive expression of *Upd2-AIM-* has on starvation survival. We subjected flies expressing fat-specific Upd2-WT (*upd2Δ; Lpp-Gal4>Upd2-WT)* and Upd2-AIM^{-} (*upd2Δ*; *Lpp-Gal4>Upd2-AIM^{-}*), to a nutrient-deprivation regime (Starvation-1% sucrose agar diet), and assayed their survival (Fig.7A). At least, 90 flies were used per genotype and the experiments were repeated thrice (see methods). We observed that fat-specific over-expression of Upd2-WT causes starvation sensitivity (Fig.7A; -20 reduction in median survival; Mantel-Cox test: $\chi 2$= 5.28, p=0.026). This effect on survival of Upd2 overexpression in starved flies resembles the detrimental effects of artificial Leptin repletion in starved mice [1]. By contrast, nuclear retention of Upd2 (*upd2Δ; Lpp-Gal4> UAS-Upd2-AIM-*) caused flies to perform better in comparison to control (Fig.7A; Mantel-Cox test: $\chi 2$= 32.41, p<0.0001). Also, of note, Upd2-AIM- displays a resilience to starvation when constitutively expressed even in a background which has Upd2-WT expression (Extended Data Fig.6A; compare *Lpp-Gal4>Upd2-AIM^{-} vs. Upd2-WT and UAS-control*). Taken together, these results show that Atg8's control of Upd2 nuclear retention during starvation provides fruit flies an ability to withstand starvation.

Leptin is a satiety signal in mammals [11], therefore we reasoned that Upd2 overexpression could indicate a satiety state. Hence, we set out to test feeding behavior (see Methods) using a widely used [81] feeding behavior assay in flies, the FLIC assay [82]. In the baseline state, i.e., flied fed *ad libitum,* overexpression of both Upd2-AIM- (*upd2Δ; Lpp-Gal4> UAS-Upd2-AIM-)* and Upd2-WT (*upd2Δ; Lpp-Gal4> UAS-Upd2-WT)* showed reduced feeding events (-50 to -80%) compared to control transgene (Extended Data Fig.6B). We next assayed hunger-driven feeding

bioRxiv preprint doi: https://doi.org/10.1101/2021.01.29.428913; this version posted April 2, 2021. The copyright holder for this preprint (which was not certified by peer review) is the author/funder, who has granted bioRxiv a license to display the preprint in perpetuity. It is made available under aCC-BY 4.0 International license.

motivation (Fig.7B) and events (Fig.7C) by subjecting flies to an over-night starvation regime and measuring their feeding behavior in relation to their *ad libitum* fed siblings. We observed that flies expressing a control transgene in a *upd2Δ* background (*upd2Δ; Lpp-Gal4>UAS-Luc*) exhibited increased motivation to feed (Fig.7Ba; +197%; p=0.05) and increased feeding events (Fig.7Ca), and that this increase in hunger-driven feeding events for the control was consistent with what we documented in a WT- background (*Lpp-Gal4>UAS-Luc*; Extended Data Fig.6Ca; +76% p=0.02). Constitutive expression of Upd2-WT (*upd2Δ; Lpp-Gal4> UAS-Upd2-WT)*, in keeping with the idea that it acts as a satiety signal like Leptin, does not display any increase in hunger-driven feeding motivation following starvation (Fig.7Bb; -28%; p=0.59) or events (Fig.7Cb; -10%; p=0.8). However, constitutive expression of Upd2-AIM-, despite showing reducing feeding events in an *ad libitum* state compared to control transgene (Extended Data Fig.6B), displayed strong hunger-driven feeding motivation. Specifically, compared to its fed sibs, fat-specific Upd2-AIM- expressing flies (*upd2Δ; Lpp-Gal4> UAS-Upd2-AIM-)*, after an overnight fast, exhibit strong motivation to feed (Fig.7Bc; +471%; p=0.0031) and feeding events (Fig.7Cc; +502%' p=0.0014). Increased hunger-driven feeding events (Extended Data Fig.6Cb; +867; p=0.0114) are observed even in a WT background (Extended Data Fig.6Cb; *Lpp-Gal4>UAS-Upd2-AIM-*). Altogether, these results suggest that fasting-induced Upd2 nuclear accumulation, controlled by Atg8, sensitizes the hunger response, thus improving an organism's adaptation to nutrient scarcity.

Discussion

By exploring how cells retain adipokines during fasting, we identified a previously unknown, non-degradative role for Atg8 in licensing adipokine nuclear export in fed cells (see working model Fig.7D-top left panel). When interactions between Atg8 and the adipokine Upd2 are disrupted (AIM-), adipokine nuclear retention occurs, even in a fed state (see working model Fig.7D-middle panel). During fasting, Atg8 is lipidated and recruited to the cytosol; this depletes the nuclear Atg8 pool. A result of Atg8's reduced availability in the nucleus on fasting is adipokine nuclear retention (see model Fig.7D-top right panel). Thus, nuclear retention promotes organismal fitness by ensuring adipokine secretion does not occur during fasting. Furthermore, we illustrate that adipokine retention on fasting has beneficial effects, promoting resilience on fasting and driving post-fasting hunger response. Therefore we reveal that Atg8 lipidation not only enables cells to intrinsically manage nutrient stress [16, 17], but because Atg8 controls adipokine release or retention, it enables an entire organism to adapt its neuroendocrine axes

bioRxiv preprint doi: https://doi.org/10.1101/2021.01.29.428913; this version posted April 2, 2021. The copyright holder for this preprint (which was not certified by peer review) is the author/funder, who has granted bioRxiv a license to display the preprint in perpetuity. It is made available under aCC-BY 4.0 International license.

to respond to nutrient stress. We term this ability of Atg8, to promote adipokine nuclear exit in fed cells and to conversely cause adipokine nuclear retention in starved cells, 'adipokine licensing'. Altogether, we have identified a cell-intrinsic mechanism of Atg8-mediated adipokine licensing that coordinates nutrient state with organismal physiology and behavior.

Critically, our report provides a specific answer to an outstanding question: whether in fed cells Atg8/LC3's localization in the nucleus has a functional role. A recent study by Liu and colleagues [23], presented compelling evidence that the nuclear pool of Atg8, translocates to the cytosol on starvation and is primary the source of lipidated Atg8 for autophagosome formation [68]. Also, nuclear Atg8 is known to associate with lamin-associated domains and degrade nuclear lamina during oncogenic stress [30] as well as act in repression of several genes in *Drosophila* fat during starvation [83]. However, it remains possible that Atg8 has other, yet to be uncovered functions in the nucleus of fed cells. By uncovering Atg8's ability to serve as a context-dependent 'licensing factor' to promote adipokine Upd2's nuclear exit, we provide an insight into the functional significance of nuclear Atg8 in fed cells.

More broadly, our findings indicate that Atg8 is likely to perform a context-dependent role in protein localization of other AIM/LIR bearing client proteins. Atg8 is a ubiquitin-like protein [20]. Ubiquitin and ubiquitin-like proteins have been shown to function in cellular localization. [84-86]. Specifically, SUMO (small ubiquitin-like modifier) is conjugated to proteins and modulates protein localization [87], in particular NC transport [88]. Interestingly, SUMO conjugation is not essential for NC transport itself, but positions its target protein (RanGAP1) to the NPC, therefore increasing the efficiency of its translocation. Similarly, Atg8 might position adipokine Upd2, and other such 'client' proteins, to enable efficient export via the classical nuclear export pathway or may serve to direct its larger client proteins to other mechanisms of nuclear export such as nuclear budding [89].

In support of this possibility, we observed that *CRM1*/*Emb* plays a role in Upd2 nuclear export (Fig.3Ab). Our evidence comes from a *Emb-KD* test, which is a genetic approach, and leaves open the possibility that Upd2 may need an adapter protein to access Emb/CRM1 export pathway. This idea is consistent with our analysis that Upd2 has a strong predicted NLS(sequence GRVIKRKHLE with score 10.5: a GUS-GFP reporter protein fused to an NLS with a score of 8, 9, or 10 is exclusively localized to the nucleus) allowing it to enter the nucleus. However, Upd2's predicted NES is 248-254 (LCEIELTI) and the Glutamate residues in position 251 and 253 do not broach the threshold, making it difficult to say if this whole sequence is

bioRxiv preprint doi: https://doi.org/10.1101/2021.01.29.428913; this version posted April 2, 2021. The copyright holder for this preprint (which was not certified by peer review) is the author/funder, who has granted bioRxiv a license to display the preprint in perpetuity. It is made available under aCC-BY 4.0 International license.

indeed an NES. Thus, perhaps Upd2 requires an adapter to access the CRM1 export pathway. This is reminiscent of a mechanism where-in a nuclear import importin-α requires a specific nuclear export factor, CAS, to access the cytosol [90]. Whether Atg8 serves as such an adapter itself, or if Upd2's association with Atg8 changes its conformation allowing the cryptic NES to be exposed so that it can bind CRM1/Emb, and/or Atg8 enables Upd2 to associate with other proteins that then serve to link up Upd2 to a classical nuclear export pathway are all possibilities. Preliminary evidence that our lab gathered, using mass-spectrometry (MS) analysis of immunoprecipitated (IP) Atg8-WT, Upd2-WT and Upd2-AIM- indicate that while Atg8 and Upd2-WT, both pull-down Emb/CRM1 as a MS interactor, the Upd2-AIM- IP-MS interaction list does not contain Emb. This supports the idea that Atg8 may serve as an adapter to enable Upd2 access Emb/CRM1. However, the IP-MS interactors will need further biochemical validation that is being actively pursued. Importantly, despite having a putative NES, Atg8/LC3 itself does not seem to require CRM1 for its nuclear export [22]. This is consistent with the idea that it can diffuse freely across the NPC barrier gives its size (<15kDa). In sum, how Atg8 interacts with the nuclear export machinery to enable context-dependent nuclear exit of adipokine Upd2, and whether other AIM/LIR containing proteins are regulated in such a fashion, will be developed in future work.

Another unexpected observation is that Upd2 requires both nuclear import, and then subsequent nuclear export, in order to be secreted (Fig.3). Impeding its nuclear entry by either pharmacological means, using Importazole (Fig. 3C, D, D'), or using an ectopic NES to shuttle Upd2 out of the nucleus (Fig. 3E, F), results in an abnormal cytosolic localization that is more diffuse, as opposed to its WT punctate localization (Compare Fig. 3Ea to 3Ee), and results in a significant reduction in secretion. Furthermore, the ectopic nuclear export of Upd2 interferes with its ability to co-localize with Atg8 (Fig. 4B). This is consistent with the idea that Upd2 requires the nuclear environment for a productive interaction with Atg8. We surmise that on entry into the nucleus, Upd2, via its AIM sequence, gains access to Atg8, which then routes it not only to a nuclear exit pathway, but to an appropriate secretory route (Schematic in Fig. 7D, top left panel). Consistent with this, Upd2-AIM- mutant protein is unable to effectively complex with GRASP (Fig. 4D) and our lab has previously shown that Upd2 uses a GRASP-mediated unconventional secretory route [3]. A tantalizing possibility is that Atg8 leads Upd2 through the outer nuclear envelope, which is continuous with the endoplasmic reticulum (ER) and, thus, with the cellular secretory route [91, 92]. However, further characterization is needed to define precisely how Atg8

bioRxiv preprint doi: https://doi.org/10.1101/2021.01.29.428913; this version posted April 2, 2021. The copyright holder for this preprint (which was not certified by peer review) is the author/funder, who has granted bioRxiv a license to display the preprint in perpetuity. It is made available under aCC-BY 4.0 International license.

targets Upd2 to the correct cytosolic location for secretion. It will also be interesting to test whether Atg8 enables Upd2 secretion via a mechanism akin to the one described by Debnath, Leidal and colleagues for RNA binding proteins, in which in a novel secretory process, called LDELS, the Atg8/LC3 conjugation pathway controls extracellular vesicle (EV) cargo loading and secretion [28, 45, 93].

While much is known about Atg8 lipidation being a key node of regulation during autophagic degradation [94], we reveal new insight on the a non-degradative outcome of fasting induced lipidation. Our results (Fig. 5B) show that adipokine nuclear retention is an outcome of fasting-induced lipidation. We show that lipidation induced depletion of the Atg8 nuclear pool (Fig. 7D, top panel) causes Upd2 retention. Consistent, with this we show that the presence of lipidation-defective nuclear Atg8 is sufficient to promote Upd2 nuclear exit even in fasting (Fig.5Cf; see schematic model Fig. 7D bottom panel). Whether lipidation-defective Atg8 can produce a productive, bioactive secretion event, is still under investigation. It therefore remains possible that lipidation of Atg8, even in fed cells, may very well be an important requirement for productive Upd2 secretion and its subsequent access to the blood-brain barrier by following an LDELS like route [45]. But we show here that lipidation of Atg8 is not required for Upd2 nuclear exit, and in fact, we show the opposite. We show that Atg8 lipidation is the molecular switch which controls ‘adipokine licensing’ and determines whether Upd2 is targeted to the cytosol or is retained in the nucleus.

From a physiological standpoint, the *Upd2-AIM-* mutation, provided us a unique opportunity to examine the systemic effect of Atg8’s role in adipokine regulation. *Atg8-KD* based mosaic clonal analysis would not provide answers to its systemic effects on adipokine signaling. While The Upd2-AIM- allele, which is impaired in its ability to interact with Atg8 (Fig. 2C), not only phenocopies *Atg8-KD’s* effects on Upd2 localization and secretion (Fig. 2D), but displays an almost exclusive nuclear accumulation phenotype with barely detectable cytosolic puncta (Fig. 2Eb,b’), coupled with a -96% reduction in Upd2 secretion (Fig. 2D). These observations suggest that a Upd2-AIM- mutation represents an “Atg8-null”-like state for Upd2. By expressing the *UAS-Upd2-AIM-* transgene in adult fly fat in an *upd2Δ* background, we were able to investigate how the Atg8-mediated adipokine nuclear licensing mechanism impacts an organism’s ability to cope with nutrient deprivation. We identified that adipokine nuclear retention promotes resilience to nutrient stress and increased hunger-driven feeding behavior (Fig. 7B, C and Extended Data Fig. 6C), despite having reduced basal feeding rate (Extended Data Fig.6B).

bioRxiv preprint doi: https://doi.org/10.1101/2021.01.29.428913; this version posted April 2, 2021. The copyright holder for this preprint (which was not certified by peer review) is the author/funder, who has granted bioRxiv a license to display the preprint in perpetuity. It is made available under aCC-BY 4.0 International license.

Thus, expression of *Upd2-AIM-* displays a dominant effect, even though it does not interfere with Upd2-WT localization (Extended Data Fig.5C). These results suggest that nuclear accumulation of Upd2 not only prevents its release, but also affects gene regulation, reminiscent of SREBP, a master-regulator of lipogenesis that activates transcription of lipogenic genes [74, 75]. This regulation of gene expression could occur either indirectly, through regulation of Insulin signaling, or directly via Upd2-dependent regulation of the nuclear landscape; thus, meriting further investigation.

In sum, we have uncovered an unexpected role for Atg8 in licensing the nuclear exit of a fly adipokine, Upd2, in fed cells, and in nuclear retention during fasting. This mechanism provides resilience during nutrient scarcity and sensitizes the post-fasting hunger response of an organism. Upd2 is a fly ortholog of human Leptin [4] and Leptin, just like Upd2, must be retained during fasting in order to signal a starved state in mammals [1, 6, 13]. Prior studies have shown that Leptin signaling and its regulation closely mirrors findings in the *Drosophila* model [3, 12]. A sequence analysis reveals that human Leptin has two AIM-like sequences, suggesting that it will be important to study the evolutionary conservation of Atg8's control of fasting-induced Leptin retention. Dysfunctional Leptin signaling- 'Leptin resistance' -is a leading cause of obesity. Our report that Atg8-mediated adipokine nuclear retention sensitizes an organism's hunger response, suggests a new mechanism to tackle adipokine resistance.

Acknowledgments: We are grateful to Gabor Juhasz for sharing Atg8 antibodies and to the late Suzanne Eaton for Lpp-Gal4 flies. We are grateful for advice from Scott Pletcher for the FLIC assay. We thank Brooke Figureoa and Laura Holderbaum for assistance with cell culture and immunoprecipitation experiments. Zach Goldberg for technical assistance with setting up the FLIC assay. We thank Susan Parkhurst for advice on the NES sequences and Prashant Raghavan for discussions. **Funding:** This work is possible due to grants awarded to AR from NIDDK (DK101605), NIGMS (GM124593), and New Development funds from Fred Hutch. Genomic reagents from the DGRC which is funded by NIH grant 2P40OD010949 were used in this study. Stocks obtained from the Bloomington Drosophila Stock Center (NIH P40OD018537) and Transgenic RNAi Resource project (NIGMS R01 GM084947 and NIGMS P41 GM132087) were used in this study. **Author contributions:** Conceptualization: AR; Investigation: MEP, CES, AEB, AR; Formal analysis, Data Curation: MEP, CES, AB, AR; Visualization: MEP, CS,

bioRxiv preprint doi: https://doi.org/10.1101/2021.01.29.428913; this version posted April 2, 2021. The copyright holder for this preprint (which was not certified by peer review) is the author/funder, who has granted bioRxiv a license to display the preprint in perpetuity. It is made available under aCC-BY 4.0 International license.

AR, AB, TH; Supervision: AR; Writing- original draft: AR; Writing- review and editing: AEB; Funding acquisition: AR. **Competing interests:** Authors declare no competing interests.

RESOURCE AVAILABILITY

Lead Contact

Requests for further information, reagents, and resources should be directed to and will be fulfilled by the corresponding author Akhila Rajan (akhila@fredhutch.org).

Materials Availability

Drosophila strains generated in this study are available from the corresponding author, Akhila Rajan (akhila@fredhutch.org).

Data and Code Availability

The datasets generated in this study are available from the corresponding author, Akhila Rajan (akhila@fredhutch.org).

EXPERIMENTAL MODEL AND SUBJECT DETAILS

Experimental Animals

Drosophila melanogaster

Only males were used in experiments at an age of 5-10 days post-eclosion. Flies were cultured in a humidified incubator at 25°C with a 12h light-12h dark cycle, and were fed a standard lab diet, containing per liter: 15 g yeast, 8.6 g soy flour, 63 g corn flour, 5g agar, 5g malt, 74 mL corn syrup. For acute starvation, adult male flies which were 7 days old, were subjected to 4-hour starvation on 0% sucrose in agar at 29°C. For survival curves, flies were subjected to 1% sucrose in agar diet. For RNAi experiments, flies were raised at 18°C until 7 days post-eclosion, after which they were shifted to 29°C for 7 days.

The following fly strains used in this study were from our previous work [3, 4] and/or obtained from other investigators or the Bloomington *Drosophila* stock center (BDSC): upd2Δ3-62 (upd2Δ; [39]), *Lpp-Gal4* [95], *Ppl-Gal4, TubGal80ts* [96], Atg8-Trojan-Gal4 ([97]; BDSC 77836). The control UAS strain used for over-expression experiments is UAS-Luciferase [4]. RNAi lines from the TRiP facility at Harvard Medical School (http://www.flyrnai.org/TRiP-HOME.html) include: Luciferase-RNAi (JF01801), Atg8-RNAi #1 (JF02895, BDSC 28989), Atg8-RNAi #2 (HMS01328, BDSC 34340).

bioRxiv preprint doi: https://doi.org/10.1101/2021.01.29.428913; this version posted April 2, 2021. The copyright holder for this preprint (which was not certified by peer review) is the author/funder, who has granted bioRxiv a license to display the preprint in perpetuity. It is made available under aCC-BY 4.0 International license.

The following UAS lines were generated for this study: *UAS-Upd2::mCherry*, *UAS-Upd2-AIM-::mCherry, UAS-GFP::Atg8; UAS-GFP::Atg8-PE-*. To control for expression levels, all transgenes pertaining to the same gene were inserted at the same att site. Either attp40 or attP2.

For RNAi experiments, in Fig.6B, flies were generated with the following genotype: *Upd2-crGFP; Ppl-Gal4, TubGal80^{ts}* and *Upd2-crGFP; Lpp-Gal4*. This strain was used for crossing to Atg8-RNAi lines for analysis. The parents of this cross (F0 generation) were maintained at 18c for both the strains, F1s were allowed to eclose at 18c. A week after eclosion, the F1s were moved to 29c for 5-7 days prior to dissection and staining.

Ability of UAS-GFP::Atg8 and UAS-GFP::Atg8-PE- to rescue loss of Atg8 function was tested by introducing Atg8 variant transgenes into the Atg8-Trojan-Gal4 line [97], in which insertion of the Trojan-Gal4 into the Atg8 locus generates a lethal allele.

Cell lines

Drosophila S2R+ cells were used for all cell culture related experiments. This cell line was chosen because previous studies have validated their applicability to study autophagy [69, 98, 99] and protein secretion [100]. The cells were maintained in Schneider's medium (GIBCO), 10% heat-inactivated FBS (SIGMA) and 5% Pen-Strep (GIBCO) at 25˚C. For starvation, cells were incubated in Schneider's Insect Medium without Amino Acids (United States Biological, Cat# S0100-01.10) for indicated amount of time.

METHOD DETAILS:

Cloning and Transgenic Flies

All cloning was done using the Gateway® Technology. For Atg8, entry cDNA was PCR amplified from *Atg8* cDNA (clone LD05816 DGRC-Gold collection) and cloned into pENTR-D/TOPO using BP reaction (Gateway® BP Clonase II enzyme mix, Cat#11789-020, Invitrogen). pENTR-GRASP was previously described [3]. For *Drosophila* Upd2 variants, pENTR-Upd2 [3] made for previous work in our lab was used. For site directed mutagenesis of putative AIM sites, pENTR-Upd2 was mutagenized to convert tryptophan and leucine encoding codons to alanine. For addition of a canonical NES+, sequence corresponding to amino acids LQELLELLRL [64] was inserted after the start codon in either pENTER-Upd2-WT or p-ENTR-Upd2-AIM-. For site directed mutagenesis of Atg8 lipidation site, pENTR-Atg8 was mutagenized to convert its penultimate Glycine to Alanine. All mutagenesis was done using the Q5® Site-Directed

bioRxiv preprint doi: https://doi.org/10.1101/2021.01.29.428913; this version posted April 2, 2021. The copyright holder for this preprint (which was not certified by peer review) is the author/funder, who has granted bioRxiv a license to display the preprint in perpetuity. It is made available under aCC-BY 4.0 International license.

Mutagenesis Kit from NEB (Cat # E0554S). The sequence of oligonucleotides used for this mutagenesis reaction are available on request. The entry vectors were then moved using LR clonase reaction (Gateway® LR Clonase® II Enzyme mix, Cat#11791-020, Invitrogen) into destination vectors compatible with fly transformation, or cell culture and with the appropriate C-terminal tags for Upd2 and N-terminal tags for Atg8. Transgenic flies were generated by Bestgene.

Generation of C-terminal tagged Upd2 CRISPR lines

GFP or HA-tagged Upd2 CRISPR lines were developed in collaboration with WellGenetics Inc. using modified methods of Kondo and Ueda [101]. In brief, for HA lines, following gRNA sequence were cloned into U6 promoter plasmids: TCCAATGAGTCTTGAGCCCT[CGG]/GCCGAGGGCTCAAGACTCAT[TGG]. Cassette 3xHA RFP containing 3xHA and 3xP3 RFP and two homology arms were cloned into pUC57 Kan as donor template for repair. upd2/CG5988 targeting gRNAs and hs-Cas9 were supplied in DNA plasmids, together with donor plasmid for microinjection into embryos of control strain w^{1118}. F1 flies carrying selection marker of 3xP3 RFP were further validated by genomic PCR and sequencing. CRISPR generates a break in upd2/CG5988 and is replaced by cassette 3xHA RFP. 3XP3 RFP, which facilitates the genetic screening, was flipped out by Cre recombinase. RE loxP RE (46 bp) remains after excision between Stop codon and 3'UTR. For GFP lines, gRNA sequence TCCAATGAGTCTTGAGCCCT[CGG] was used.

Tissue culture:

The day before transfection, cells were passaged to 60-80% confluency. For transfections related to ELISA experiments, cells were cultured in 96 well plates, and for co-immunoprecipitations in 6-well plates. For ELISAs, cells were transfected with 20ng/well of *pAc-upd2::GFP* [39] or indicated Upd2 variants, 10ng/well *pACRenilla::Luciferase*, and 150ng of dsRNA/well for knockdown experiments. For coimmunoprecipitations, cells were transfected with 200ng/well of indicated plasmid.

For imaging experiments, cells were seeded on poly-D-lysine coated 8-well chambered culture slides for fixed imaging (MatTek CCS-8) and glass bottom FluoroDish (World Precision I: FD3510-100) for live imaging. The T7 flasks which were 100% confluent were used for seeing cells at 1:10 dilution at 400µl per well of the 8-well chamber dish or 1:20 dilution at 200µl per

bioRxiv preprint doi: https://doi.org/10.1101/2021.01.29.428913; this version posted April 2, 2021. The copyright holder for this preprint (which was not certified by peer review) is the author/funder, who has granted bioRxiv a license to display the preprint in perpetuity. It is made available under aCC-BY 4.0 International license.

dish for FluoroDish. Transfections were done with plasmids indicated. For 8-chamber slides 100ng/well and for FluoroDish 10ng/dish of each plasmid was transfected.

Transfections were done using the Effectene kit (Cat# 301427**,** QIAGEN) as per the manufacturer's instructions.

dsRNA production and cell treatments:

Amplicons for dsRNAs were designed using the SnapDragon dsRNA design tool (https://www.flyrnai.org/snapdragon) and in vitro transcribed (IVT) using MEGAscript® T7 Transcription Kit (Cat# AMB1334-5, ThermoFisher). IVT reactions were carried out as per the protocol provided by the DRSC (available at: http://www.flyrnai.org/DRSC-PRS.html). Sequence of amplicons used in this study can be found in the table below. *LacZ* dsRNA was used as controls. All dsRNA knockdown experiments were carried out using 2 independent dsRNAs per gene. We found that this produced a knockdown efficiency of >85% (based on qPCR analysis) in S2R+ cells. S2R+ transfected with dsRNAs were incubated for 4 days to allow for gene knockdown. On the 4th day, media was changed, and the ELISA assay was carried out on the 5th day. Note the data is represented as percent change in Upd2/Leptin secretion normalized to transfection efficiency with 0% change indicating baseline level of secretion. See ELISA assay procedure below.

Primer sequences used for dsRNA production.

Target	Primer name	Sequence 5' → 3'
LacZ	LacZ F1	TTTCCAGTTCCGTTTATCCG
	LacZ R1	CAAAAATCCATTTCGCTGGT
Atg8a	Atg8a F1	GTACAGGGAGCCCATGGTA
	Atg8a R1	CGAGAAGGCTCCCAAGG
Atg8a	Atg8a F2	GCCCTGCGTATCAGATCAAT
	Atg8a R2	CGATGAGAATGTTTACGGCA
Emb	Emb F1	AGAGGTACATGCAACTGCCC
	Emb R1	GTTGGAACGAGACACCCACT

bioRxiv preprint doi: https://doi.org/10.1101/2021.01.29.428913; this version posted April 2, 2021. The copyright holder for this preprint (which was not certified by peer review) is the author/funder, who has granted bioRxiv a license to display the preprint in perpetuity. It is made available under aCC-BY 4.0 International license.

Emb	Emb F2	ACTAAGGCCAAGCACCTGAA
	Emb R2	TGAACCATCGTGTCCTTGAA

Treatment of cells with drugs:

For drug treatment experiments, the media was replaced with media containing the drug on day 3 after transfection with *upd2::GFP*. 4 hours later the conditioned media was used for ELISA or imaging. Drugs used in this study include Torin1 (Cat# ab218606, Abcam) and Importazole (Cat# CAYM-21491-5, Neta Scientific). Stocks solutions of the drugs were made in DMSO as per the manufacturer's instructions and used at a working concentration indicated in the Fig.legends of each experiment. DMSO treated replicates were used as controls. Note that for ELISAs, the data is represented as percent change in Upd2 secretion normalized to transfection efficiency, with 0% change indicating baseline level of secretion.

ELISA assays:

GFP sandwich ELISA assay was used for detecting Upd2::GFP. On day 1, 96 well medium bind polystyrene plates (Cat#CLS3368-100EA, Sigma) were incubated overnight at 4C with coating antibody (Cat# ACT-CM-GFPTRAP, Allele Biotechnology) diluted in 0.01M pH8.0 bicarbonate buffer at a concentration of 1µg/ml. On day 2, plates were washed briefly with PBS, blocked for 30 minutes with 1% BSA block in PBS, and coated with conditioned media and incubated overnight at 4C. Recombinant GFP protein (Cat# MB-0752, Vector labs), diluted in S2R+ cell growth media (64ng/µl to 4 ng/µl), was used in every ELISA plate as positive control to ensure linearity of GFP readings. On day 3, the plates were washed with PBS+0.05% Tween-20 (PBS-T), blocked with 1% BSA in PBS for 30 minutes at RT. GFP detection antibody (Cat# 600-401-215, Rockland) was added to the diluted 1:1000 in 0.1% BSA in PBS-T. Plates were washed with PBS-T and incubated with secondary HRP conjugated anti Rabbit secondary antibodies (Cat# ab136636, Abcam) diluted at 1:5000 in 1% BSA block. Plates were washed in PBS-T with a final wash in PBS. For detection, each well was incubated 100µl 1-step Ultra-TMB ELISA substrate (Cat# 34028, Pierce), which was previously equilibrated to RT, for approximately 5-15 minutes until detectable blue colorimetric reaction occurred. Reaction was stopped with 2N sulphuric acid and absorbance was measured at 450nm. The TMB readings were normalized to transfection efficiency as measured from Renilla Luciferase assays (see below).

bioRxiv preprint doi: https://doi.org/10.1101/2021.01.29.428913; this version posted April 2, 2021. The copyright holder for this preprint (which was not certified by peer review) is the author/funder, who has granted bioRxiv a license to display the preprint in perpetuity. It is made available under aCC-BY 4.0 International license.

Renilla Luciferase assay:

On day 2 of the ELISA assay, after the conditioned medium was transferred for use in ELISA assays, cells were re-suspended in 50µl of PBS, and incubated with 50µl/well Renilla-Glo® Luciferase reagent (Cat# E2710, Promega) for 10 minutes and read using a multiwell luminometer.

Immunoprecipitation and Western blots:

For Immunoprecipitation (IP) from S2R+ cells, protein for each condition was prepared by lysing 1 well of a 6-well dish, 4 days after transfection. 2mg/ml was used per IP experiments performed with camelid antibodies GFP-Trap Magnetic Agarose (Cat# gtma-20, Chromotek); RFP-Trap Magnetic Agarose (Cat# rtma-20, Chromotek); Myc-Trap magnetic agarose (Cat# ytma-20; ChromoTek); as per the manufacturer's protocol.

Western blots were performed detailed in our prior publication [3]. Antibodies used include Chicken anti-GFP (Cat#ab13970, abcam) 1:2000 in TBS-0.05% tween-20 (TBS-T), Rabbit- anti Upd2 [custom antibody AR4398 generated at YenZym Inc., to Upd2 peptide 318-334: RRPRRNSAERRHLAAIHC; antibody was verified by its recognition of GFP tagged Upd2 pull down in western blots] 1:2000 in TBS-T 0.05%; Rabbit- anti-GRASP (Cat# ab 30315, Abcam) 1:10000 in 1% BSA TBS-T 0.1%; Rabbit-anti RFP (Cat# 600-401-379, Rockland) 1:2500 in0.1% TBS-T ; Mouse-anti-Myc (abcam 9E10) 1:5000 in 0.1% TBS-T; mouse-Anti-Tubulin 1:5000 in 0.05% TBS-T(Cat# T5168, Sigma). The secondary antibodies used were HRP conjugated Goat antibodies directed to appropriate species and the western blot was developed using Amersham ECL kit Start or Prime (Cat# RPN3243 or # RPN2232 , GE life sciences).

Tissue preparation for fixed immunostaining:

For fat body preparation, incisions, using dissection scissors (Cat# 500086, World Precision Instruments Inc), were made to release the ventral abdomen from the rest of the fly body. Flies used for dissection were adult males, 7-10 days old. Dissections were done in Ringer's medium (1.8 mM $CaCl_2$, 2mM Kcl, 128mM Nacl, 4mM $MgCl_2$. 35mM sucrose, 5mM HEPES). Tissue was fixed in 4% formaldehyde for 20 minutes and rinsed with PBS. For immunohistochemistry the fixed fat tissue was permeabilized in PBS+ 1.0% Triton-X-100 for 3X washes 5 minutes, subsequently washed with PBS+0.3% Triton-X-100 (Fat wash). Blocked for 30 minutes at room temperature (RT) with gentle agitation in Fat wash+ 5% Normal donkey serum (Block). Primary

bioRxiv preprint doi: https://doi.org/10.1101/2021.01.29.428913; this version posted April 2, 2021. The copyright holder for this preprint (which was not certified by peer review) is the author/funder, who has granted bioRxiv a license to display the preprint in perpetuity. It is made available under aCC-BY 4.0 International license.

antibodies, diluted in block, included Rabbit-anti-RFP (1:500, Rockland, #600-401-379); Chicken-anti-GFP (1:2000, Abcam, #ab13970); Mouse-anti-HA (1:200; Abcam, #ab18181); mouse-anti-Lamin (1:100; ADL67.10 DSHB); Rabbit-anti-GABARAP (Atg8) (1:500; Abcam, # ab109364); and incubated overnight at 4C. Washed multiple times following day in fat wash at (RT) incubated with appropriate secondary antibody (from Jackson Immunoresearch) in block for 2-4 hours at RT. Washed 3X-5X for 5-15 minutes in fat wash, mounted in SlowFade Gold antifade reagent with DAPI (Cat# S36938, Invitrogen).

Dissection and immunostaining of adult brains was performed as previously described (Rajan et al., 2017). In brief: Adult brains were dissected in PBS, then fixed overnight in cold 0.8% Para-formaldehyde (PFA) in PBS at 4°C. The following day, tissues were washed multiple times in 0.5% BSA and 0.5% Triton X-100 in PBS (PAT). Tissues were pre-blocked in PAT+ 5% NDS for 2 hours at RT, then incubated overnight with primary antibodies chicken anti-Dilp2 (1:250; [12]) and rabbit anti-Dilp5 (1:500; [12]) at 4°C. The following day, tissues were washed multiple times in PAT, re-blocked for 30 minutes in PAT+ 5% NDS, then incubated in secondary antibody in block (final concentration of 1:500, from Jackson Immunoresearch) for 4 hours at RT. Samples were washed 3X-5X, 15 minutes per wash, in PAT, then mounted on slides with one layer of Scotch Tape spacers in Slowfade gold antifade.

Images were captured with Zeiss LSM 800 confocal system and analyzed with Zeiss ZenLite or ImageJ.

Cell staining and live imaging:

For immunohistochemistry, cells were fixed for 20 minutes in 4% formaldehyde, washed in PBS for 5 quick changes, permeabilized in PBS+ 0.1% Triton-X-100 for 3X washes 5 minutes, subsequently washed with PBS+0.1% Triton-X-100 (Cell wash). Blocked for 30 minutes at room temperature (RT) with gentle agitation in Cell wash+ 5% Normal donkey serum (Block). Primary antibodies--Rabbit-anti-RFP (1:500, Rockland, #600-401-379); Chicken-anti-GFP (1:2000, Abcam, #ab13970); mouse-anti-Lamin (1:100; ADL67.10 DSHB)--were diluted in block incubated overnight at 4°C. Washed multiple times following day in fat wash at (RT) incubated with appropriate secondary antibody (from Jackson Immunoresearch) in block for 2-4 hours at RT. Washed 3X-5X for 5-15 minutes in cell wash, mounted with SlowFade Gold antifade reagent with DAPI (Cat# S36938, Invitrogen). Images were captured with Zeiss LSM 800 or Zeiss Elyra 7 with Lattice SIM confocal systems, and analyzed with Zeiss ZenLite or ImageJ [102].

bioRxiv preprint doi: https://doi.org/10.1101/2021.01.29.428913; this version posted April 2, 2021. The copyright holder for this preprint (which was not certified by peer review) is the author/funder, who has granted bioRxiv a license to display the preprint in perpetuity. It is made available under aCC-BY 4.0 International license.

For live imaging (Extended Data Fig.1), cells were incubated with ProLong Live antifade reagent (Cat# P36974, ThermoFisher), LysoView™ -633 (Cat# 70058, Biotium), and NucBlue (Cat# R37605, Thermofisher) as per manufacturer's instructions, prior to imaging in appropriate media condition. Images were captured in time lapse mode on Zeiss LSM800 in the sequential scan setting.

FLIC assay:

The Fly Liquid Interaction Counter (FLIC) assay was performed as detailed previously in Ro et al., [82] and provides a measure of continuous feeding behavior and motivation. The Digital feeding monitor (DFM) used to run FLIC assays was purchased from Sable System Inc. and instructions provided in the manufacturers model were followed for set up. Flies used in experiment were aged 7 days and un-sedated flies were loaded into each DFM chamber using mouth pipettes as sedation affected the assay. For recording basal feeding behavior well-fed flies (6 replicates per condition) on standard lab-food were recorded in individual chambers for their interactions and feeding events for 3 hours. For recording hunger-driven feeding behavior flies were fasted for 16hrs at 29^{o}C on 0% sucrose, 1% agar and then loaded into chambers. The feeding behaviors of fed versus fasted (6-replicates per condition) loaded onto the same DFM were used for analysis. Analysis was performed using R. Macros used for R analysis were kindly provided by Scott Pletcher via a github open source code and are available upon request.

qPCR analysis:

qPCR Total RNA prepared from 12-15 fat bodies per genotype, using the Direct-zol RNA miniprep kit (Zymo Research, cat#R2071). cDNA prepared with iScript cDNA Synthesis (Bio-Rad, cat#1708891), and 1mg RNA applied per reaction. qPCR performed with iQ SYBR Green Supermix (Bio-Rad, cat#1708882). rpl13A and robl employed to normalize RNA levels. Relative quantification of mRNA levels calculated with comparative CT method. Primers used in this study can be found in the table below.

Primer sequences used in this study.

Target	Primer name	Sequence 5' → 3'

bioRxiv preprint doi: https://doi.org/10.1101/2021.01.29.428913; this version posted April 2, 2021. The copyright holder for this preprint (which was not certified by peer review) is the author/funder, who has granted bioRxiv a license to display the preprint in perpetuity. It is made available under aCC-BY 4.0 International license.

rpl13A	rpl13A F1	AGCTGAACCTCTCGGGACAC
	rpl13A R1	TGCCTCGGACTGCCTTGTAG
Robl	robl F1	AGCGGTAGTGTCTGCCGTGT
	robl R1	CCAGCGTGGATTTGACCGGA
SREBP	SREBP F1	AGTCGCCGCTTCTCGTCTA
	SREBP R1	TGTATGGTGGCTGTTGGTTGG
FASN1	FASN1 F1	TGACCAACAGTTCTTCGGTGT
	FASN1 R1	GCGTCAATAATAGCTTCATGGGT
Apolpp	Apolpp F1	TTGGAATCCTAGCTTCTGTGCT
	Apolpp R1	AGTCATAGTAGTTGCCGGGTAT
Mtp	Mtp F1	GTTTGGAGTGGAGATGAGGACC
	Mtp R1	GGGTATCCGGGTAATTGAGCG
InR	InR F1	AAGCGTGGGAAAATTAAGATGGA
	InR R1	GGCTGTCAACTGCTTCTACTG
Bmm	Bmm F1	TTTTGCAGTTGAACCACGCC
	Bmm R1	CACGGGGTCCATATAAGCGG
4ebp	4ebp F1	GAAGGGAGTACGCGGAGTG
	4ebp R1	TCCCCATTGAGCCAAACTC

Triglyceride Measurements:

TAG assays were carried out as previously described (Rajan et al., 2017). In brief: Flies were homogenized in PBST (PBS + 0.1% Triton X-100) using 1mm zirconium beads (Cat#ZROB10, Next Advance) in a Bullet Blender® Tissue homogenizer (Model BBX24, Next Advance). Samples were heated to 70^{o}C for 10 minutes, then centrifuged at 14,000 rpm (in refrigerated

bioRxiv preprint doi: https://doi.org/10.1101/2021.01.29.428913; this version posted April 2, 2021. The copyright holder for this preprint (which was not certified by peer review) is the author/funder, who has granted bioRxiv a license to display the preprint in perpetuity. It is made available under aCC-BY 4.0 International license.

tabletop centrifuge). 10.0 µl of the supernatant was applied to determine level of TAG in sample, using the following reagents obtained from Sigma: Free glycerol (cat # F6428-40ML), Triglyceride reagent (cat# T2449-10ML), and Glycerol standard (cat# G7793-5ML).Three adult males employed per biological replicate. Note: For adult TAG assays, the most consistent results, with lowest standard deviations, were obtained with 10 day old males. TAG readings from whole fly lysate (n=4 replicates of 3 flies each) were normalized to number of flies per experiment. Normalized ratio from the control served as baseline, and data is represented as fold change of experimental genotypes with respect to the control.

Starvation Survival Assays:

Survival curves were done using flies that were harvested in a 24hour time frame and aged for 7 days. 10 males per vial were flipped onto 1% sucrose and 1% agar starvation food. The number of dead flies were recorded each day until every fly had died. Flies were kept in a 25^{o}C incubator with a 12 hour light dark cycle for the entirety of the experiment. Survival analysis was performed using the Survival Curve module of GraphPad Prism. A Mantel-cox test was the test used to determine statistical significance. Greater than 90 flies were used per genotype per curve.

Image quantification and statistical analysis:

Excel or GraphPad Prism 7 software was used for data quantification and generation of graphs. Quantification of nuclear localization in S2R+ was performed as follows: Using Zeiss ZenLite, each cell exhibiting transfected expression was visualized in LUT Rainbow2 mode. Whole Cell fraction (WC) was generated from subsets of z-stacks covering an entire cell (using DIC as reference). For nuclear fraction (Nuc), DAPI or Lamin was used as a reference to generate a subset of the WC z-stack representing the nucleus. Maximum Intensity Projections (MIPs) were generated for both WC and Nuc stacks, and ImageJ was used to measure the Integrated Density of protein being quantified in compartment. The fraction of protein in the nucleus was determined as Nuc Integrated Density/WC Integrated Density. An average was calculated and 2-tailed t-test performed between control and experimental groups. Error bars represent %SD (Standard Deviation). For quantification of nuclear localization in fat tissue, Integrated Density was measured in ImageJ from MIPs of z-stacks covering the fat cell nucleus (based on DAPI or

bioRxiv preprint doi: https://doi.org/10.1101/2021.01.29.428913; this version posted April 2, 2021. The copyright holder for this preprint (which was not certified by peer review) is the author/funder, who has granted bioRxiv a license to display the preprint in perpetuity. It is made available under aCC-BY 4.0 International license.

Lamin staining). An average was calculated and 2-tailed t-test performed between control and experimental groups.

To measure intensity of Dilp expression, ImageJ-calculated mean gray values were averaged from maximum intensity projections (MIPs) of a similar number of confocal stacks. Average values were normalized to control and t-test performed between control and experimental groups. Error bars represent %SD (Standard Deviation). Manders coefficients were calculated using the JACoP plugin for ImageJ on z-stacks through entire cells. Significance was calculated by 2-tailed t-test. Error bars represent %SD (Standard Deviation). For ELISA assays, the ELISA signal readings are normalized to transfection efficiency; the data is represented as percent fold change from control used as baseline. Specifically, the ratio of TMB readings to Renilla Luciferase readings is calculated. This ratio from the control is used as a baseline and the data is represented as percent fold change of experimental conditions with respect to the control. Statistical significance quantified by 2-tailed t-test on 6 biological replicates per condition. Error bars represent %SD (Standard Deviation). For TAG analysis, statistical significance was quantified by 2-tailed t-test on 3-6 biological replicates per condition. Error bars indicate %SD (Standard Deviation). For qPCR analysis, normalized levels of gene expression were analyzed using one-way ANOVA. Error bars represent standard error of the mean (SEM).

We determined that our data-points were normally distributed, based on two measures: i) A GraphPad outlier test did not identify any outliers in our data; and ii) the majority of our data points for a particular condition were relatively similar to one other, with only a small standard error of mean or standard deviation.

References

1. Ahima, R.S. *et al.* Role of leptin in the neuroendocrine response to fasting. *Nature* **382**, 250-252 (1996).

2. Ahima, R.S. & Flier, J.S. Leptin. *Annu Rev Physiol* **62**, 413-437 (2000).

3. Rajan, A*., Housden, B.E., Wirtz-Peitz, F., Holderbaum, L. & Perrimon, N. A Mechanism Coupling Systemic Energy Sensing to Adipokine Secretion. *Dev Cell* **43**, 83-98 e86 (2017).* lead author and corresponding author.

4. Rajan, A. & Perrimon, N. *Drosophila* Cytokine Unpaired 2 Regulates Physiological Homeostasis by Remotely Controlling Insulin Secretion. *Cell* **151**, 123-137 (2012).

5. Ichimura, Y. *et al.* A ubiquitin-like system mediates protein lipidation. *Nature* **408**, 488-492 (2000).

6. Flier, J.S. & Maratos-Flier, E. Leptin's Physiologic Role: Does the Emperor of Energy Balance Have No Clothes? *Cell Metab* **26**, 24-26 (2017).

7. Munzberg, H. Leptin-signaling pathways and leptin resistance. *Forum Nutr* **63**, 123-132 (2010).

bioRxiv preprint doi: https://doi.org/10.1101/2021.01.29.428913; this version posted April 2, 2021. The copyright holder for this preprint (which was not certified by peer review) is the author/funder, who has granted bioRxiv a license to display the preprint in perpetuity. It is made available under aCC-BY 4.0 International license.

8. Kolaczynski, J.W., Ohannesian, J.P., Considine, R.V., Marco, C.C. & Caro, J.F. Response of leptin to short-term and prolonged overfeeding in humans. *J Clin Endocrinol Metab* **81**, 4162-4165 (1996).

9. Kolaczynski, J.W. *et al.* Responses of leptin to short-term fasting and refeeding in humans: a link with ketogenesis but not ketones themselves. *Diabetes* **45**, 1511-1515 (1996).

10. Hickey, M.S. *et al.* Leptin is related to body fat content in male distance runners. *Am J Physiol* **271**, E938-940 (1996).

11. Farooqi, I.S. & O'Rahilly, S. Leptin: a pivotal regulator of human energy homeostasis. *The American journal of clinical nutrition* **89**, 980S-984S (2009).

12. Brent, A.E. & Rajan, A. Insulin and Leptin/Upd2 Exert Opposing Influences on Synapse Number in Fat-Sensing Neurons. *Cell Metab* **32**, 786-800 e787 (2020).

13. Flier, J.S. Starvation in the Midst of Plenty: Reflections on the History and Biology of Insulin and Leptin. *Endocr Rev* **40**, 1-16 (2019).

14. Knight, Z.A., Hannan, K.S., Greenberg, M.L. & Friedman, J.M. Hyperleptinemia is required for the development of leptin resistance. *PloS one* **5**, e11376 (2010).

15. Baggio, L.L. & Drucker, D.J. Glucagon-like peptide-1 receptor co-agonists for treating metabolic disease. *Mol Metab*, 101090 (2020).

16. Kaushik, S., Singh, R. & Cuervo, A.M. Autophagic pathways and metabolic stress. *Diabetes Obes Metab* **12 Suppl 2**, 4-14 (2010).

17. Singh, R. & Cuervo, A.M. Autophagy in the cellular energetic balance. *Cell Metab* **13**, 495-504 (2011).

18. Singh, R. *et al.* Autophagy regulates lipid metabolism. *Nature* **458**, 1131-1135 (2009).

19. Singh, R. *et al.* Autophagy regulates adipose mass and differentiation in mice. *J Clin Invest* **119**, 3329-3339 (2009).

20. Shpilka, T., Weidberg, H., Pietrokovski, S. & Elazar, Z. Atg8: an autophagy-related ubiquitin-like protein family. *Genome Biol* **12**, 226 (2011).

21. Kirisako, T. *et al.* Formation process of autophagosome is traced with Apg8/Aut7p in yeast. *J Cell Biol* **147**, 435-446 (1999).

22. Drake, K.R., Kang, M. & Kenworthy, A.K. Nucleocytoplasmic distribution and dynamics of the autophagosome marker EGFP-LC3. *PLoS One* **5**, e9806 (2010).

23. Huang, R. *et al.* Deacetylation of nuclear LC3 drives autophagy initiation under starvation. *Mol Cell* **57**, 456-466 (2015).

24. Nakatogawa, H., Ichimura, Y. & Ohsumi, Y. Atg8, a ubiquitin-like protein required for autophagosome formation, mediates membrane tethering and hemifusion. *Cell* **130**, 165-178 (2007).

25. Galluzzi, L. & Green, D.R. Autophagy-Independent Functions of the Autophagy Machinery. *Cell* **177**, 1682-1699 (2019).

26. Cunha, L.D. *et al.* LC3-Associated Phagocytosis in Myeloid Cells Promotes Tumor Immune Tolerance. *Cell* **175**, 429-441 e416 (2018).

27. Reggiori, F. *et al.* Coronaviruses Hijack the LC3-I-positive EDEMosomes, ER-derived vesicles exporting short-lived ERAD regulators, for replication. *Cell Host Microbe* **7**, 500-508 (2010).

bioRxiv preprint doi: https://doi.org/10.1101/2021.01.29.428913; this version posted April 2, 2021. The copyright holder for this preprint (which was not certified by peer review) is the author/funder, who has granted bioRxiv a license to display the preprint in perpetuity. It is made available under aCC-BY 4.0 International license.

28. Leidal, A.M. & Debnath, J. LC3-dependent extracellular vesicle loading and secretion (LDELS). *Autophagy* **16**, 1162-1163 (2020).

29. Heckmann, B.L. *et al.* LC3-Associated Endocytosis Facilitates beta-Amyloid Clearance and Mitigates Neurodegeneration in Murine Alzheimer's Disease. *Cell* **178**, 536-551 e514 (2019).

30. Dou, Z. *et al.* Autophagy mediates degradation of nuclear lamina. *Nature* **527**, 105-109 (2015).

31. Neufeld, T.P. & Baehrecke, E.H. Eating on the fly: function and regulation of autophagy during cell growth, survival and death in Drosophila. *Autophagy* **4**, 557-562 (2008).

32. Zirin, J. & Perrimon, N. Drosophila as a model system to study autophagy. *Semin Immunopathol* **32**, 363-372 (2010).

33. Tennessen, J.M., Barry, W.E., Cox, J. & Thummel, C.S. Methods for studying metabolism in Drosophila. *Methods* **68**, 105-115 (2014).

34. Baker, K.D. & Thummel, C.S. Diabetic larvae and obese flies-emerging studies of metabolism in Drosophila. *Cell Metab* **6**, 257-266 (2007).

35. King-Jones, K. & Thummel, C.S. Nuclear receptors--a perspective from Drosophila. *Nat Rev Genet* **6**, 311-323 (2005).

36. Teleman, A.A., Ratzenbock, I. & Oldham, S. Drosophila: a model for understanding obesity and diabetic complications. *Exp Clin Endocrinol Diabetes* **120**, 184-185 (2012).

37. Musselman, L.P. & Kuhnlein, R.P. Drosophila as a model to study obesity and metabolic disease. *J Exp Biol* **221** (2018).

38. Welte, M.A. & Gould, A.P. Lipid droplet functions beyond energy storage. *Biochim Biophys Acta Mol Cell Biol Lipids* **1862**, 1260-1272 (2017).

39. Hombria, J.C., Brown, S., Hader, S. & Zeidler, M.P. Characterisation of Upd2, a Drosophila JAK/STAT pathway ligand. *Dev Biol* **288**, 420-433 (2005).

40. Goldstein, I. & Hager, G.L. Transcriptional and Chromatin Regulation during Fasting - The Genomic Era. *Trends Endocrinol Metab* **26**, 699-710 (2015).

41. Shu, X.E., Swanda, R.V. & Qian, S.B. Nutrient Control of mRNA Translation. *Annu Rev Nutr* **40**, 51-75 (2020).

42. Mortimore, G.E., Hutson, N.J. & Surmacz, C.A. Quantitative correlation between proteolysis and macro- and microautophagy in mouse hepatocytes during starvation and refeeding. *Proc Natl Acad Sci U S A* **80**, 2179-2183 (1983).

43. Zhang, M., Kenny, S., Ge, L., Xu, K. & Schekman, R. Translocation of interleukin-1beta into a vesicle intermediate in autophagy-mediated secretion. *Elife* **4** (2015).

44. Dupont, N. *et al.* Autophagy-based unconventional secretory pathway for extracellular delivery of IL-1beta. *Embo J* **30**, 4701-4711 (2011).

45. Leidal, A.M. *et al.* The LC3-conjugation machinery specifies the loading of RNA-binding proteins into extracellular vesicles. *Nat Cell Biol* **22**, 187-199 (2020).

46. Bruns, C., McCaffery, J.M., Curwin, A.J., Duran, J.M. & Malhotra, V. Biogenesis of a novel compartment for autophagosome-mediated unconventional protein secretion. *J Cell Biol* **195**, 979-992 (2011).

bioRxiv preprint doi: https://doi.org/10.1101/2021.01.29.428913; this version posted April 2, 2021. The copyright holder for this preprint (which was not certified by peer review) is the author/funder, who has granted bioRxiv a license to display the preprint in perpetuity. It is made available under aCC-BY 4.0 International license.

47. Duran, J.M., Anjard, C., Stefan, C., Loomis, W.F. & Malhotra, V. Unconventional secretion of Acb1 is mediated by autophagosomes. *J Cell Biol* **188**, 527-536 (2010).

48. Cadwell, K. & Debnath, J. Beyond self-eating: The control of nonautophagic functions and signaling pathways by autophagy-related proteins. *J Cell Biol* **217**, 813-822 (2018).

49. Mizushima, N. & Yoshimori, T. How to interpret LC3 immunoblotting. *Autophagy* **3**, 542-545 (2007).

50. Noda, N.N., Ohsumi, Y. & Inagaki, F. Atg8-family interacting motif crucial for selective autophagy. *FEBS letters* **584**, 1379-1385 (2010).

51. Noda, N.N. *et al.* Structural basis of target recognition by Atg8/LC3 during selective autophagy. *Genes Cells* **13**, 1211-1218 (2008).

52. Davis, L.I. The nuclear pore complex. *Annu Rev Biochem* **64**, 865-896 (1995).

53. Kaffman, A. & O'Shea, E.K. Regulation of nuclear localization: a key to a door. *Annu Rev Cell Dev Biol* **15**, 291-339 (1999).

54. Gorlich, D. & Kutay, U. Transport between the cell nucleus and the cytoplasm. *Annu Rev Cell Dev Biol* **15**, 607-660 (1999).

55. Mattaj, I.W. & Englmeier, L. Nucleocytoplasmic transport: the soluble phase. *Annu Rev Biochem* **67**, 265-306 (1998).

56. Kosugi, S. *et al.* Design of peptide inhibitors for the importin alpha/beta nuclear import pathway by activity-based profiling. *Chem Biol* **15**, 940-949 (2008).

57. Kosugi, S., Hasebe, M., Tomita, M. & Yanagawa, H. Systematic identification of cell cycle-dependent yeast nucleocytoplasmic shuttling proteins by prediction of composite motifs. *Proc Natl Acad Sci U S A* **106**, 10171-10176 (2009).

58. Kosugi, S. *et al.* Six classes of nuclear localization signals specific to different binding grooves of importin alpha. *J Biol Chem* **284**, 478-485 (2009).

59. la Cour, T. *et al.* Analysis and prediction of leucine-rich nuclear export signals. *Protein Eng Des Sel* **17**, 527-536 (2004).

60. Fukuda, M. *et al.* CRM1 is responsible for intracellular transport mediated by the nuclear export signal. *Nature* **390**, 308-311 (1997).

61. Fasken, M.B., Saunders, R., Rosenberg, M. & Brighty, D.W. A leptomycin B-sensitive homologue of human CRM1 promotes nuclear export of nuclear export sequence-containing proteins in Drosophila cells. *J Biol Chem* **275**, 1878-1886 (2000).

62. Mason, D.A. & Goldfarb, D.S. The nuclear transport machinery as a regulator of Drosophila development. *Semin Cell Dev Biol* **20**, 582-589 (2009).

63. Soderholm, J.F. *et al.* Importazole, a small molecule inhibitor of the transport receptor importin-beta. *ACS Chem Biol* **6**, 700-708 (2011).

64. Verboon, J.M. *et al.* Wash interacts with lamin and affects global nuclear organization. *Curr Biol* **25**, 804-810 (2015).

65. Thoreen, C.C. *et al.* An ATP-competitive mammalian target of rapamycin inhibitor reveals rapamycin-resistant functions of mTORC1. *J Biol Chem* **284**, 8023-8032 (2009).

bioRxiv preprint doi: https://doi.org/10.1101/2021.01.29.428913; this version posted April 2, 2021. The copyright holder for this preprint (which was not certified by peer review) is the author/funder, who has granted bioRxiv a license to display the preprint in perpetuity. It is made available under aCC-BY 4.0 International license.

66. Galluzzi, L., Bravo-San Pedro, J.M., Levine, B., Green, D.R. & Kroemer, G. Pharmacological modulation of autophagy: therapeutic potential and persisting obstacles. *Nat Rev Drug Discov* **16**, 487-511 (2017).

67. Stolz, A. *et al.* Fluorescence-based ATG8 sensors monitor localization and function of LC3/GABARAP proteins. *EMBO J* **36**, 549-564 (2017).

68. Huang, R. & Liu, W. Identifying an essential role of nuclear LC3 for autophagy. *Autophagy* **11**, 852-853 (2015).

69. Lin, L. *et al.* Complement-Related Regulates Autophagy in Neighboring Cells. *Cell* **170**, 158-171 e158 (2017).

70. Geminard, C., Rulifson, E.J. & Leopold, P. Remote control of insulin secretion by fat cells in Drosophila. *Cell Metab* **10**, 199-207 (2009).

71. Nassel, D.R., Kubrak, O.I., Liu, Y., Luo, J. & Lushchak, O.V. Factors that regulate insulin producing cells and their output in Drosophila. *Front Physiol* **4**, 252 (2013).

72. DiAngelo, J.R. & Birnbaum, M.J. Regulation of fat cell mass by insulin in Drosophila melanogaster. *Mol Cell Biol* **29**, 6341-6352 (2009).

73. Palm, W. *et al.* Lipoproteins in Drosophila melanogaster--assembly, function, and influence on tissue lipid composition. *PLoS Genet* **8**, e1002828 (2012).

74. Kunte, A.S., Matthews, K.A. & Rawson, R.B. Fatty acid auxotrophy in Drosophila larvae lacking SREBP. *Cell Metab* **3**, 439-448 (2006).

75. Porstmann, T. *et al.* SREBP activity is regulated by mTORC1 and contributes to Akt-dependent cell growth. *Cell Metab* **8**, 224-236 (2008).

76. Garrido, D. *et al.* Fatty acid synthase cooperates with glyoxalase 1 to protect against sugar toxicity. *PLoS Genet* **11**, e1004995 (2015).

77. Parvy, J.P. *et al.* Drosophila melanogaster Acetyl-CoA-carboxylase sustains a fatty acid-dependent remote signal to waterproof the respiratory system. *PLoS Genet* **8**, e1002925 (2012).

78. Eijkelenboom, A. & Burgering, B.M. FOXOs: signalling integrators for homeostasis maintenance. *Nat Rev Mol Cell Biol* **14**, 83-97 (2013).

79. Gronke, S. *et al.* Brummer lipase is an evolutionary conserved fat storage regulator in Drosophila. *Cell Metab* **1**, 323-330 (2005).

80. Teleman, A.A., Chen, Y.W. & Cohen, S.M. 4E-BP functions as a metabolic brake used under stress conditions but not during normal growth. *Genes & development* **19**, 1844-1848 (2005).

81. Deshpande, S.A. *et al.* Quantifying Drosophila food intake: comparative analysis of current methodology. *Nat Methods* **11**, 535-540 (2014).

82. Ro, J., Harvanek, Z.M. & Pletcher, S.D. FLIC: high-throughput, continuous analysis of feeding behaviors in Drosophila. *PLoS One* **9**, e101107 (2014).

83. Jacomin, A.-C. *et al.* Regulation of Expression of Autophagy Genes by Atg8a-Interacting Partners Sequoia, YL-1, and Sir2 in Drosophila. *Cell Rep* **31**, 107695-107695 (2020).

84. Jura, N., Scotto-Lavino, E., Sobczyk, A. & Bar-Sagi, D. Differential modification of Ras proteins by ubiquitination. *Molecular Cell* **21**, 679-687 (2006).

bioRxiv preprint doi: https://doi.org/10.1101/2021.01.29.428913; this version posted April 2, 2021. The copyright holder for this preprint (which was not certified by peer review) is the author/funder, who has granted bioRxiv a license to display the preprint in perpetuity. It is made available under aCC-BY 4.0 International license.

85. Xu, L., Lubkov, V., Taylor, L.J. & Bar-Sagi, D. Feedback regulation of Ras signaling by Rabex-5-mediated ubiquitination. *Curr Biol* **20**, 1372-1377 (2010).

86. Nakagawa, T. & Nakayama, K. Protein monoubiquitylation: targets and diverse functions. *Genes Cells* **20**, 543-562 (2015).

87. Melchior, F. SUMO--nonclassical ubiquitin. *Annu Rev Cell Dev Biol* **16**, 591-626 (2000).

88. Mahajan, R., Delphin, C., Guan, T., Gerace, L. & Melchior, F. A small ubiquitin-related polypeptide involved in targeting RanGAP1 to nuclear pore complex protein RanBP2. *Cell* **88**, 97-107 (1997).

89. Speese, S.D. *et al.* Nuclear envelope budding enables large ribonucleoprotein particle export during synaptic Wnt signaling. *Cell* **149**, 832-846 (2012).

90. Kutay, U., Bischoff, F.R., Kostka, S., Kraft, R. & Gorlich, D. Export of importin alpha from the nucleus is mediated by a specific nuclear transport factor. *Cell* **90**, 1061-1071 (1997).

91. Rapoport, T.A., Jungnickel, B. & Kutay, U. Protein transport across the eukaryotic endoplasmic reticulum and bacterial inner membranes. *Annu Rev Biochem* **65**, 271-303 (1996).

92. Puddington, L., Lively, M.O. & Lyles, D.S. Role of the nuclear envelope in synthesis, processing, and transport of membrane glycoproteins. *J Biol Chem* **260**, 5641-5647 (1985).

93. Leidal, A.M. & Debnath, J. Unraveling the mechanisms that specify molecules for secretion in extracellular vesicles. *Methods* **177**, 15-26 (2020).

94. Geng, J. & Klionsky, D.J. The Atg8 and Atg12 ubiquitin-like conjugation systems in macroautophagy. 'Protein modifications: beyond the usual suspects' review series. *EMBO Rep* **9**, 859-864 (2008).

95. Brankatschk, M. & Eaton, S. Lipoprotein particles cross the blood-brain barrier in Drosophila. *J Neurosci* **30**, 10441-10447 (2010).

96. Zinke, I., Kirchner, C., Chao, L.C., Tetzlaff, M.T. & Pankratz, M.J. Suppression of food intake and growth by amino acids in Drosophila: the role of pumpless, a fat body expressed gene with homology to vertebrate glycine cleavage system. *Development* **126**, 5275-5284 (1999).

97. Lee, P.T. *et al.* A gene-specific T2A-GAL4 library for Drosophila. *Elife* **7** (2018).

98. Anding, A.L. & Baehrecke, E.H. Vps15 is required for stress induced and developmentally triggered autophagy and salivary gland protein secretion in Drosophila. *Cell Death Differ* **22**, 457-464 (2015).

99. Shravage, B.V., Hill, J.H., Powers, C.M., Wu, L. & Baehrecke, E.H. Atg6 is required for multiple vesicle trafficking pathways and hematopoiesis in Drosophila. *Development* **140**, 1321-1329 (2013).

100. Bard, F. *et al.* Functional genomics reveals genes involved in protein secretion and Golgi organization. *Nature* **439**, 604-607 (2006).

101. Kondo, S. & Ueda, R. Highly improved gene targeting by germline-specific Cas9 expression in Drosophila. *Genetics* **195**, 715-721 (2013).

102. Schindelin, J. *et al.* Fiji: an open-source platform for biological-image analysis. *Nat Methods* **9**, 676-682 (2012).

Figure 1

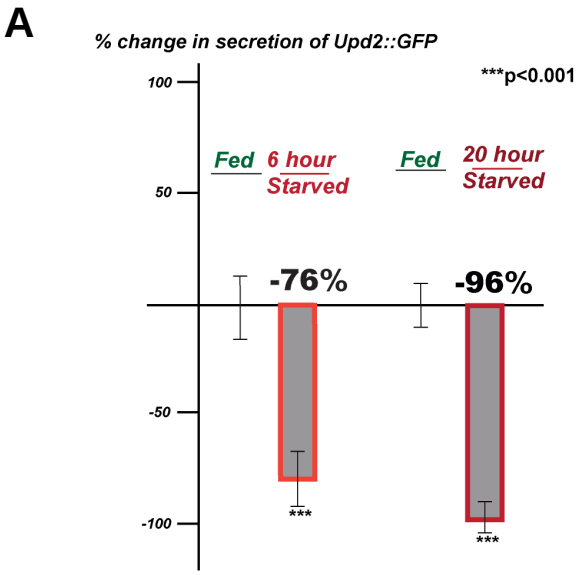
A
% change in secretion of Upd2::GFP
***p<0.001
100
50
-50
-100
Fed
6 hour Starved
Fed
20 hour Starved
-76%
-96%
***
***

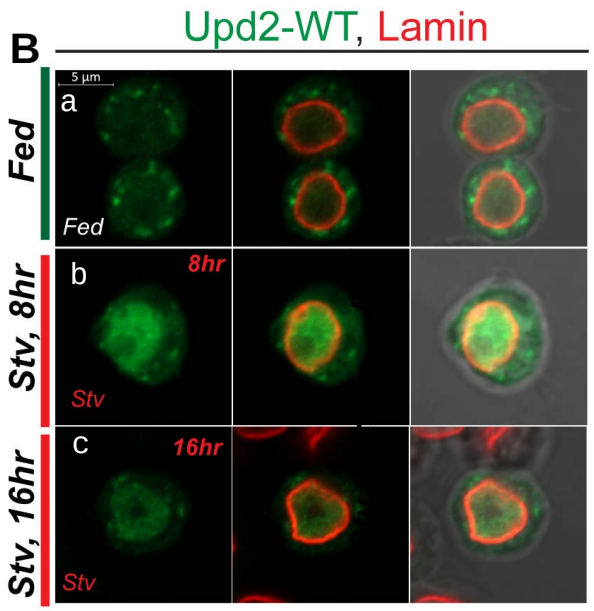
B
Upd2-WT, Lamin
5 µm
Fed
Stv, 8hr
Stv, 16hr
a
Fed
b
8hr
Stv
c
16hr
Stv

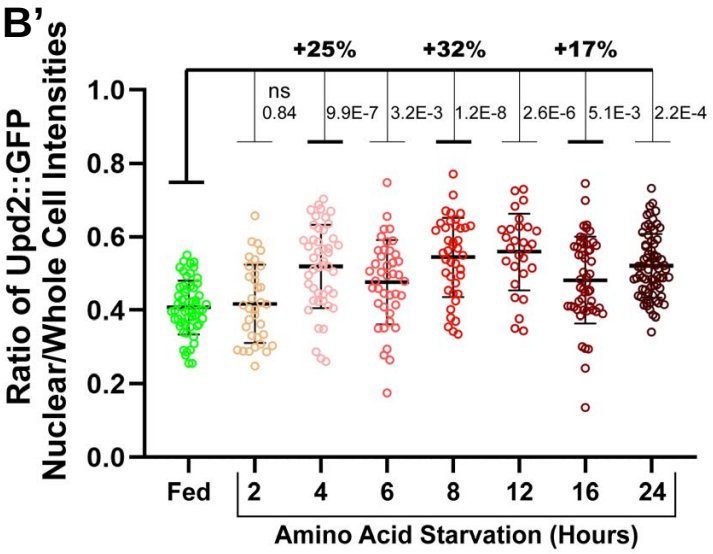
B'
Ratio of Upd2::GFP Nuclear/Whole Cell Intensities
+25%
+32%
+17%
ns
0.84
9.9E-7
3.2E-3
1.2E-8
2.6E-6
5.1E-3
2.2E-4
1.0
0.8
0.6
0.4
0.2
0.0
Fed
2
4
6
8
12
16
24
Amino Acid Starvation (Hours)

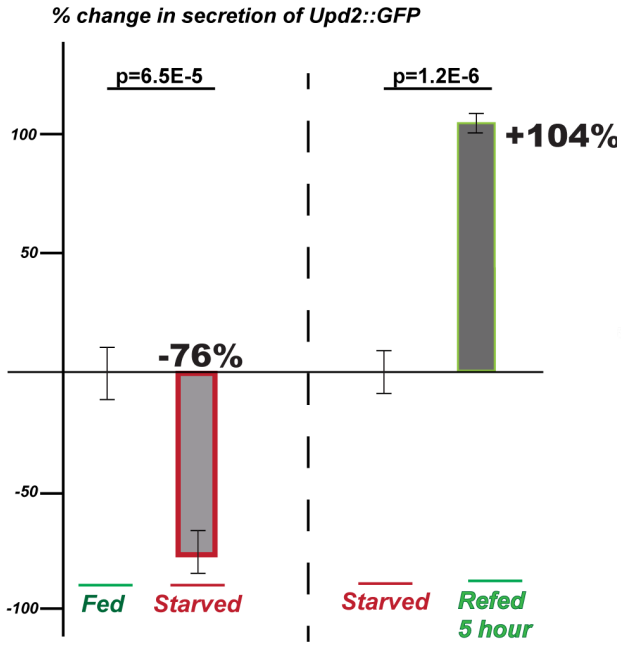
C
% change in secretion of Upd2::GFP
p=6.5E-5
p=1.2E-6
100
50
-50
-100
-76%
+104%
Fed
Starved
Starved
Refed 5 hour

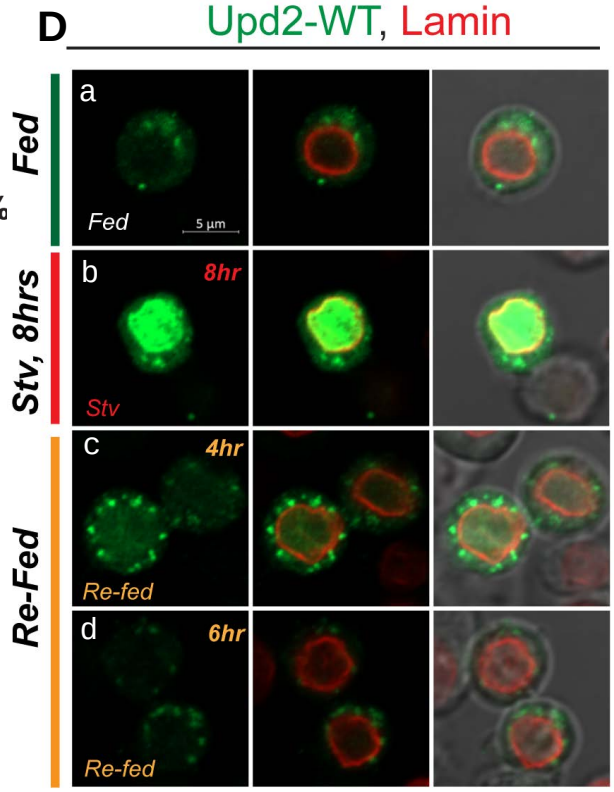
D
Upd2-WT, Lamin
Fed
Stv, 8hrs
Re-Fed
a
Fed
5 µm
b
8hr
Stv
c
4hr
Re-fed
d
6hr
Re-fed

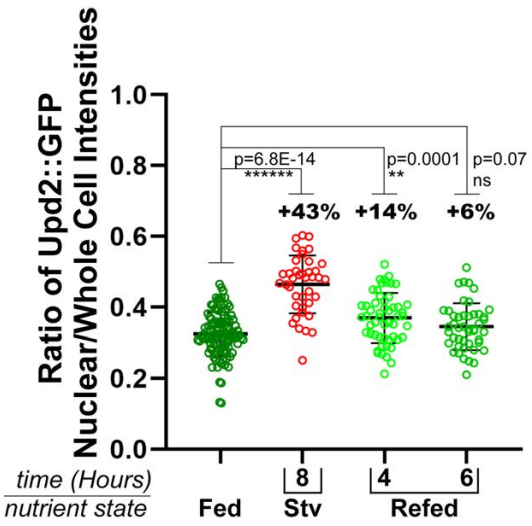
D'
Ratio of Upd2::GFP Nuclear/Whole Cell Intensities
p=6.8E-14
******
p=0.0001
**
p=0.07
ns
+43%
+14%
+6%
1.0
0.8
0.6
0.4
0.2
0.0
time (Hours)
nutrient state
Fed
8
Stv
4
6
Refed

bioRxiv preprint doi: https://doi.org/10.1101/2021.01.29.428913; this version posted April 2, 2021. The copyright holder for this preprint (which was not certified by peer review) is the author/funder, who has granted bioRxiv a license to display the preprint in perpetuity. It is made available under aCC-BY 4.0 International license.

Figure 1: Fasting induces Upd2 nuclear accumulation.

(A) Effect of amino acid starvation on Upd2's release into media. Normalized percent fold change in secreted GFP signal detected by GFP sandwich ELISA assay performed on conditioned media of S2R+ cells transiently transfected with *Upd2-WT::GFP*. Cells were incubated either with complete media (control) or Amino-Acid (AA) free media for the indicated times. Statistical significance is quantified by unpaired two-tailed t-test on 6 biological replicates per condition.

(B) Effect of amino acid starvation on Upd2's nuclear accumulation. Confocal micrographs of single optical-slices of *Drosophila* S2R+ cells transiently transfected with *Upd2-WT::GFP* (green) stained with Lamin (red). **(a)** In fed state, Upd2-WT::GFP is localizes to cytosolic puncta and its nuclear localization is not obvious. **(b, c)** In AA starved cells (8 and 16 hours post-starvation) Upd2 is visible both as cytosolic puncta and shows nuclear enrichment. Scale bar is 5um and right most panel shows DIC image merge. In **B'**, the ratio of Upd2::GFP nuclear/whole cell intensity is plotted. Each dot represents a cell, 50-100 cells were counted per time point. Statistical significance is quantified by unpaired two-tailed t-test.

(C) Effect of re-feeding on Upd2's release into media. Normalized percent fold change in secreted GFP signal detected by GFP sandwich ELISA assay performed on conditioned media of S2R+ cells transiently transfected with *Upd2-WT::GFP*. Cells were incubated either with complete media (control) or Amino-Acid (AA) free media for the indicated times. Statistical significance is quantified by unpaired two-tailed t-test on 6 biological replicates per condition.

(D) Effect of re-feeding on Upd2's nuclear accumulation. Confocal micrographs of single optical-slices of *Drosophila* S2R+ cells transiently transfected with *Upd2-WT::GFP* (green) stained with Lamin (red). **(a)** In fed state, *Upd2-WT::GFP* is localized to cytosolic puncta and nuclear localization is not obvious. **(b)** In AA starved cells (8 hours post-starvation) Upd2 is visible both as cytosolic puncta and shows nuclear enrichment. (**c, d**) On re-feeding with complete media, by 4 hours **(c)** Upd2's starvation-induced accumulation begins to reduce and is restored to pre-fasting levels by 6 hours **(d)**. Scale bar is 5um and right most panel shows DIC image merge. In **D',** the ratio of Upd2::GFP nuclear/whole cell intensity is plotted. Each dot represents a cell, 50-100 cells were counted per time point. Statistical significance is quantified by unpaired two-tailed t-test.

Figure 2

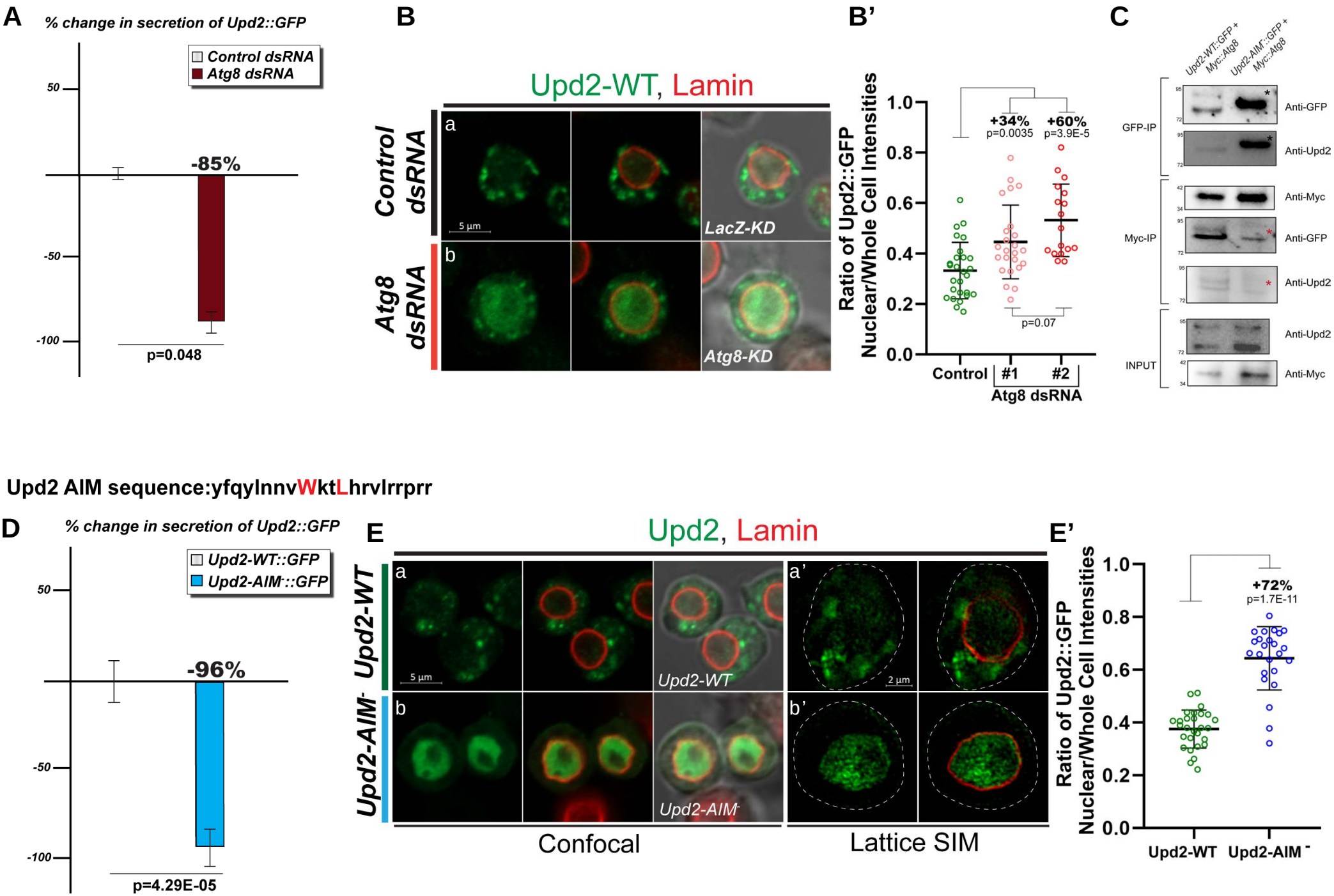
A
% change in secretion of Upd2::GFP
Control dsRNA
Atg8 dsRNA
50
-50
-100
-85%
p=0.048
B
Upd2-WT, Lamin
Control dsRNA
Atg8 dsRNA
a
b
5 µm
LacZ-KD
Atg8-KD
B'
Ratio of Upd2::GFP Nuclear/Whole Cell Intensities
1.0
0.8
0.6
0.4
0.2
0.0
+34%
p=0.0035
+60%
p=3.9E-5
p=0.07
Control
#1
#2
Atg8 dsRNA
C
Upd2-WT::GFP+ Myc::Atg8
Upd2-AIM-::GFP+ Myc::Atg8
GFP-IP
Myc-IP
INPUT
Anti-GFP
Anti-Upd2
Anti-Myc
Anti-GFP
Anti-Upd2
Anti-Upd2
Anti-Myc
Upd2 AIM sequence:yfqylnnvWktLhrvlrrprr
D
% change in secretion of Upd2::GFP
Upd2-WT::GFP
Upd2-AIM-::GFP
50
-50
-100
-96%
p=4.29E-05
E
Upd2, Lamin
Upd2-WT
Upd2-AIM-
a
b
a'
b'
5 µm
2 µm
Upd2-WT
Upd2-AIM-
Confocal
Lattice SIM
E'
Ratio of Upd2::GFP Nuclear/Whole Cell Intensities
1.0
0.8
0.6
0.4
0.2
0.0
+72%
p=1.7E-11
Upd2-WT
Upd2-AIM-

bioRxiv preprint doi: https://doi.org/10.1101/2021.01.29.428913; this version posted April 2, 2021. The copyright holder for this preprint (which was not certified by peer review) is the author/funder, who has granted bioRxiv a license to display the preprint in perpetuity. It is made available under aCC-BY 4.0 International license.

Figure 2: Atg8 regulates nucleocytoplasmic localization of Upd2.

(A) Effect of Atg8 knockdown on Upd2's release into media in fed cells. Normalized percent fold change in secreted GFP signal detected by GFP sandwich ELISA assay performed on conditioned media of S2R+ cells transiently transfected with *Upd2-WT::GFP* dsRNA for control (*LacZ*) or *Atg8* dsRNA. ELISA for *Upd2-WT::GFP* was performed after 5 days of knockdown, and the amount of Upd2-WT::GFP in a 24-hour period (Day 5) was assessed. Statistical significance is quantified by unpaired two-tailed t-test on 6 biological replicates per condition.

(B) Effect of Atg8 knockdown on Upd2's nuclear accumulation. Confocal micrographs of single optical-slices of *Drosophila* S2R+ cells transiently co-transfected with *Upd2-WT::GFP* (green) stained with Lamin (red). **(a)** In fed state, in cells co-transfected with *LacZ-dsRNA* (control) Upd2-WT::GFP is localized to cytosolic puncta and nuclear localization is not obvious. **(b)** In fed state, Atg8-KD (*Atg8 dsRNA*) significant increase in Upd2-WT::GFP nuclear accumulation is observed. Scale bar is 5um and right most panel shows DIC image merge. In **B'**, the ratio of Upd2::GFP nuclear/whole cell intensity is plotted. Each dot represents a cell, 20-40 cells were counted per dsRNA condition. Two independent *Atg8-dsRNAs* were used. Statistical significance is quantified by unpaired two-tailed t-test.

(C) Upd2-WT coimmunoprecipitates with Atg8 and this interaction relies on Upd2's AIM. GFP- and Myc-IPs were prepared from S2R+ cells transiently transfected with the indicated cDNAs. GFP, Myc IPs and 2% of the input were analyzed by immunoblotting for the indicated proteins. Note Upd2-AIM$^-$ always runs slightly higher than Upd2 (see asterisk) and is always more abundant in the lysate as the Upd2-AIM$^-$ is not secreted (see D below), but Upd2-AIM- it is not readily detectable in the Myc-IPs (see red asterisk), despite being more abundant in input. Atg8-Myc is always more abundant in Upd2-AIM- input than in Upd2 WT input, despite loading same amount of protein in input.

(D) Effect of point mutations to Upd2's AIM (*Upd2-AIM$^-$::GFP*) on its release into media in fed cells. Normalized percent fold change in secreted GFP signal detected by GFP sandwich ELISA assay performed on conditioned media of S2R+ cells transiently transfected with *Upd2-WT::GFP* or *Upd2-AIM$^-$::GFP*. Mutated residues in Upd2's AIM is shown in red. Statistical significance is quantified by unpaired two-tailed t-test on 6 biological replicates per condition.

(E) Effect of point mutations to Upd2's AIM (*Upd2-AIM$^-$::GFP*) on its nuclear accumulation. Confocal micrographs (**a, b**) and Lattice SIM images (**a', b'**) of single optical-slices of *Drosophila* S2R+ cells transiently co-transfected with (a, a') *Upd2-WT::GFP* or (b, b') *Upd2-AIM$^-$::GFP* (green) stained with Lamin (red) in a fed state. Scale bars are 5um for a, b and 2um for a', b'; right most panel of a, b shows DIC image merge. In **E'**, the ratio of Upd2::GFP nuclear/whole cell intensity is plotted. Each dot represents a cell, 20-40 cells were counted per dsRNA condition. Statistical significance is quantified by unpaired two-tailed t-test.

Figure 3

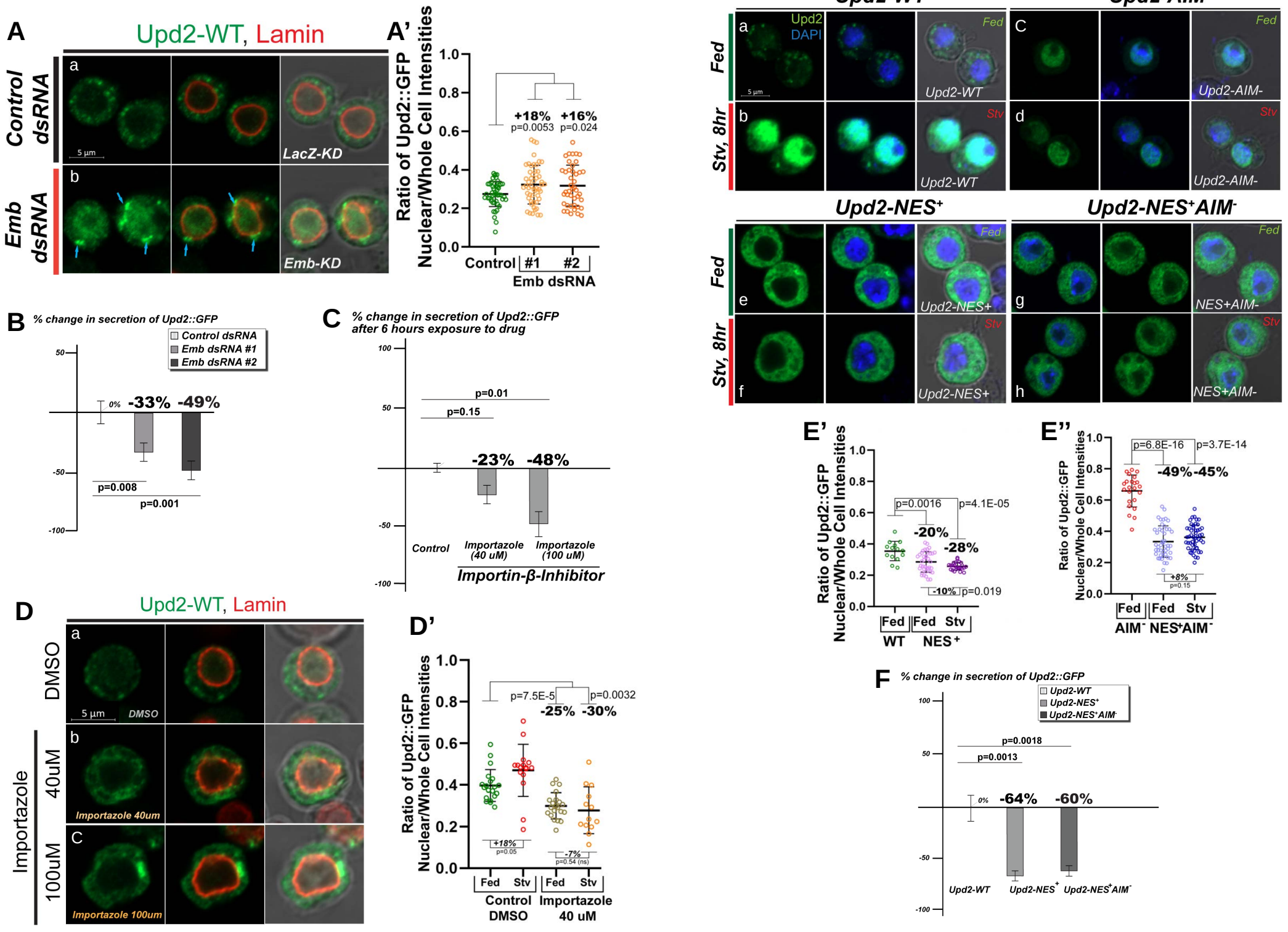
A
Upd2-WT, Lamin
Control dsRNA
Emb dsRNA
a
b
5 µm
LacZ-KD
Emb-KD
A'
Ratio of Upd2::GFP Nuclear/Whole Cell Intensities
+18%
p=0.0053
+16%
p=0.024
Control
#1
#2
Emb dsRNA
B
% change in secretion of Upd2::GFP
Control dsRNA
Emb dsRNA #1
Emb dsRNA #2
0%
-33%
-49%
p=0.008
p=0.001
C
% change in secretion of Upd2::GFP after 6 hours exposure to drug
p=0.01
p=0.15
-23%
-48%
Control
Importazole (40 uM)
Importazole (100 uM)
Importin-β-Inhibitor
D
Upd2-WT, Lamin
DMSO
Importazole
40uM
100uM
5 µm
DMSO
Importazole 40um
Importazole 100um
D'
Ratio of Upd2::GFP Nuclear/Whole Cell Intensities
p=7.5E-5
p=0.0032
-25%
-30%
+18%
p=0.05
-7%
p=0.54 (ns)
Fed
Stv
Control DMSO
Importazole 40 uM
E
Upd2-WT
Upd2-AIM-
Upd2-NES+
Upd2-NES+AIM-
Fed
Stv, 8hr
Upd2
DAPI
Upd2-WT
Upd2-AIM-
Upd2-NES+
NES+AIM-
E'
Ratio of Upd2::GFP Nuclear/Whole Cell Intensities
p=0.0016
p=4.1E-05
-20%
-28%
-10%
p=0.019
Fed
Fed
Stv
WT
NES+
E''
Ratio of Upd2::GFP Nuclear/Whole Cell Intensities
p=6.8E-16
p=3.7E-14
-49%
-45%
+8%
p=0.15
Fed
Fed
Stv
AIM-
NES+AIM-
F
% change in secretion of Upd2::GFP
Upd2-WT
Upd2-NES+
Upd2-NES+AIM-
p=0.0018
p=0.0013
0%
-64%
-60%
Upd2-WT
Upd2-NES+
Upd2-NES+AIM-

bioRxiv preprint doi: https://doi.org/10.1101/2021.01.29.428913; this version posted April 2, 2021. The copyright holder for this preprint (which was not certified by peer review) is the author/funder, who has granted bioRxiv a license to display the preprint in perpetuity. It is made available under aCC-BY 4.0 International license.

Figure 3: Nucleocytoplasmic shuttling of Upd2 is required for its subsequent release.

(A, A') Effect of Embargoed (Emb)/ CRM1 exportin knockdown on Upd2's nuclear accumulation. Confocal micrographs of single optical-slices of *Drosophila* S2R+ cells transiently co-transfected with *Upd2-WT::GFP* (green) stained with Lamin (red). In fed state, cells are co-transfected with **(a)** *LacZ-dsRNA* (control), or **(b)** Emb-KD (*Emb dsRNA*). *Emb-KD* increases Upd2-WT::GFP nuclear accumulation and shows an enrichment of Upd2-WT::GFP at the interface of nuclear lamina and cytoplasm (see blue arrows). Scale bar is 5um and right most panel shows DIC image merge. In **A'**, the ratio of Upd2::GFP nuclear/whole cell intensity is plotted. Each dot represents a cell, 50-80 cells were counted per dsRNA condition. Two independent *Emb-dsRNAs* (#1 and #2) were used. Statistical significance is quantified by unpaired two-tailed t-test.

(B) Effect of Embargoed (Emb) exportin knockdown on Upd2's release in fed cells. Normalized percent fold change in secreted GFP signal detected by GFP sandwich ELISA assay performed on conditioned media of S2R+ cells transiently transfected with *Upd2-WT::GFP* dsRNA for control (*LacZ*) or two independent *Emb* dsRNAs. ELISA for *Upd2-WT::GFP* was performed after 5 days of knockdown, and the amount of Upd2-WT::GFP in a 24-hour period (Day 5) was assessed. Statistical significance is quantified by unpaired two-tailed t-test on 6 biological replicates per condition.

(C) Effect of pharmacological inhibition of nuclear import on Upd2's release in fed cells. Quantification of relative normalized secreted GFP signal detected by GFP sandwich ELISA assay performed on conditioned media of S2R+ cells transfected with *Upd2-WT::GFP* and treated with drug Importazole, an Importin-beta inhibitor for 6 hours. Percent change in Upd2::GFP secretion relative to DMSO is depicted. Error bars represent %SD. Statistical significance quantified by t-test on 6 biological replicates per condition.

(D) Effect of pharmacological inhibition of nuclear import on Upd2's nuclear localization in fed cells. Confocal micrographs of single optical-slices of *Drosophila* S2R+ cells transiently transfected with *Upd2-WT::GFP* (green) stained with Lamin (red) and treated with DMSO **(a)** or indicated concentrations of importazole **(b, c)**. Scale bar is 5um and right most panel shows DIC image merge. In **D'**, the ratio of Upd2::GFP nuclear/whole cell intensity is plotted. Note that in starved state Upd2 nuclear accumulation does not significantly increase when treated with 40uM Importazole. Each dot represents a cell, 15-30 cells were counted per condition. Statistical significance is quantified by unpaired two-tailed t-test.

(E) Effect of nuclear export signal (NES) addition to Upd2-WT or -AIM$^-$ (*Upd2-NES$^+$::GFP or Upd2-NES$^+$AIM$^-$::GFP*) on its nuclear accumulation. Confocal micrographs of single optical-slices of *Drosophila* S2R+ cells transiently co-transfected with *Upd2::GFP* variants (a, b) WT; (c, d) AIM$^-$; (e, f) NES$^+$; (g, h) NES$^+$AIM$^-$ Upd2::GFP (green) stained with DAPI (blue) in a fed state (a ,c, e, g) or AA-starved for 8 hours (b, d, f, h). Scale bars are 5um right most panel shows DIC image merge. In **E' and E''**, the ratio of Upd2::GFP

bioRxiv preprint doi: https://doi.org/10.1101/2021.01.29.428913; this version posted April 2, 2021. The copyright holder for this preprint (which was not certified by peer review) is the author/funder, who has granted bioRxiv a license to display the preprint in perpetuity. It is made available under aCC-BY 4.0 International license.

nuclear/whole cell intensity is plotted. Note that an NES^{+} addition prevents Upd2 from accumulating in the nucleus even on starvation (E') and is epistatic to the AIM^{-} mutation (E''). Each dot represents a cell, 15-80 cells were counted per condition. Statistical significance is quantified by unpaired two-tailed t-test.

(F) Effect of nuclear export signal (NES) addition to Upd2-WT or AIM^{-} (*Upd2-NES^{+}::GFP or Upd2-$NES^{+}AIM^{-}$::GFP*) on its release. Normalized percent fold change in secreted GFP signal detected by GFP sandwich ELISA assay performed on conditioned media of S2R+ cells transiently transfected with *Upd2::GFP* variants: WT; NES^{+}; $NES^{+}AIM^{-}$ the amount of Upd2-WT::GFP in a 24-hour period was assessed. Statistical significance is quantified by unpaired two-tailed t-test on 6 biological replicates per condition.

Figure 4

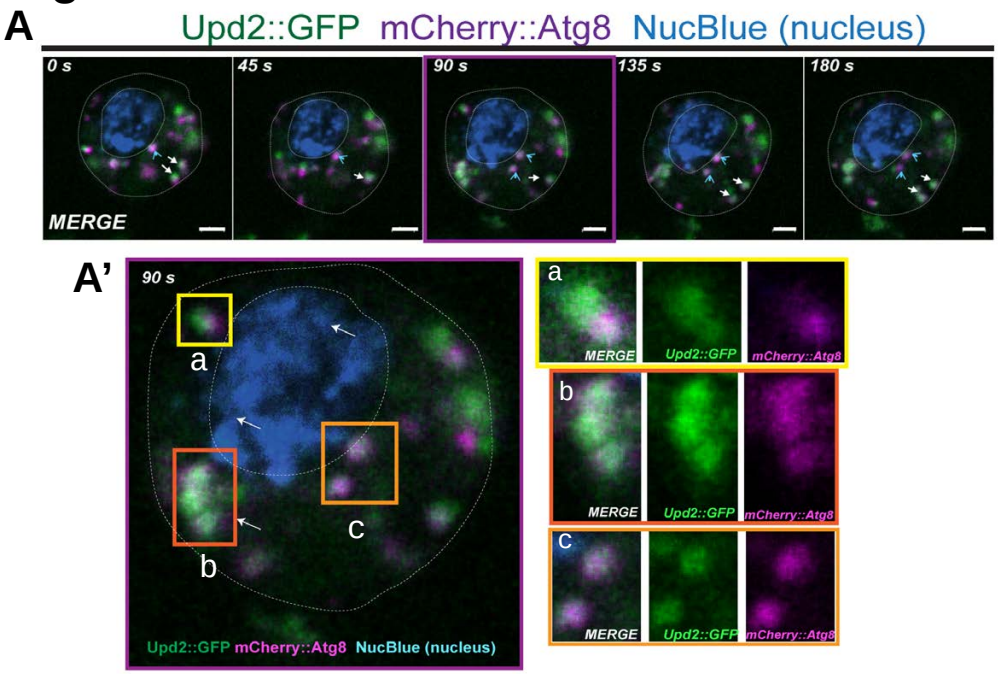
A
Upd2::GFP mCherry::Atg8 NucBlue (nucleus)
0 s
45 s
90 s
135 s
180 s
MERGE
A'
90 s
a
b
c
Upd2::GFP mCherry::Atg8 NucBlue (nucleus)
MERGE
Upd2::GFP
mCherry::Atg8

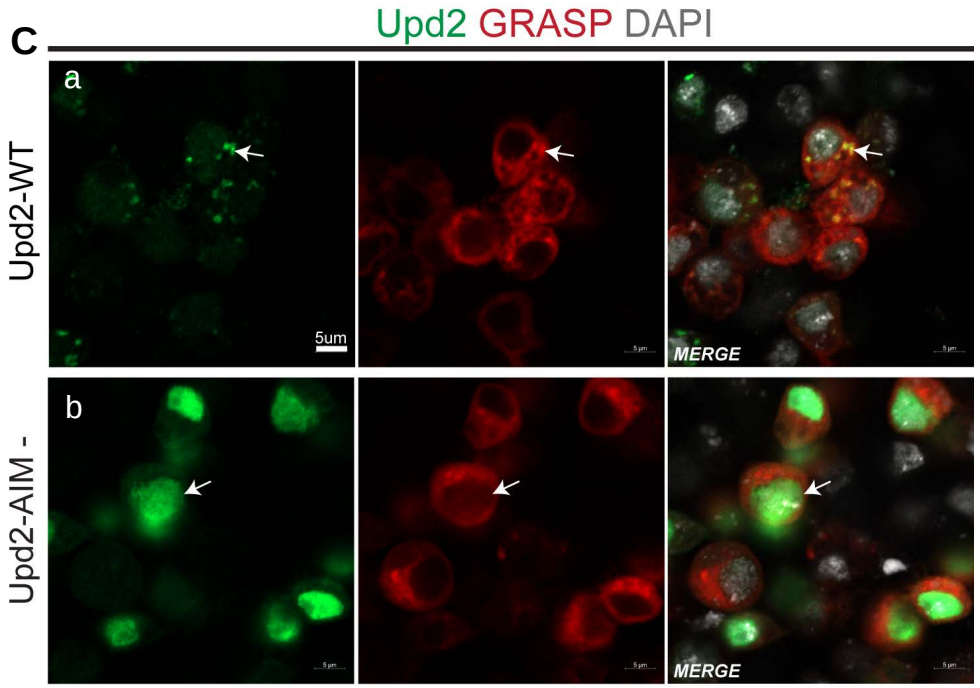
C
Upd2 GRASP DAPI
Upd2-WT
Upd2-AIM -
a
b
5um
MERGE

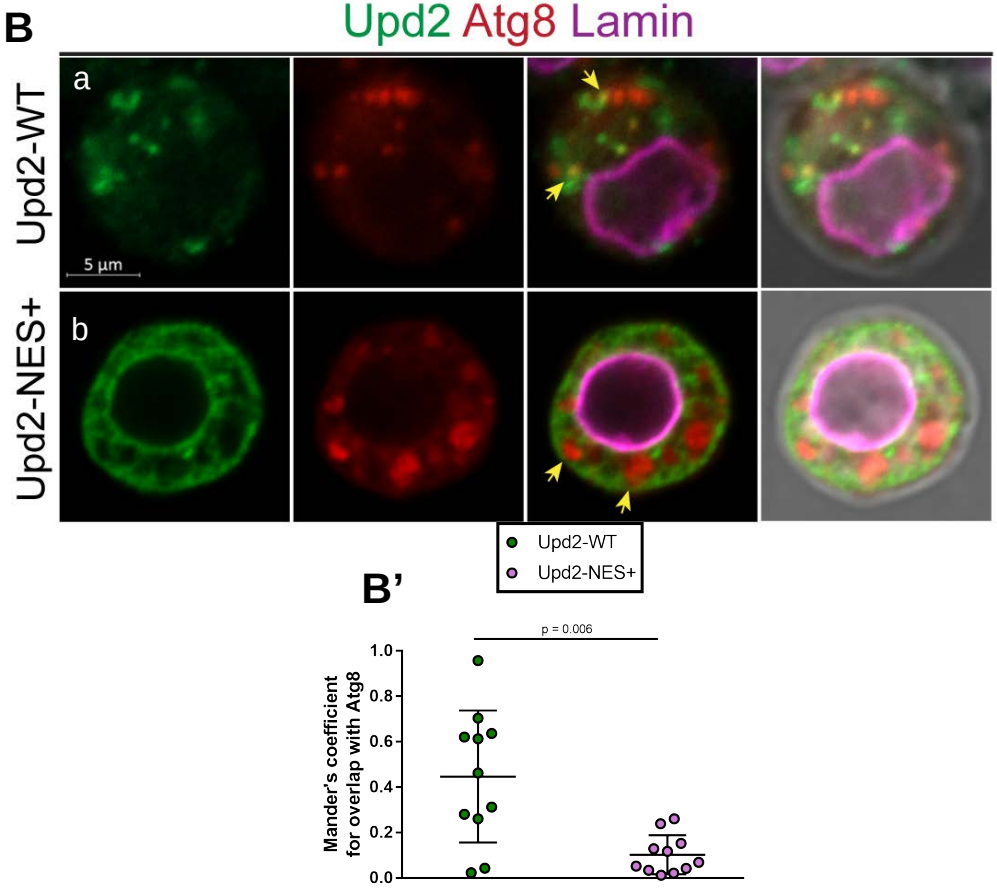
B
Upd2 Atg8 Lamin
Upd2-WT
Upd2-NES+
a
b
5 µm
Upd2-WT
Upd2-NES+
B'
p = 0.006
Mander's coefficient for overlap with Atg8
1.0
0.8
0.6
0.4
0.2
0.0

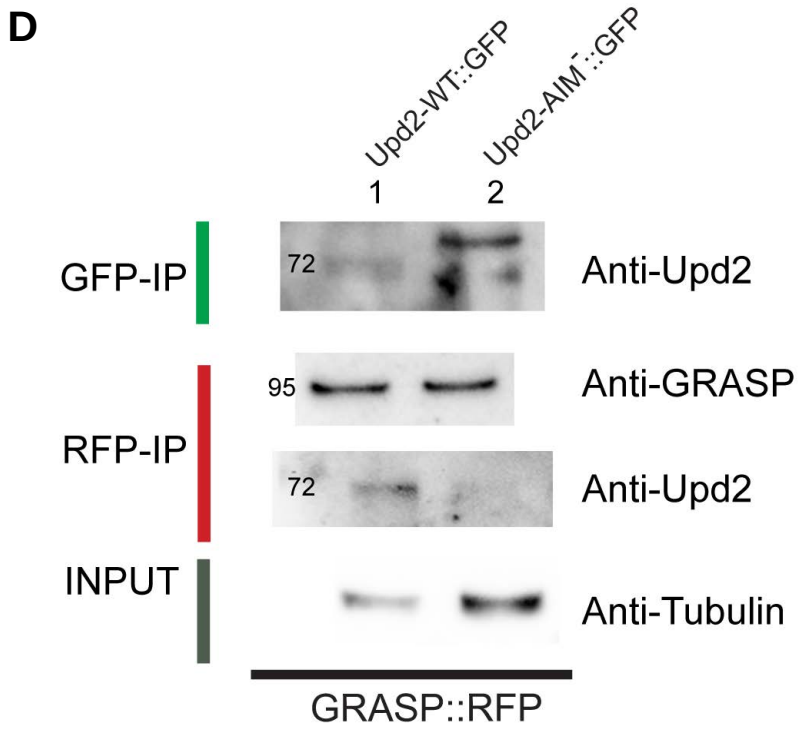
D
Upd2-WT::GFP
Upd2-AIM-::GFP
1
2
GFP-IP
RFP-IP
INPUT
72
95
72
Anti-Upd2
Anti-GRASP
Anti-Upd2
Anti-Tubulin
GRASP::RFP

bioRxiv preprint doi: https://doi.org/10.1101/2021.01.29.428913; this version posted April 2, 2021. The copyright holder for this preprint (which was not certified by peer review) is the author/funder, who has granted bioRxiv a license to display the preprint in perpetuity. It is made available under aCC-BY 4.0 International license.

Figure 4: Upd2 nucleocytoplasmic shuttling licenses its release via Atg8-GRASP pathway.

(A) Live dynamics of Upd2 and Atg8 in S2R+ cells. Confocal micrographs of live time lapse shots acquired every 45 seconds(s), of *Drosophila* S2R+ cells cultured in a fed state. Cells are transiently transfected with cDNAs for tagged Upd2::GFP (green) and mCherry::Atg8 (magenta); live cell dyes mark nucleus (NucBlue™ -dark blue). Atg8 and Upd2 exhibit discrete punctate localization. The Atg8 and Upd2 puncta show dynamics of both colocalization as well as association in: i) nuclear periphery (blue arrows), ii) cell periphery (white arrows). (**A'**) 90 second snapshot is enlarged for clarity, along with magnified insets. Inset **(a)** Upd2 and Atg8 shows association, not complete colocalization; **(b, c)** Upd2 and Atg8 show significant overlap. Cell outlines and nuclear outlines are marked for clarity and based on DIC images of the cells in Extended Data Figure 1. See also. Scale bars, 2μM.

(B) Effect of nuclear export signal (NES) addition to Upd2-WT's colocalization with Atg8. Confocal micrographs of single optical-slices of fed *Drosophila* S2R+ cells transiently transfected with *Upd2-WT::GFP* (green), mCherry-Atg8-WT (red) stained with Lamin (magenta). In WT state, Upd2 shows partial co-localization with Atg8. Addition of NES alters Upd2's punctate distribution in the cytoplasm and its co-localization with Atg8 is significantly diminished as quantified in B' using the Mander's coefficient. Statistical significance is quantified by unpaired two-tailed t-test

(C) Effect of mutating Upd2's AIM on its colocalization with GRASP. Confocal micrographs of single optical-slices of *Drosophila* S2R+ cells transiently transfected with cDNAs expressing *Upd2-WT::GFP* or *Upd2-AIM$^-$::GFP* (green) and *GRASP::RFP* (red) stained with DAPI (white). In fed state, *Upd2-WT::GFP* is localized to cytosolic puncta enriched for GRASP (white arrows). When Upd2's AIM is mutated (*Upd2-AIM$^-$::GFP*) Upd2 is nuclear (white arrows), and the cytosolic puncta are not readily detectable. GRASP is exclusively cytosolic. Scale bars are 5μM.

(D) Effect of mutating Upd2's AIM on its interaction with GRASP. GFP- and RFP-IPs were prepared from S2R+ cells transiently co-transfected with GRASP-RFP and Upd2-WT::GFP or Upd2-AIM-::GFP. GFP, RFP IPs and 2% of the input were analyzed by immunoblotting for the indicated proteins. Note Upd2-AIM$^-$ always runs slightly higher than Upd2 and is always more abundant in the lysate as the Upd2-AIM$^-$ is not secreted, but it is not readily detectable in the RFP-IPs, despite loading more input.

Figure 5

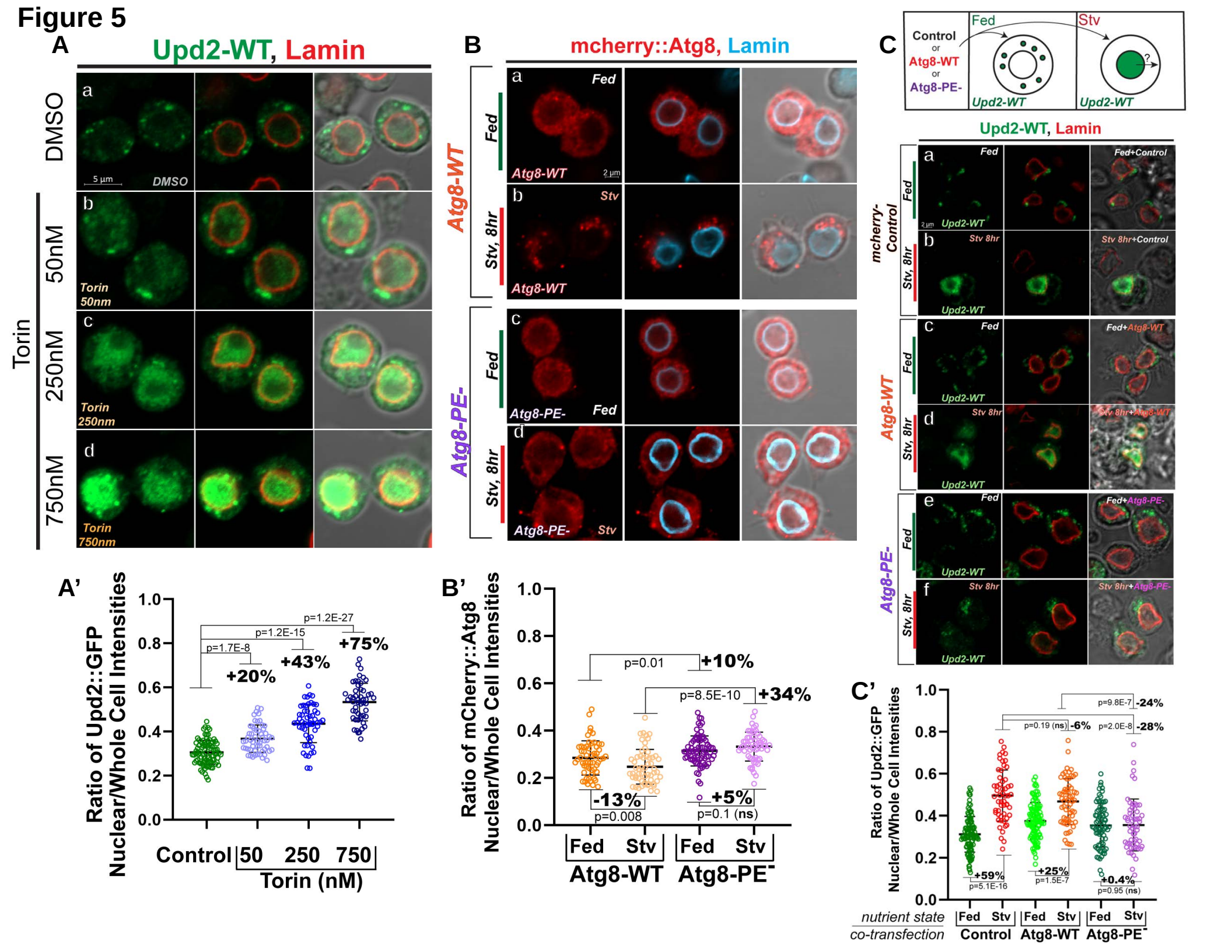
A
Upd2-WT, Lamin
DMSO
Torin
50nM
250nM
750nM
5 µm
Torin 50nm
Torin 250nm
Torin 750nm
B
mcherry::Atg8, Lamin
Atg8-WT
Atg8-PE-
Fed
Stv, 8hr
Stv
2 µm
C
Control or Atg8-WT or Atg8-PE-
Upd2-WT
Upd2-WT, Lamin
mcherry-Control
Atg8-WT
Atg8-PE-
Fed+Control
Stv 8hr+Control
Fed+Atg8-WT
Stv 8hr+Atg8-WT
Fed+Atg8-PE-
Stv 8hr+Atg8-PE-
A'
Ratio of Upd2::GFP Nuclear/Whole Cell Intensities
p=1.2E-27
p=1.2E-15
p=1.7E-8
+75%
+43%
+20%
Control
50
250
750
Torin (nM)
B'
Ratio of mCherry::Atg8 Nuclear/Whole Cell Intensities
p=0.01
+10%
p=8.5E-10
+34%
-13%
p=0.008
+5%
p=0.1 (ns)
Fed
Stv
Atg8-WT
Atg8-PE-
C'
Ratio of Upd2::GFP Nuclear/Whole Cell Intensities
p=9.8E-7
-24%
p=0.19 (ns)
-6%
p=2.0E-8
-28%
+59%
p=5.1E-16
+25%
p=1.5E-7
+0.4%
p=0.95 (ns)
nutrient state
co-transfection
Control
Atg8-WT
Atg8-PE-

bioRxiv preprint doi: https://doi.org/10.1101/2021.01.29.428913; this version posted April 2, 2021. The copyright holder for this preprint (which was not certified by peer review) is the author/funder, who has granted bioRxiv a license to display the preprint in perpetuity. It is made available under aCC-BY 4.0 International license.

Figure 5: Atg8 lipidation induces Upd2 nuclear accumulation.

(A) Effect of pharmacological autophagy activation on Upd2 nuclear accumulation. Confocal micrographs of single optical-slices of *Drosophila* S2R+ cells transiently transfected with *Upd2-WT::GFP* (green) stained with Lamin (red) and treated with DMSO **(a)** or indicated concentrations of autophagy activator Torin1 **(b, c, d)**. Scale bar is 5um and right most panel shows DIC image merge. In B**'**, the ratio of Upd2::GFP nuclear/whole cell intensity is plotted. Each dot represents a cell, 50-100 cells were counted per condition. Statistical significance is quantified by unpaired two-tailed t-test.

(B) Effect of starvation induced changes in the nuclear pool of mCherry-tagged Atg8 wild-type (*Atg8-WT*) versus lipidation-defective Atg8 (*Atg8-PE-*). Confocal micrographs of single optical-slices of *Drosophila* S2R+ cells transiently transfected with (**a, b**) *mCherry::Atg8-WT* (red) or (**c, d**) *mCherry::Atg8-PE-* (red) stained with Lamin (blue) in either well-fed state (a, c) or AA-starved (b, d). Scale bar is 2um and right most panel shows DIC image merge. In **C'**, the ratio of mCherry::Atg8 nuclear/whole cell intensity is plotted. While Atg8-WT pool in the nucleus is reduced on starvation, lipidation-defective pool of Atg8 is similar between fed and starved states. Each dot represents a cell, 50-80 cells were counted per condition. Statistical significance is quantified by unpaired two-tailed t-test.

(C) Effect of providing exogenous mCherry-tagged Atg8 wild-type (*Atg8-WT*) versus lipidation-defective Atg8 (*Atg8-PE-*) on Upd2 nuclear localization during starvation: Schematic, in the top panel, shows experimental design; an assay for the effect of increasing the dose of lipidation-defective Atg8 on Upd2 nuclear accumulation. Below, confocal micrographs of representative single optical-slices of *Drosophila* S2R+ cells transiently co-transfected with *Upd2-WT::GFP* and (**a, b**) *mCherry* or (**c, d**) *mCherry::Atg8-WT* or (**e, f**) *mCherry::Atg8-PE-* stained with GFP (green) and Lamin (red) in either well-fed state (a, c, e) or AA-starved (b, d, f). Scale bar is 2um and right most panel shows DIC image merge. In **D'**, the ratio of Upd2::GFP nuclear/whole cell intensity is plotted. While Atg8-WT and control show that Upd2 nuclear accumulation increases on starvation, cells co-transfected with lipidation-defective Atg8-PE-, do not show Upd2 nuclear accumulation increase on starvation. Each dot represents a cell, 80-130 cells were counted per condition. Statistical significance is quantified by unpaired two-tailed t-test.

Also see companion Figure S2, that assays Upd2's ability to immunoprecipitate with lipidation-defective Atg8-PE-.

Figure 6

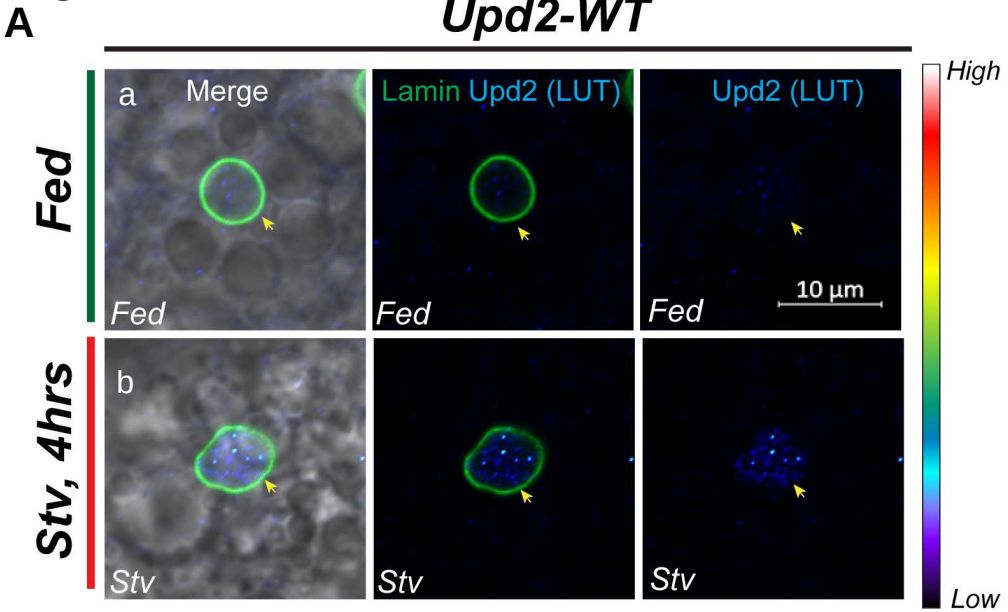
A
Upd2-WT
Fed
Stv, 4hrs
a
Merge
Lamin Upd2 (LUT)
Upd2 (LUT)
Fed
10 µm
b
Stv
High
Low

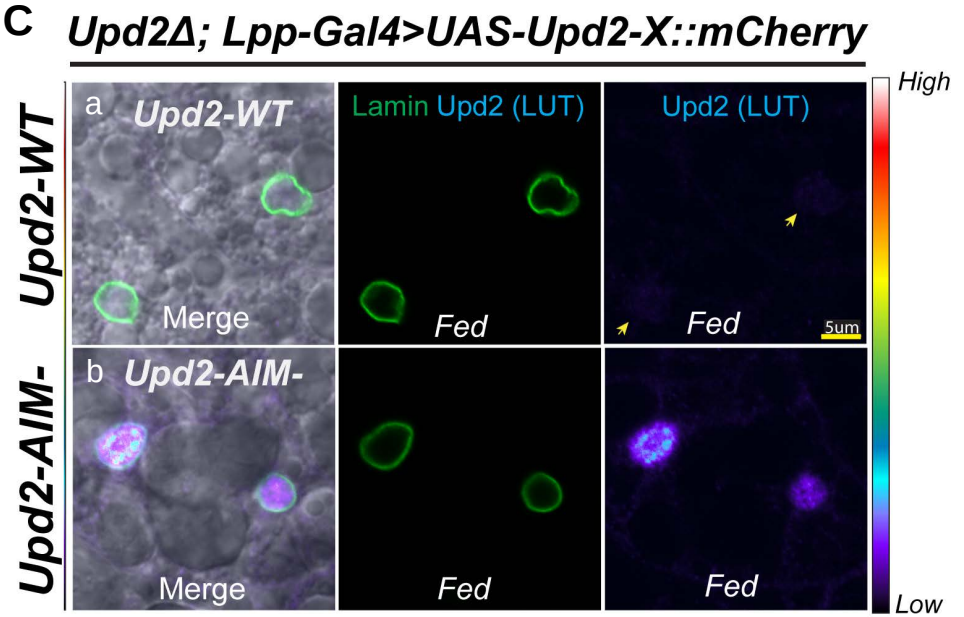
C
Upd2Δ; Lpp-Gal4>UAS-Upd2-X::mCherry
Upd2-WT
Upd2-AIM-
a Upd2-WT
b Upd2-AIM-
Lamin Upd2 (LUT)
Upd2 (LUT)
Merge
Fed
5um
High
Low

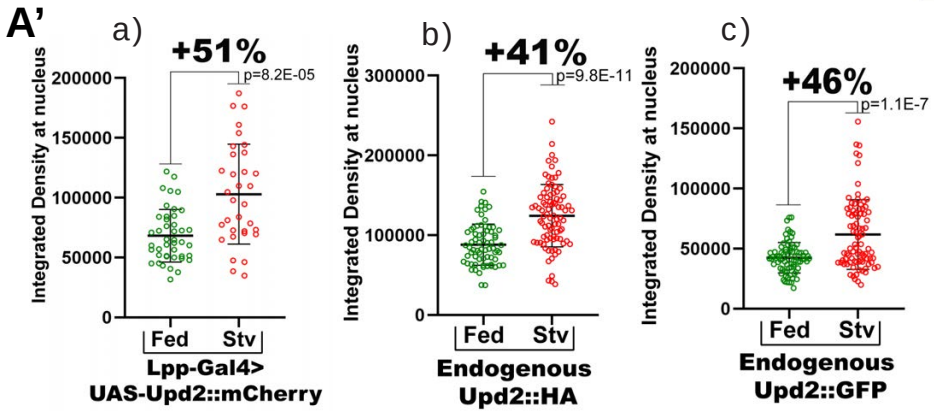
A'
a)
+51%
p=8.2E-05
Integrated Density at nucleus
Fed
Stv
Lpp-Gal4>
UAS-Upd2::mCherry
b)
+41%
p=9.8E-11
Endogenous
Upd2::HA
c)
+46%
p=1.1E-7
Endogenous
Upd2::GFP

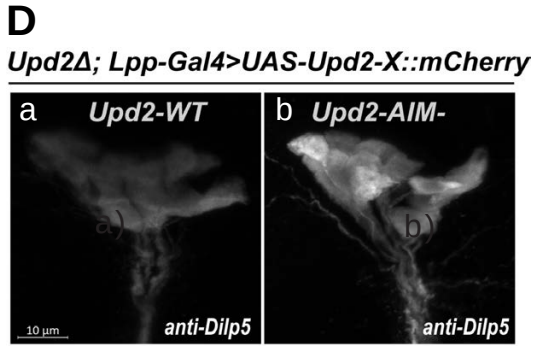
D
Upd2Δ; Lpp-Gal4>UAS-Upd2-X::mCherry
a Upd2-WT
b Upd2-AIM-
10 µm
anti-Dilp5
anti-Dilp5

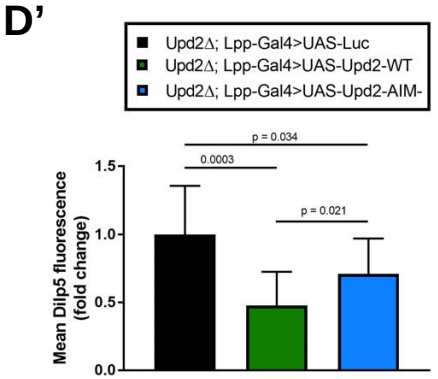
D'
Upd2Δ; Lpp-Gal4>UAS-Luc
Upd2Δ; Lpp-Gal4>UAS-Upd2-WT
Upd2Δ; Lpp-Gal4>UAS-Upd2-AIM-
p = 0.034
0.0003
p = 0.021
Mean Dilp5 fluorescence
(fold change)

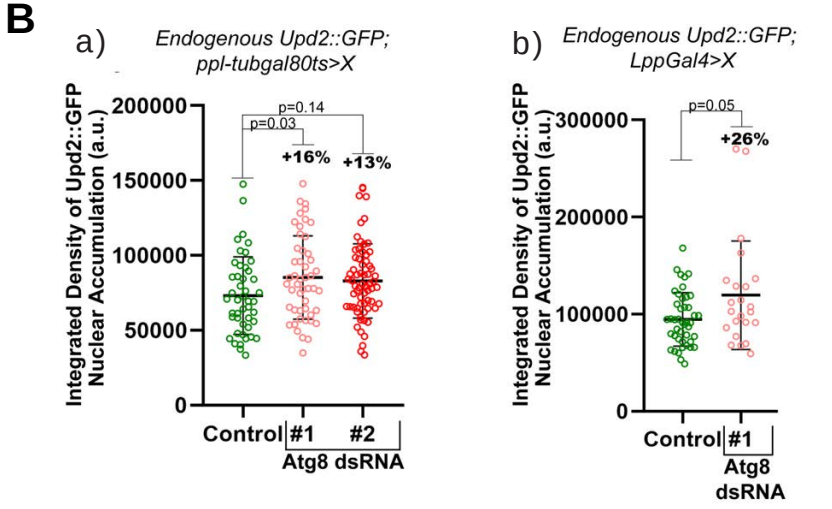
B
a)
Endogenous Upd2::GFP;
ppl-tubgal80ts>X
p=0.14
p=0.03
+16%
+13%
Integrated Density of Upd2::GFP
Nuclear Accumulation (a.u.)
Control
#1
#2
Atg8 dsRNA
b)
Endogenous Upd2::GFP;
LppGal4>X
p=0.05
+26%
Control
#1
Atg8
dsRNA

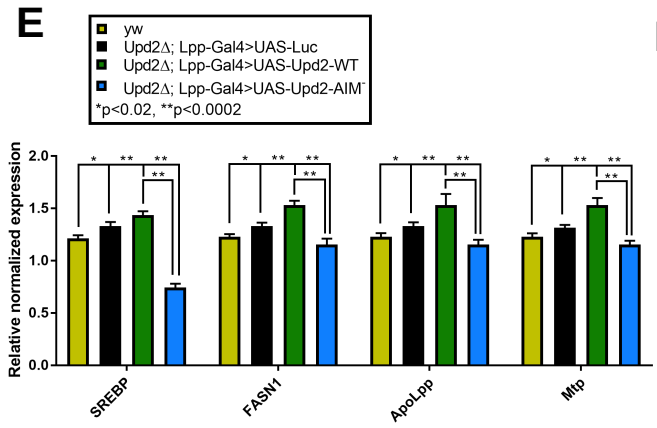
E
yw
Upd2Δ; Lpp-Gal4>UAS-Luc
Upd2Δ; Lpp-Gal4>UAS-Upd2-WT
Upd2Δ; Lpp-Gal4>UAS-Upd2-AIM-
*p<0.02, **p<0.0002
Relative normalized expression
SREBP
FASN1
ApoLpp
Mtp

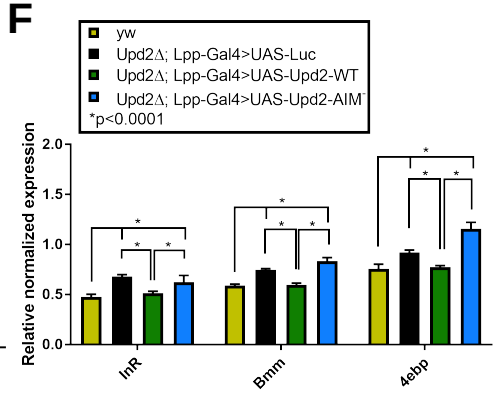
F
yw
Upd2Δ; Lpp-Gal4>UAS-Luc
Upd2Δ; Lpp-Gal4>UAS-Upd2-WT
Upd2Δ; Lpp-Gal4>UAS-Upd2-AIM-
*p<0.0001
Relative normalized expression
InR
Bmm
4ebp

bioRxiv preprint doi: https://doi.org/10.1101/2021.01.29.428913; this version posted April 2, 2021. The copyright holder for this preprint (which was not certified by peer review) is the author/funder, who has granted bioRxiv a license to display the preprint in perpetuity. It is made available under aCC-BY 4.0 International license.

Figure 6: On fasting Upd2 accumulates in fly fat and Upd2-AIM- systemically signals a state of chronic starvation.

(A) Effect of starvation on Upd2 nuclear accumulation in adult fly fat tissue: Confocal micrographs of fixed and immunostained adult fly fat from flies CRISPR engineered (see methods) with HA and GFP tag in the endogenous Upd2 locus (that rescues the upd2Δ mutant- see Figure S3). Fat is stained with RFP antibody (in a, b) in well-fed flies, or flies starved on agarose for 4 hours. Upd2-WT in fed state is detectable in very low levels in the nucleus (see look up table (LUT)) and yellow arrows in a. Upd2 shows increased nuclear accumulation on starvation. Scale bar is 10um and left post panel shows merges DIC image. (A') Upd2 nuclear accumulation is quantified three different Upd2 tagged genotypes: (a) mCherry tagged Upd2 (*UAS-X*) under the control of a fat-cell specific promoter (*Lpp-Gal4*); (b) Upd2-HA endogenous tag and ; (c) Upd2-GFP endogenous tag. Each dot represents a fat cell nucleus, 30-100 fat nuclei were counted per condition per genotype. Statistical significance is quantified by unpaired two-tailed t-test.

(B) Effect of *Atg8-KD* on Upd2 nuclear accumulation in adult fly fat tissue: Confocal micrographs of fixed and immunostained adult fly fat from flies CRISPR engineered with GFP tag in the endogenous Upd2 locus (*upd2-crGFP*) expressing dsRNA for Atg8 or control (Luciferase) in fat cells. Two different fat specific promoters, one of them with fat-specific temporal control *upd2-crGFP; ppl-Gal4tubGal80^{ts}* (a) or *upd2-crGFP; Lpp-Gal4* chronic fat-specific (b) knockdown were used (see Methods for how we controlled knock-down only to adult stages). Fat is stained with GFP antibody Upd2 nuclear accumulation is quantified and graphs of the total integrated density of Upd2 levels -as measured by GFP- are represented. Each dot on the graph is a fat cell nucleus, 50-80 nuclei were counted for the temporal knockdown (a) 18-20 fat cell nuclei were counted per condition per genotype for (b). Statistical significance is quantified by unpaired two-tailed t-test.

(C) Effect of point mutations to Upd2's AIM (*Upd2-AIM$^-$*) on its nuclear accumulation in adult fly fat: Confocal micrographs of single optical sections of fixed and immunostained adult fly fat from transgenic flies expressing mCherry tagged Upd2-cDNAs for (a) Upd2-WT (*UAS-Upd2-WT*) or (b) Upd2's AIM mutated (*UAS-Upd2-AIM$^-$*) under the control of a fat-cell specific promoter (*Lpp-Gal4*) in a *upd2-deletion* background (*upd2Δ; Lpp-Gal4*). In Upd2-WT in fed state is detectable in very low levels in the nucleus (see look up table (LUT)) and yellow arrows in a. Upd2-AIM- shows significantly nuclear accumulation even in a fed state.

(D) Effect of point mutations to Upd2's AIM (*Upd2-AIM$^-$*) on its ability to rescue the insulin accumulation defect in the IPCs of Upd2 deletion mutants (Insulin producing cells): Confocal micrographs of fixed and immunostained adult brain of well-fed transgenic flies expressing mCherry tagged Upd2-cDNAs for (a) Upd2-WT (*UAS-Upd2-WT*) or (b) Upd2's AIM mutated (*UAS-Upd2-AIM$^-$*) under the control of a fat-cell specific promoter (*Lpp-Gal4*) in a *upd2-deletion* background (*upd2Δ; Lpp-Gal4*). Scale bar is 10um. While *Upd2-WT* transgene rescue insulin accumulation defect of *upd2Δ*, the *Upd2-AIM$^-$* as quantified in C'. Statistical significance is quantified by unpaired two-tailed t-test and 11-12 brains were used per genotype. Also see companion Extended Data Figure 4.

bioRxiv preprint doi: https://doi.org/10.1101/2021.01.29.428913; this version posted April 2, 2021. The copyright holder for this preprint (which was not certified by peer review) is the author/funder, who has granted bioRxiv a license to display the preprint in perpetuity. It is made available under aCC-BY 4.0 International license.

(**E, F**) Effect of point mutations to Upd2's AIM (*Upd2-AIM*$^{-}$) on gene expression profiles relevant for fat storage and starvation response: Relative normalized expression, of steady-state mRNA levels, assayed by qPCR on adult fat tissue (see methods) from *Upd2Δ* mutants in which either Upd2-WT or Upd2-AIM- was over-expressed in fat. *yw and updΔ* flies with control transgene serves as baseline (*Upd2Δ; Lpp-Gal4>UAS-Luc*). **In E**, expression of genes involved in either de-novo lipid synthesis or LPP production are examined. **In F**, expression of FOXO target genes- *InR*, *brummer* (*Bmm*), and *4ebp/Thor*- provide a readout of Insulin signaling. One-way ANOVA followed by Turkey's multiple comparisons test. Error bars represent standard error of the mean (SEM). N = 3 replicates per primer pair. See companion Figure S5.

Figure 7

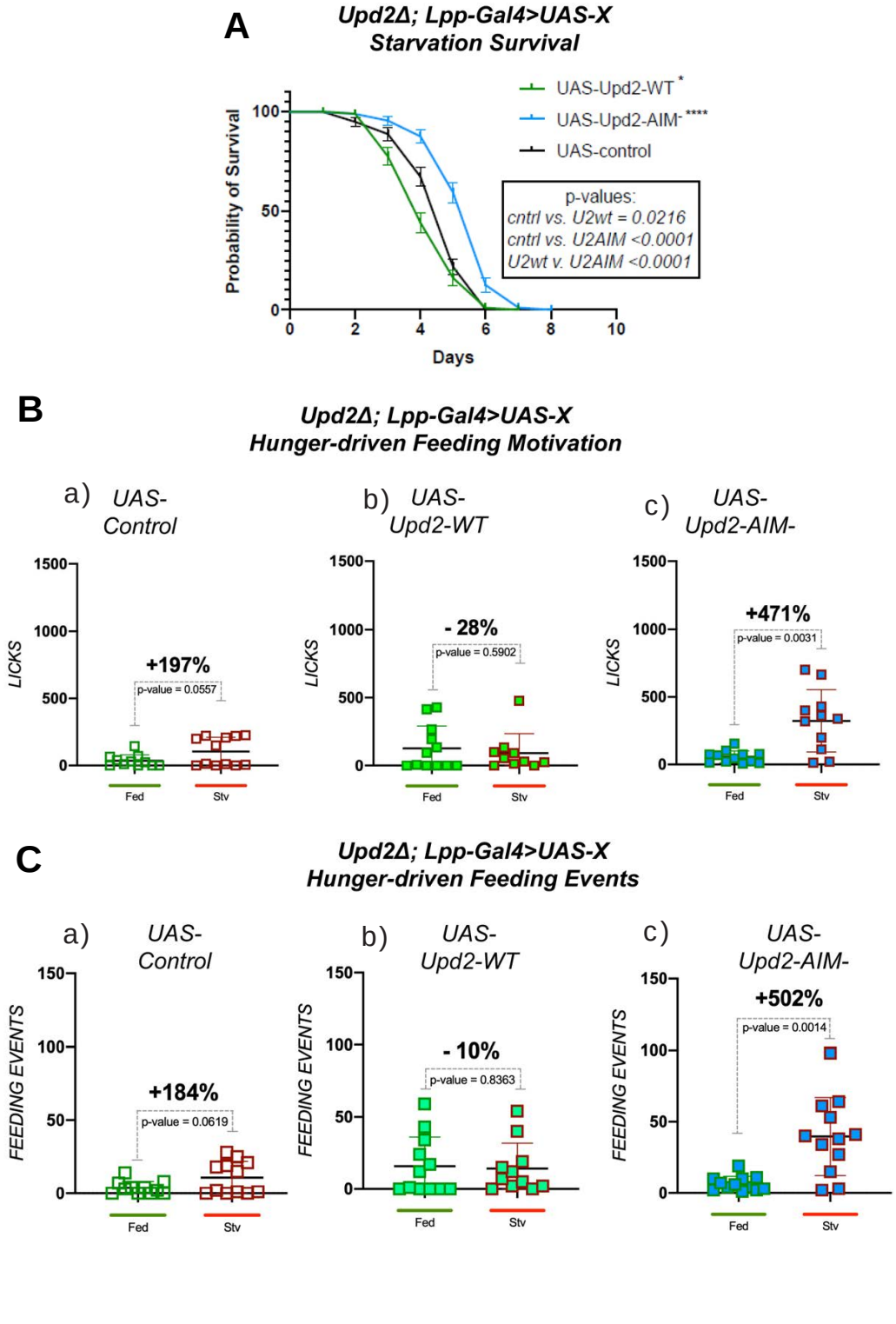
A
Upd2Δ; Lpp-Gal4>UAS-X
Starvation Survival
UAS-Upd2-WT *
UAS-Upd2-AIM- ****
UAS-control
p-values:
cntrl vs. U2wt = 0.0216
cntrl vs. U2AIM <0.0001
U2wt v. U2AIM <0.0001
Probability of Survival
Days
B
Upd2Δ; Lpp-Gal4>UAS-X
Hunger-driven Feeding Motivation
a) UAS-Control
b) UAS-Upd2-WT
c) UAS-Upd2-AIM-
LICKS
+197%
p-value = 0.0557
- 28%
p-value = 0.5902
+471%
p-value = 0.0031
Fed
Stv
C
Upd2Δ; Lpp-Gal4>UAS-X
Hunger-driven Feeding Events
a) UAS-Control
b) UAS-Upd2-WT
c) UAS-Upd2-AIM-
FEEDING EVENTS
+184%
p-value = 0.0619
- 10%
p-value = 0.8363
+502%
p-value = 0.0014
Fed
Stv
D
Fed
Fasting
Upd2-WT
Atg8-WT
Nucleus
Cytoplasm
Upd2-AIM-
Atg8-WT
X
Upd2-WT
Atg8-PE-
?
?
Upd2/Leptin -Wild-Type
Upd2/Leptin AIM-
AIM
AIM-
Atg8-WT
Lipidated Atg8
Phagophore
Lipidation defective Atg8-PE-
GRASP

bioRxiv preprint doi: https://doi.org/10.1101/2021.01.29.428913; this version posted April 2, 2021. The copyright holder for this preprint (which was not certified by peer review) is the author/funder, who has granted bioRxiv a license to display the preprint in perpetuity. It is made available under aCC-BY 4.0 International license.

Figure 7: Atg8-controlled Upd2 retention in nucleus is a mechanism to resist starvation and increase post-fasting hunger response.

(A) Effect of fat-specific expression of Upd2-AIM- on starvation survival: Flies expressing cDNAs (*UAS-X*) for *Upd2-WT*, *Upd2-AIM-* and control (*UAS-Luciferase)* specifically in fly fat (*Upd2Δ; Lpp-Gal4>UAS-X*). Transgenic flies with fat-specific overexpression of *Upd2-AIM-* are starvation-resistant, whereas overexpression of normal Upd2 (*Upd2-WT*) results in starvation-sensitivity with a median life span of 4 days compared to 6 days *for Upd2-AIM-* that lives significantly longer than the control as assessed by the Log-rank (Mantel-Cox) test. See companion Extended Data Figure 6A.

(B, C) Effect of fat-specific expression of Upd2-AIM- on post-fasting hunger driven feeding: Quantification of feeding behavior in transgenic flies, expressing indicated cDNAs (*UAS-X*) specifically in fat-tissue (*Upd2Δ; Lpp-Gal4>UAS-X*), measured using the Fly Liquid Interaction Counter (FLIC-see methods). Each dot represents a fly. 10-12 flies were used per experiment per genotype. The flies were starved for 16 hours prior to testing. The difference between fed and starved flies of the same genotype were assayed as licks i.e., interactions with food, which is a measure of feeding motivation (B) and feeding events (C). Error bars represent percent standard deviation and statistical significance was calculated using 2-tailed unpaired t-test. See companion Extended Data Figure 6 B, C.

(D) Working model: Atg8 mediates adipokine nuclear exit and its subsequent release: In a fed state, the ortholog of human Leptin in flies, Upd2, enters the nucleus; via its Atg8-interaction motif (AIM) Upd2 complexes with Atg8. Atg8 then enables Upd2 nuclear exit via an Exportin/CRM1 based mechanism. Atg8 subsequently targets Upd2 to the GRASP secretory pathway. On fasting, Atg8 lipidation and recruitment to autophagy decreases the Atg8 nuclear pool. In turn, this increases Upd2 nuclear accumulation and causes cells to retain the adipokine on fasting. When Upd2's interaction with Atg8 is disrupted (AIM-), Upd2 localizes to the nucleus even in a fed state and is not secreted. In flies, constitutive expression of Upd2-AIM- in fat cells, results in a chronic starvation phenotype. Upd2-AIM- flies are starvation resistant and exhibit higher hunger-driven feeding motivation. Altogether, this suggests that fasting-induced Upd2 accumulation facilitates organismal adaptation to nutrient deprivation and drives post-fasting hunger response. When cells are dosed with lipidation-defective nuclear Atg8, Upd2 export from the nucleus occurs even on fasting. Future studies, indicated by question marks, are required to evaluate whether Upd2 which is exported from the nucleus by lipidation-defective Atg8 can be targeted to the appropriate secretory compartment. If indeed Upd2 can be subsequently released via a lipidation-defective route, then ensuing investigations should explore whether such a lipidation-defective Atg8 mediated secretion allows Upd2 to reach its appropriate neuronal target.

Extended Data Figure 1

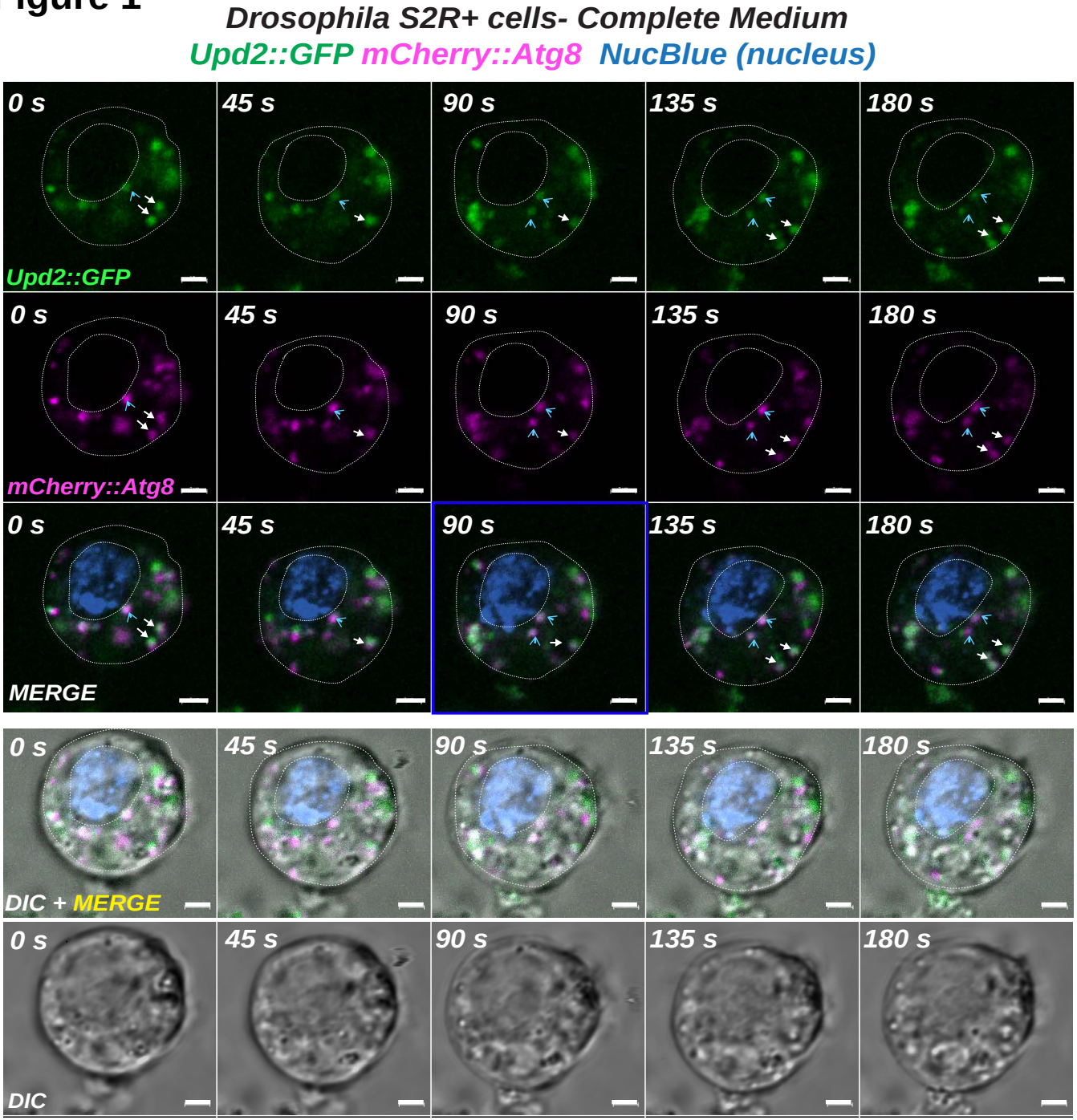

bioRxiv preprint doi: https://doi.org/10.1101/2021.01.29.428913; this version posted April 2, 2021. The copyright holder for this preprint (which was not certified by peer review) is the author/funder, who has granted bioRxiv a license to display the preprint in perpetuity. It is made available under aCC-BY 4.0 International license.

Extended Data Figure 1 ***(companion to Figure 4A)***

Confocal micrographs of time-lapse shots, acquired every 45 seconds(s), of *Drosophila* S2R+ cells cultured in complete media and transiently transfected with cDNAs for tagged Upd2::GFP (green) and mCherry::Atg8 (magenta); live cell dyes mark nucleus (NucBlue™ -dark blue). Atg8 and Upd2 exhibit discrete punctate localization. The Atg8 and Upd2 puncta show dynamics of both colocalization as well as association in: i) nuclear periphery (blue arrows), ii) cell periphery (white arrows). Cell outlines and nuclear outlines are marked for clarity and based on DIC images of the cells. Scale bars, 2μM.

Extended Data Figure 2

A

a) $\frac{\text{Atg8-Trojan-Gal4}}{\text{FM7a}}$;; $\frac{+}{+}$ ♀ X $\frac{\text{w1118}}{\text{Y}}$;; $\frac{\text{UAS-Atg8-WT}}{\text{UAS-Atg8-WT}}$ *or* $\frac{\text{UAS-Atg8-PE}^-}{\text{UAS-Atg8-PE}^-}$ ♂

b)

X chromosome genotype	Transgene on chromosome III			
	UAS-Atg8-WT		UAS-Atg8-PE$^-$	
	# males	% males	# males	% males
Atg8-Trojan-Gal4	36	46.8	0	0
FM7a	41	53.2	36	100

c)

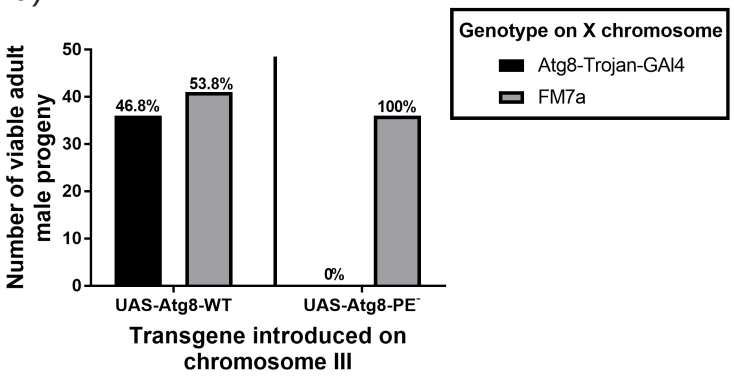

B

Fat depots from adult flies starved for 4-6 hours

GFP-tagged Atg8 transgene, anti-Atg8 (antibody), Lamin

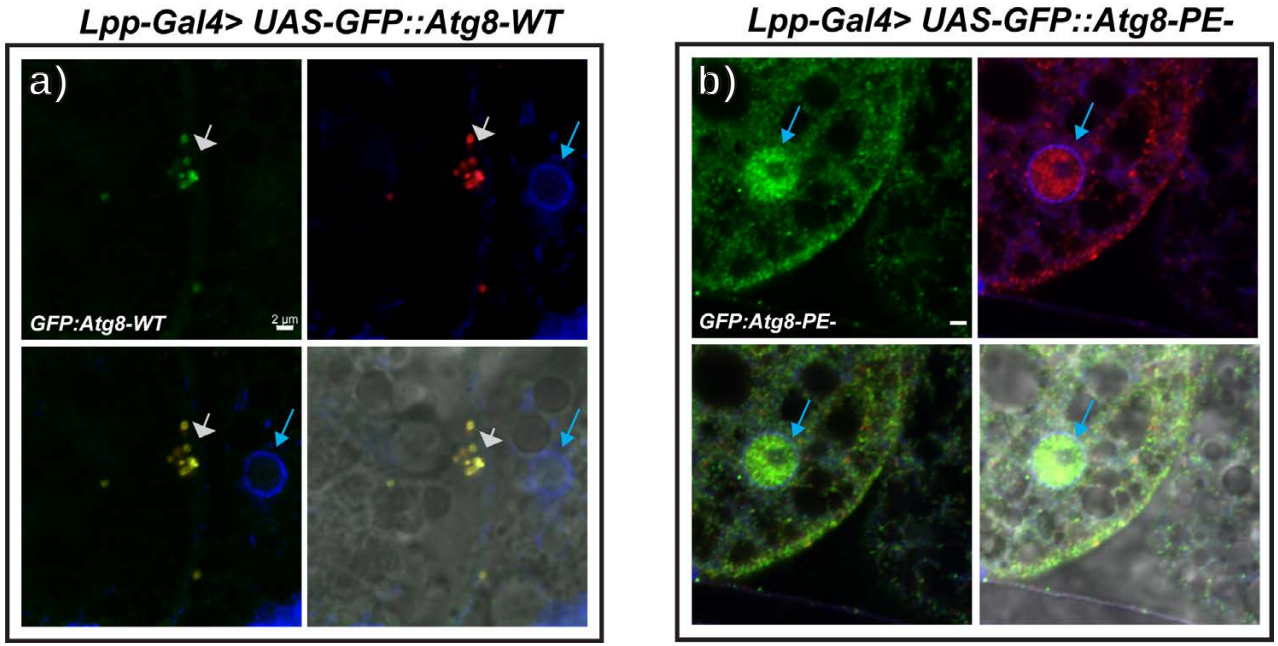

C

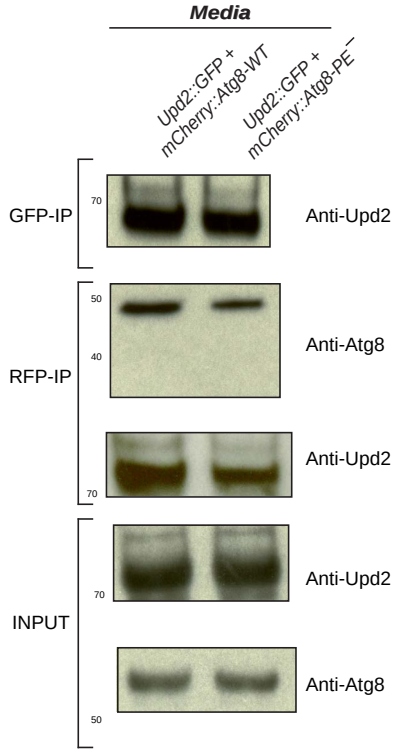

bioRxiv preprint doi: https://doi.org/10.1101/2021.01.29.428913; this version posted April 2, 2021. The copyright holder for this preprint (which was not certified by peer review) is the author/funder, who has granted bioRxiv a license to display the preprint in perpetuity. It is made available under aCC-BY 4.0 International license.

Extended Data Figure 2 ***(companion to Figure 5)***

A) Rescue of an Atg8 knock out allele- *Atg8-Trojan-Gal4* (see methods), which is lethal. **a)** The crossing scheme depicting the *Atg8-Trojan-Gal4* allele rescue with wild-type Atg8 transgene (*UAS-GFP::Atg8-WT*) or the lipidation-defective Atg8 transgene (*UAS-GFP::Atg8-PE-*). b,c) Outcome of cross to rescue lethality. In b) table shows the number of progenies counted from the cross and the % of transgenic rescue. C) graph of the %progeny of each genotype. While the expected percentage of flies with UAS-GFP-Atg8-WT, as expected the UAS-Atg8-PE- (lipidation-defective version) does not rescue the Atg8 knockout allele.

B) Confocal micrographs of single optical sections of fixed and immunostained [anti-GFP(green); anti-Atg8 (red); anti-Lamin (blue)] adult fly fat from transgenic flies- starved for 4 hours- expressing GFP-tagged Atg8-cDNAs for (a) Atg8-WT (*UAS-GFP::Atg8-WT*) or (b) lipidation-defective Atg8 (*UAS-GFP::Atg8-PE*$^{-}$) under the control of a fat-cell specific promoter (*Lpp-Gal4*) in an *Atg8-WT* background. Within 4 hours of starvation in adult fly fat: (a) GFP::Atg8-WT (green) is localized to punctate structures (white arrows) in the cytoplasm, that also co-stain with an Atg8 antibody. GFP::Atg8-WT is barely detectable in the nucleus (blue arrows). (b) In starved fat, lipidation-defective Atg8 continues to be enriched in the nucleus (blue arrows), it is present in the cytoplasm but in a diffuse pattern as opposed to being localized to distinct punctae.

C) Upd2 coimmunoprecipitates with Atg8-WT and lipidation-defective Atg8 (Atg8-PE^{-}) in the extracellular media fractions. GFP and mCherry immunoprecipitates (IPs) were prepared from cell lysates and conditioned media of *Drosophila* S2R+ cells transiently transfected with the indicated cDNAs. GFP-, mCherry- IPs and 2% of the input were analyzed by immunoblotting for the indicated proteins.

Extended Data Figure 3

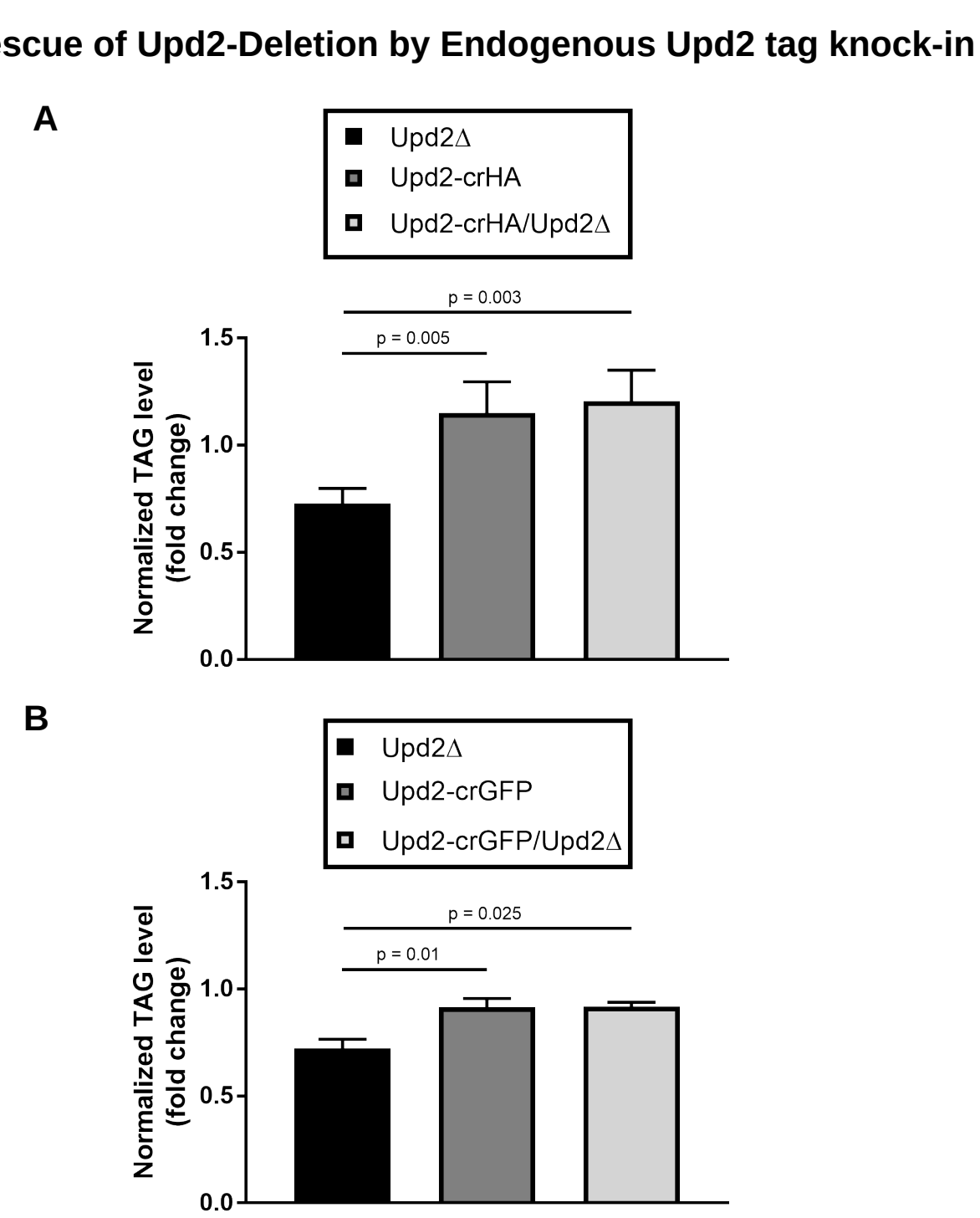

bioRxiv preprint doi: https://doi.org/10.1101/2021.01.29.428913; this version posted April 2, 2021. The copyright holder for this preprint (which was not certified by peer review) is the author/funder, who has granted bioRxiv a license to display the preprint in perpetuity. It is made available under aCC-BY 4.0 International license.

Extended Data Figure 3 ***(companion to Figure 6A)***

Rescue of *Upd2Δ* triglyceride (TAG) storage reduction phenotype by endogenous CRISPR tag knock-in of HA [*Upd2-crHA*] (A) and GFP [*Upd2-crGFP*] (B) in the Upd2 locus.

Extended Data Figure 4

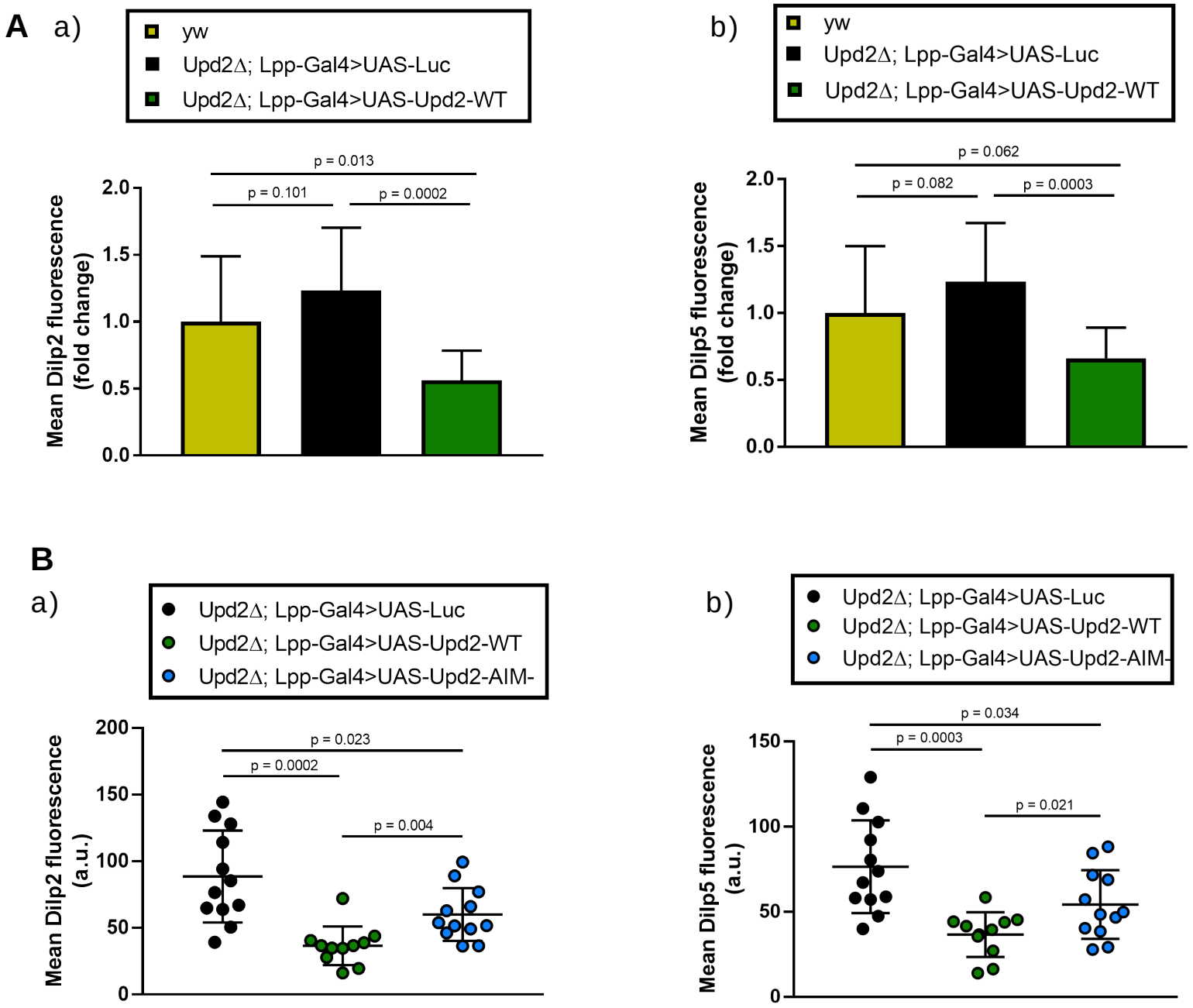

bioRxiv preprint doi: https://doi.org/10.1101/2021.01.29.428913; this version posted April 2, 2021. The copyright holder for this preprint (which was not certified by peer review) is the author/funder, who has granted bioRxiv a license to display the preprint in perpetuity. It is made available under aCC-BY 4.0 International license.

Extended Data Figure 4 ***(companion to Figure 6C, C')***

(A) Mean change in Dilp2 (a) or Dilp5 (b) accumulation in a *upd2Δ* mutant compared to background control (yw) that is rescued by the Upd2 transgene.

(B) Plot of Dilp2 (a) or Dilp5 (b) fluorescence intensity (see methods) calculated from maximum intensity projections of immunostaining of the insulin producing cells (IPCs) in adult brains of the indicated genotypes. Each dot represents an adult fly brain IPC and 10-12 brains we quantified per genotype.

Extended Data Figure 5

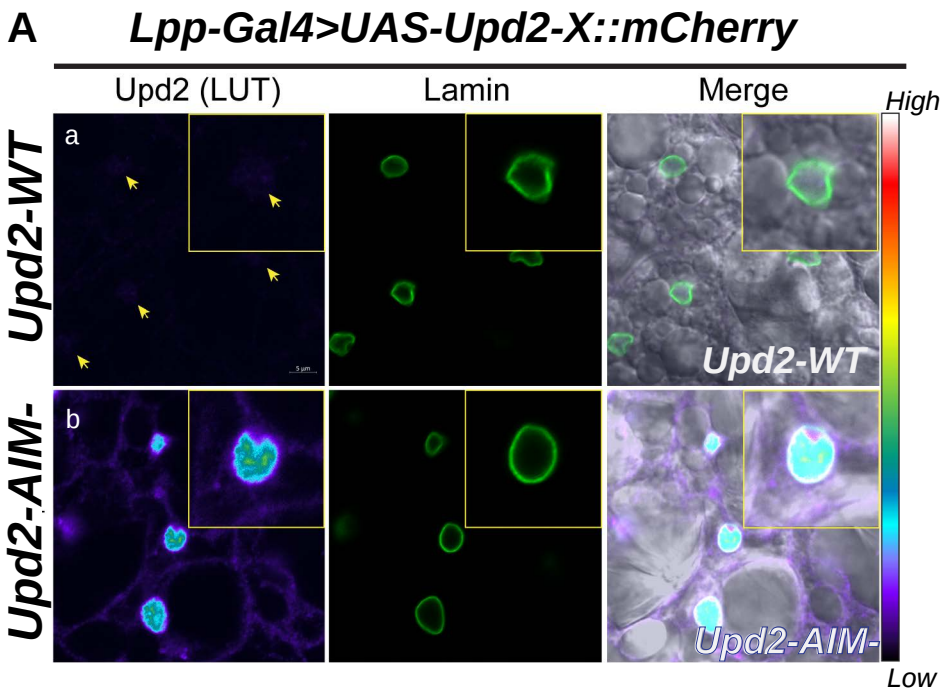

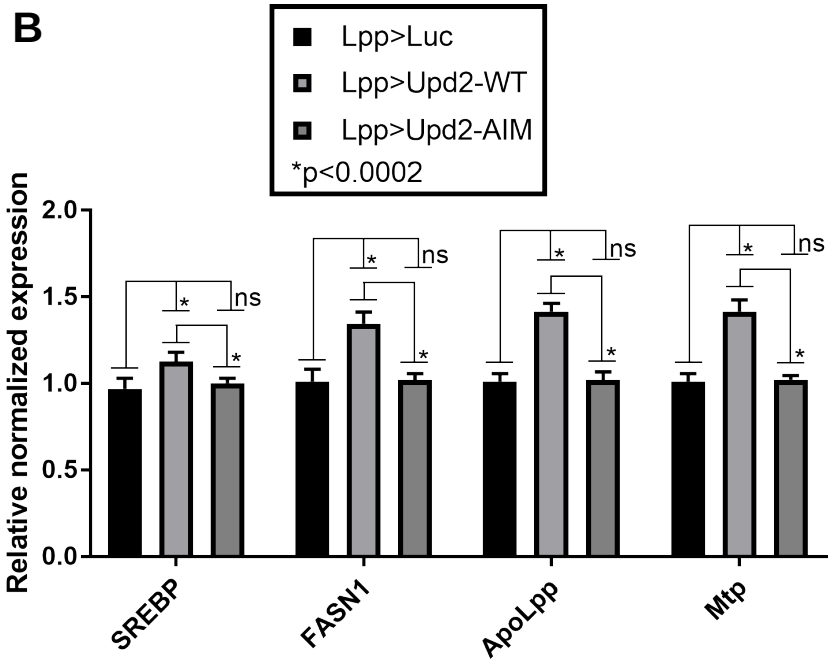

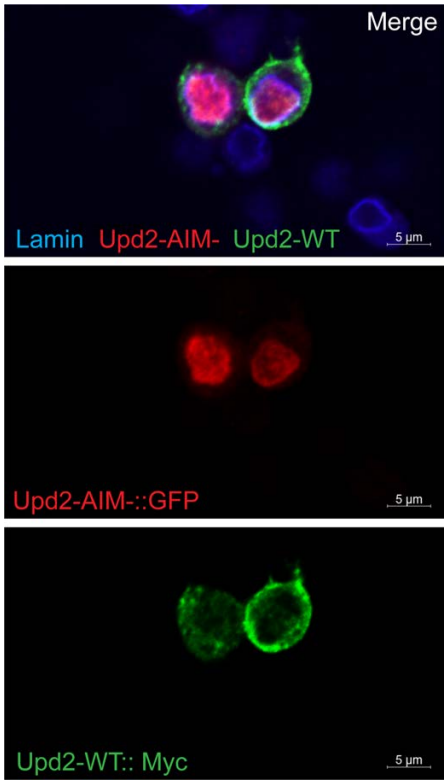

bioRxiv preprint doi: https://doi.org/10.1101/2021.01.29.428913; this version posted April 2, 2021. The copyright holder for this preprint (which was not certified by peer review) is the author/funder, who has granted bioRxiv a license to display the preprint in perpetuity. It is made available under aCC-BY 4.0 International license.

Extended Data Figure 5 ***(companion to Figure 6A, D)***

(A) Confocal micrographs of single optical sections of fixed and immunostained adult fly fat of well-fed transgenic flies expressing mCherry tagged Upd2-cDNAs for (a) Upd2-WT (*UAS-Upd2-WT*) or (b) Upd2's AIM mutated (*UAS-Upd2-AIM^{-}*) under the control of a fat-cell specific promoter (*Lpp-Gal4*). In Upd2-WT in fed state is detectable in very low levels in the nucleus (see look up table (LUT)) and yellow arrows in a. Upd2-AIM- shows significantly nuclear accumulation even in a fed state.

(B) Relative normalized expression, of steady-state mRNA levels, assayed by qPCR on adult fat tissue in which either Upd2-WT or Upd2-AIM- was over-expressed in fat under the control of *Lpp-Gal4.* Flies expressing UAS-Luciferase control transgene serves as baseline (*Lpp-Gal4>UAS-Luc*). Expression of genes involved in either de-novo lipid synthesis or LPP production are examined. One-way ANOVA followed by Turkey's multiple comparisons test. Error bars represent standard error of the mean (SEM). N = 3 replicates per primer pair. Also see Figure 6D.

(C) Confocal micrographs of single optical-slices of complete media fed *Drosophila* S2R+ cells transiently transfected with *Upd2-WT::Myc* (green), *Upd2-AIM-::GFP* (red) stained with Lamin (blue). Note that while Upd2-AIM- is nuclear, the Upd2-WT is cytoplasmic.

Extended Data Figure 6

A

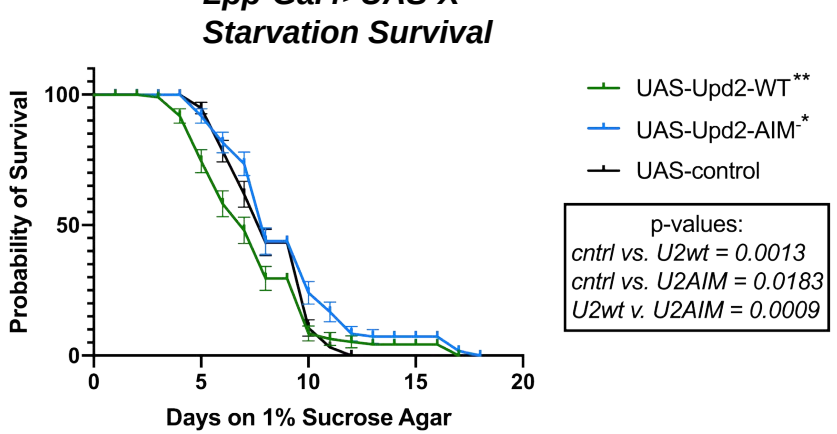

B

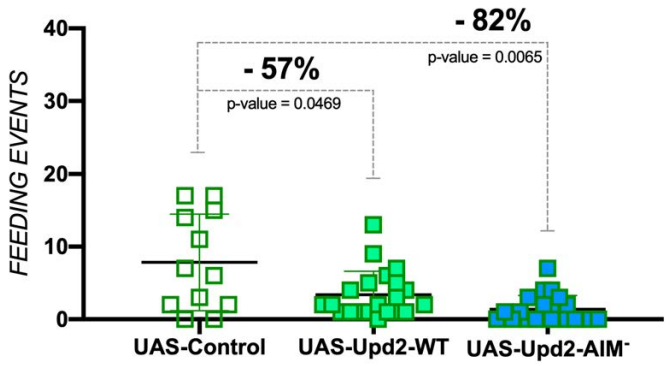

C

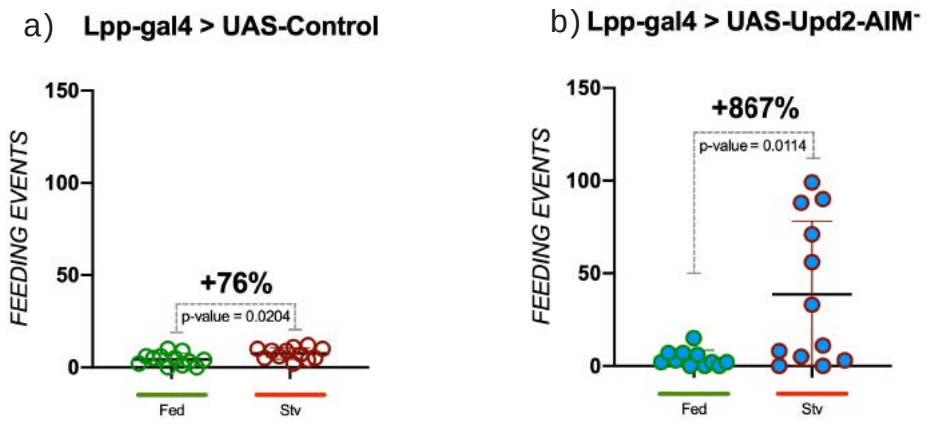

bioRxiv preprint doi: https://doi.org/10.1101/2021.01.29.428913; this version posted April 2, 2021. The copyright holder for this preprint (which was not certified by peer review) is the author/funder, who has granted bioRxiv a license to display the preprint in perpetuity. It is made available under aCC-BY 4.0 International license.

Extended Data Figure 6 ***(companion to Figure 7)***

(A) Flies expressing cDNAs (*UAS-X*) for *Upd2-WT*, *Upd2-AIM-* and control (*UAS-Luciferase)* specifically in fly fat (*Lpp-Gal4>UAS-X*) in a background with endogenous Upd2 intact. Transgenic flies with fat-specific overexpression of *Upd2-AIM-* are starvation-resistant, whereas overexpression of normal Upd2 (*Upd2-WT*) results in starvation-sensitivity. Statistical significance assessed by Log-rank (Mantel-Cox) test. Also see Figure 7A.

(B) Quantification of feeding behavior in transgenic flies, expressing indicated cDNAs (*UAS-X*) specifically in fat-tissue (*Upd2Δ; Lpp-Gal4>UAS-X*), measured using the Fly Liquid Interaction Counter (FLIC-see methods). Each dot represents a fly. 10-12 flies were used per experiment per genotype. The difference between Upd2-AIM- and Upd2-WT transgene expressing flies have reduced baseline feeding. Error bars represent percent standard deviation and statistical significance was calculated using 2-tailed unpaired t-test. Also see Figure 7B, C.

(C) Quantification of feeding behavior in transgenic flies, expressing indicated cDNAs (*UAS-X*) specifically in fat-tissue (*Upd2Δ; Lpp-Gal4>UAS-X*), measured using the Fly Liquid Interaction Counter (FLIC-see methods). Each dot represents a fly. 10-12 flies were used per experiment per genotype. The flies were starved for 16 hours prior to testing. The difference between fed and starved flies of the same genotype were assayed as feeding events. Also see Figure 7B, C.